Technical Report

TR-04-02

Earthquake induced rock shear through a deposition hole

Effect on the canister and the buffer

Lennart Börgesson, Lars-Erik Johannesson
Clay Technology AB

Jan Hernelind, FemTech AB

December 2003

Earthquake induced rock shear through a deposition hole

Effect on the canister and the buffer

Lennart Börgesson, Lars-Erik Johannesson
Clay Technology AB

Jan Hernelind, FemTech AB

December 2003

Keywords: Canister, Copper, Cast iron insert, Bentonite, Buffer, Earth quake, Rock, Shear, Laboratory test, Modelling, Calculation.

Abstract

Existing fractures crossing a deposition hole may be activated and sheared by an earthquake. The effect of such a rock shear has been investigated in a project that includes both laboratory tests and finite element calculations.

The buffer material in a deposition hole acts as a cushion between the canister and the rock, which reduces the effect of a rock shear substantially. Lower density of the buffer yields softer material and reduced effect on the canister. However, at the high density that is suggested for a repository the stiffness of the buffer is rather high. The stiffness is also a function of the rate of shear, which means that there may be a substantial damage on the canister at very high shear rates.

In order to investigate the stiffness and shear strength of the buffer material a number of laboratory test series has been performed with shearing of water1saturated bentonite samples at different densities and shear rates. From those tests a material model of the buffer that takes into account the density and shear rate has been formulated. Shear rates up to 6 m/s have been tested.

The rock shear has been modelled with finite element calculations with the code ABAQUS. A three-dimensional finite element mesh of the buffer and the canister has been created and a number of calculations with simulation of a rock shear have been performed.

The rock shear has been assumed to take place perpendicular to the canister axis in either the centre of the deposition hole or at the quarter point. The shear calculations have been driven to a total shear of 20 cm. Four buffer densities between 1950 and 2100 kg/m^3 at water saturation and shear rates between 0.0001 and 1000 mm/s have been modelled. The influence of buffer density, shear plane location, shear rate and magnitude of the shear displacement are analysed and discussed.

The results show that the influence of especially the density of the buffer and the location of the shear plane are very strong but also that the shear rate and the magnitude of the shear displacement have a significant effect. At the two lower densities an eccentric shear plane is more dangerous but at the two higher densities a centric shear is worst. At the conservative combination of a shear rate of 1 m/s, a shear displacement of 20 cm and the density 2100 kg/m^3 the cast iron insert is strongly affected with maximum plastic strain of 19% but at the reference case with the buffer density 2000 kg/m^3 and the shear displacement 10 cm the plastic strain is reduced to 1.6%.

Sammanfattning

Befintliga sprickor som skär deponeringshål kan aktiveras och skjuvas genom ett jordskalv. Inverkan av en sådan bergskjuvning har undersökts i ett projekt som omfattar både laboratorieförssök och finita element beräkningar.

Bentonitbufferten i ett deponeringshål fungerar som en kudde mellan kapseln och berget, som avsevärt reducerar inverkan av en bergskjuvning. Ju lägre densitet desto mjukare buffert och desto mindre påverkan på kapseln. Vid de höga densiteter som föreslås för bufferten i ett slutförvar är den däremot ganska styv. Styvheten är också en funktion av skjuvhastigheten, vilket medför att kanistern kan skadas avsevärt vid mycket höga skjuvhastigheter.

För att undersöka styvheten och skjuvhållfastheten hos buffertmaterialet har flera serier laboratorieförsök utförts varvid vattenmättade bentonitprover med olika densitet har skjuvats vid olika skjuvhastigheter. Med hjälp av dessa tester har en materialmodell som tar hänsyn till skjuvhastighet och densitet formulerats. Försöken har utförts med skjuvhastigheter upp till 6 m/s.

Bergskjuvningen har modellerats och beräknats med finita-element-koden ABAQUS. Ett tredimensionellt elementnät som modellerar bufferten och kapseln har skapats och ett antal beräkningar som simulerar olika bergskjuvningar har untförts.

Bergskjuvningen antas ske vinkelrätt mot kapselns axel antingen i centrum av deponeringshålet eller i fjärdedelspunkten. Skjuvberäkningen har drivits till en total skjuvning av 20 cm. Bufferten har modellerats vid fyra densiteter mellan 1950 och 2100 kg/m^3 vid vattenmättnad och vid skjuvhastigheter mellan and 0.0001 och 1000 mm/s. Påverkan av buffertens densitet, skjuvplanets placering, skjuvhastigheten och skjuvningens storlek analyseras och diskuteras.

Resultaten visar att inverkan av särskilt buffertens densitet och skjuvplanets läge är stor, men också att skjuvhastigheten och storleken hos skjuvrörelsen har en signifikant påverkan. Vid de två lägre densiteterna är ett excentriskt skjuvplan farligare men vid de två högre densiteterna är en centrisk skjuvning värst. Vid den konservativa kombinationen av skjuvhastigheten 1 m/s, skjuvrörelsen 20 cm och densiteten 2100 kg/m^3 blir järnkapslen starkt påverkad med plastiska töjningar upp till 19% men vid refernsfallet med buffertdensiteten 2000 kg/m^3 och skjuvrörelsen 10 cm reduceras den plastiska töjningen till 1.6%.

Contents

1 Introduction

One important function of the buffer material in a deposition hole in a repository for nuclear waste disposal is to reduce the damage of rock movements on the canister. The worst case of rock movements is probably a very fast shear that takes place along a fracture and occurs as a result of an earthquake.

The consequences of such rock shear has been investigated earlier, both by laboratory tests /1/, laboratory simulations in the scale 1:10 /2/ and finite element modelling /3/ and /4/.

In order to update the results a new investigation has been performed. The changes mainly concern the following items:

- the canister design – a new geometry with a copper/cast iron canister /5/,
- the magnitude of the shear displacement has been driven to 20 cm,
- the bentonite model has been updated for very fast shearing,
- a shear rate up to 1 m/s has been applied.

A number of laboratory tests with very fast shearing have been performed and used as basis for the bentonite model.

2 Earlier investigations

The main investigations concerning rock shear through a deposition hole have been the following:

Model shear tests of a canister in a deposition hole

In this investigation /2/ a laboratory model in the scale 1:10 of a deposition hole with bentonite buffer and a canister was sheared with different shear rates. The canister was made of solid copper and it was surrounded by highly compacted water saturated MX-80 bentonite. Before shearing the swelling pressure was measured by six transducers in order to follow the water uptake process. During shearing pressure, strain, force and deformation were measured in altogether 18 points. The shearing was made at different rates in the various tests.

An extensive sampling after shear was made and the density, water content, degree of saturation, homogenisation and the effect of shear on the bentonite and canister were measured and studied. The results from the shear tests were compared to different calculations. The relevance of the calculations and the need for improved mathematical models could then be studied.

One important conclusion from these tests was that the rate dependence is about 10% increased shear resistance per decade of increased rate of shear. This resulted also in a very clear increase in strain in the canister with increased rate. The results also showed that the saturated bentonite has excellent stress distributing properties. However, the high density of the clay (ρ_m = 2.05 t/m^3) made the bentonite produce such a high swelling pressure that the material was rather stiff resulting in a strong deformation of the canister. Since the canister was made of solid copper, it was deformed more than would be expected from a canister with a cast iron insert.

Finite element calculations for evaluating the material model and investigate the influence of different factors

The model test was simulated in finite element calculations with the purpose to check the reliability of the material models and the calculation technique and to investigate the influence of some factors /3/. A good agreement between calculated and measured results was reached and it was concluded that the elasto-plastic material model was relevant for this type of fast shear. It was also concluded that the buffer was completely plasticized around the influenced parts of the canister and that the influence of buffer thickness was small but the influence of density large.

Finite element calculations for investigating the mechanical interaction between bentonite buffer and the canister in a deposition hole.

The function of the bentonite buffer as a mechanical protection of the canister in a repository was investigated in a number of finite element calculations /4/. Three canister types (KBS3 HIP canister, KBS3 Cu/Fe composite canister and VLH large canister) and two repository concepts (KBS3 and VLH) were compared.

The functions and scenarios were simulated by the finite element code ABAQUS. The bentonite was modelled with the effective stress theory with Porous Elasticity and Drucker Prager Plasticity according to a model derived from laboratory investigations.

The most important results from the calculations were the following:

The water and swelling pressure will close the gap between the copper and the cast iron in the composite canisters except at the edges of the lids when the canister has flat ends.

A rock displacement of 10 cm across the deposition hole will cause some plastic strain in the copper in all concepts and for all canisters investigated but the plastic strain will be small with a maximum of 4% which was achieved at a density higher than intended for actual use in repositories.

Laboratory tests for investigating the influence of shear rate on shear strength

The shear strength of MX-80, which is the main buffer property required for the rock shear calculation, was measured in a number of shear tests with shear rates varying from 0.025 to 25% per hour /1/. These rather slow tests showed that the shear strength increased linearly with shear rate in a double logarithmic scale. The increase was 16% per 10 times increased shear rate.

3 Basic bentonite shear properties

3.1 General

The most important buffer property for modelling the effect of a rock shear is the shear strength of the bentonite. The shear strength and the stress-strain properties of compacted bentonite after complete water saturation have been investigated in a number of different tests. The shear strength is a function of mainly the following factors:

- the swelling pressure, which is a function of the density of the bentonite,
- the rate of shear.

The relation between the density and the swelling pressure is well known from earlier investigations. The influence of shear rate on the shear strength has also been investigated earlier but only for rather slows tests. These tests have been supplemented by very fast tests (see chapter 3.4).

3.2 Material model

Two types of material models have been used in previous calculations. In the first calculations /3/ a total stress model that did not consider the pore water pressure was applied. In the later calculations /4/ the effective stress concept was applied. According to the effective stress concept the effective stress (the total stress minus the pore water pressure) is controlling the stress strain behaviour of a soil. A general experience regarding clays, which also is valid for swelling clays, is that the total stress concept is applicable for fast or undrained conditions while the effective stress is necessary to apply at drained processes that take place over longer times. The difference is mainly that the effective stress theory is required when there is time enough for the pore water to move in the clay and thus change the state of the clay.

The experience from the previous calculations was that the total stress approach, applied for the calculations of the model tests /3/, was well fitted for the fast shear movements used in these tests. The effective stress approach was motivated for the combined slow shear and creep studies made for the full-scale simulations /4/ but was also more complicated and more difficult to run.

Since the aim of this study e.g. is to study the effect of the fastest possible shear the conclusion is that the total stress approach is the best model for these calculations.

3.3 Derived shear strength model

Equations 3-1 to 3-3 are used for defining the shear strength and the influence of density, pressure and rate of shear /6/.

Relation between swelling pressure and void ratio

The relation between swelling pressure and void ratio can be described according to Equation 3-1 (Equation 3-4 in /6/):

$$p = p_0 \left(\frac{e}{e_0} \right)^{\frac{1}{\beta}} \tag{3-1}$$

where

e = void ratio
e_0 = reference void ratio (=1.1)
p = swelling pressure (at e)
p_0 = reference swelling pressure (at e_0) (=1000 kPa)
β = –0.19

e_0, p_0 and β are derived for MX-80.

Relation between shear strength and swelling pressure

The relation between shear strength and swelling pressure can be described according to Equation 3-2 (Equation 3-29 in /6/):

$$q_f = q_{f0} \left(\frac{p}{p_0} \right)^b \tag{3-2}$$

where

q_f = deviator stress at failure at the swelling pressure p
q_{f0} = 500 kPa (deviator stress at failure at the swelling pressure p_0)
p_0 = 1000 kPa
b = 0.77

The parameter values are based on triaxial tests on MX-80 with the very low shear rate $v_s = 5 \cdot 10^{-5}$ mm/s.

Relation between shear strength and shear rate

The relation between shear strength and shear rate can be described according to Equation 3-3 (Equation 3-27 in /6/):

$$q_{fs} = q_{fs0} \left(\frac{v_s}{v_{s0}} \right)^n \tag{3-3}$$

where

v_s = shear rate
v_{s0} = reference shear rate
q_{fs} = deviator stress at failure at the shear rate v_s
q_{fs0} = deviator stress at failure at the reference shear rate v_{s0}
n = 0.065

The values set for Equations 3-1 to 3-3 are evaluated for MX-80 bentonite with distilled water added as saturating water.

Equations 3-1 and 3-2 are well-founded and based on a large number of tests (Figures 3-16 and 3-6 in /6/) while Equation 3-3 originally was based on direct shear tests with rather low shear rate (strain rates γ =0.025–25%/h corresponding to shear rates $v_s = 3.5 \cdot 10^{-5} – 3.5 \cdot 10^{-2}$ mm/s). The new very fast shear tests were made in order to check Equation 3-3 at the very fast shear rates that may take place at an earthquake (see chapter 3-4).

The shear strengths at the shear rates 1 m/s have been used in the calculations for 4 different densities. Table 3-1 shows the data and how it has been derived from Equations 3-1 to 3-3.

Table 3-1 shows that the influence on the shear strength of the density is very strong and also that the expected very high shear rate has an influence with increasing shear strength at increasing density and shear rate. It is thus possible to substitute a change in density with a change in shear rate. E.g. the density 2000 kg/m^3, which is calculated for the shear rate 1 m/s as case 2, can also be evaluated with the results from case 1 corresponding to the shear rate 0.0013 m/s. The recalculation can be done with Equation 3-4, which is a reformulation of Equation 3-3.

$$v_s = v_{s0}\left(\frac{q_{fs}}{q_{fs0}}\right)^{\frac{1}{n}} \tag{3-4}$$

Table 3-2 shows the shear rate that the different calculations correspond to for the different densities (some very high shear rates are excluded).

Table 3-1. Shear strength q_f used in the rock shear calculations.

Calculation case No	ρ_m (kg/m^3)	e	p (kPa)	q_f (kPa) at $v_s = 5 \cdot 10^{-8}$ m/s	q_{fs} (kPa) at v_s = 1 m/s	q_{fs} (kPa) used in the calculations
1	1 950	0.87	3 436	1 294	3 858	3 900
2	2 000	0.78	6 106	2 014	6 006	6 000
3	2 050	0.69	11 642	3 310	9 871	10 000
4	2 100	0.62	20 442	5 106	15 228	15 200

ρ_m = density at saturation
e = void ratio
p = swelling pressure derived from Equation 3-1.
q_f = deviator (Mises) stress at failure derived from Equation 3-2.
q_{fs} = deviator (Mises) stress at failure derived from Equation 3-3.
v_s = shear rate

Table 3-2. Translation of calculation case to shear rate for different densities.

ρ_m kg/m^3	Shear rate m/s Case 1	Case 2	Case 3	Case 4
1 950	1.0	$1.6 \cdot 10^{3}$	-	-
2 000	$1.3 \cdot 10^{-3}$	1.0	$1.4 \cdot 10^{3}$	-
2 050	$4.4 \cdot 10^{-7}$	$7.0 \cdot 10^{-4}$	1.0	$4.4 \cdot 10^{2}$
2 100	$1.0 \cdot 10^{-9}$	$1.6 \cdot 10^{-6}$	$2.3 \cdot 10^{-3}$	1.0

3.4 Laboratory tests

In order to check the shear strengths used for the calculations, a laboratory program with very fast shear tests were planned and carried through.

The shear tests were carried out as one-axial compression tests. The tests used as bases for the shear strengths that were applied in Equation 3-3, were triaxial tests with very low shear rate ($v_s \approx 5 \cdot 10^{-8}$ m/s). In these tests the effective stress equal to the swelling pressure was applied before shearing by applying a cell pressure in the triaxial cell and the pore pressure was kept close to zero. Very fast tests cannot be done with an external pressure in such cells. Instead the effective stress in these tests were attained by the suction or negative pore pressure, which is similar to the swelling pressure when the sample is unconfined and water saturated.

Three different densities (~1860 kg/m^3, ~1960 kg/m^3 and ~2000 kg/m^3) were tested at a large number of tests with shear rates varying from 0.0001 m/s up to 6.0 m/s. All samples were cylinders with the height 40 mm and diameter 20 mm. The following two different techniques were used:

1. A very fast precision compression machine, which also measures deformation and compression force, was used for shear rates between 0.0001 m/s and 0.3 m/s. Figure 3-1 shows a picture of the a sample installed in the compression machine after completed test.

2. In order to reach at least 1 m/s a special machine was built in the form of a fall hammer. Figure 3-2 shows the apparatus. A hammerhead and a weight are fixed to the end of a 2 m long pendulum arm. The sample is placed on a pedestal, which is attached to the frame via a force transducer. By releasing the arm with the hammer from a specified height, the head will ram the sample with a speed that can be calculated. The deformation is measured with a displacement transducer placed close to the sample. The deformation is stopped after about 20 mm shear with a rubber block in order not to damage the transducers. The force and deformation were recorded with an oscilloscope. This device was used to shear samples with a shear rate varying from 1.3 m/s to 6.0 m/s.

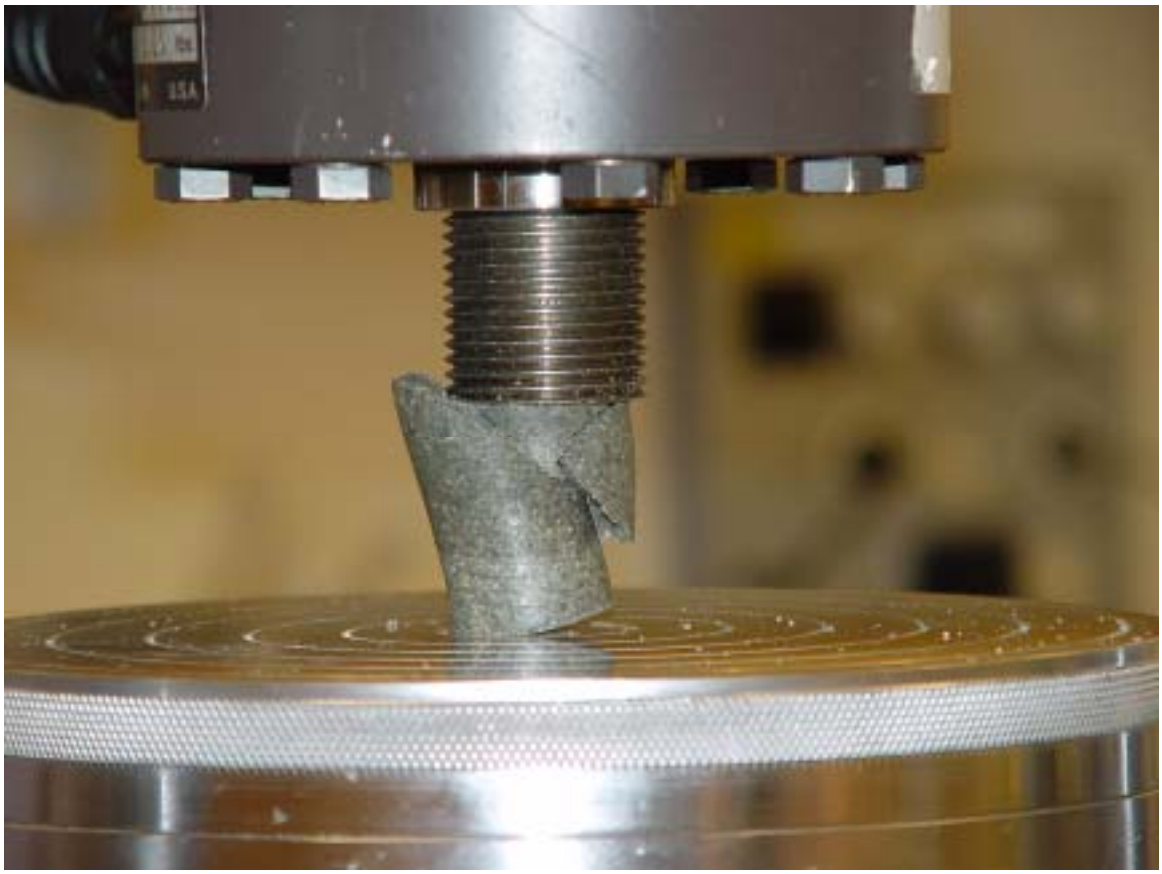

Figure 3-1. *Sheared sample in the compression machine.*

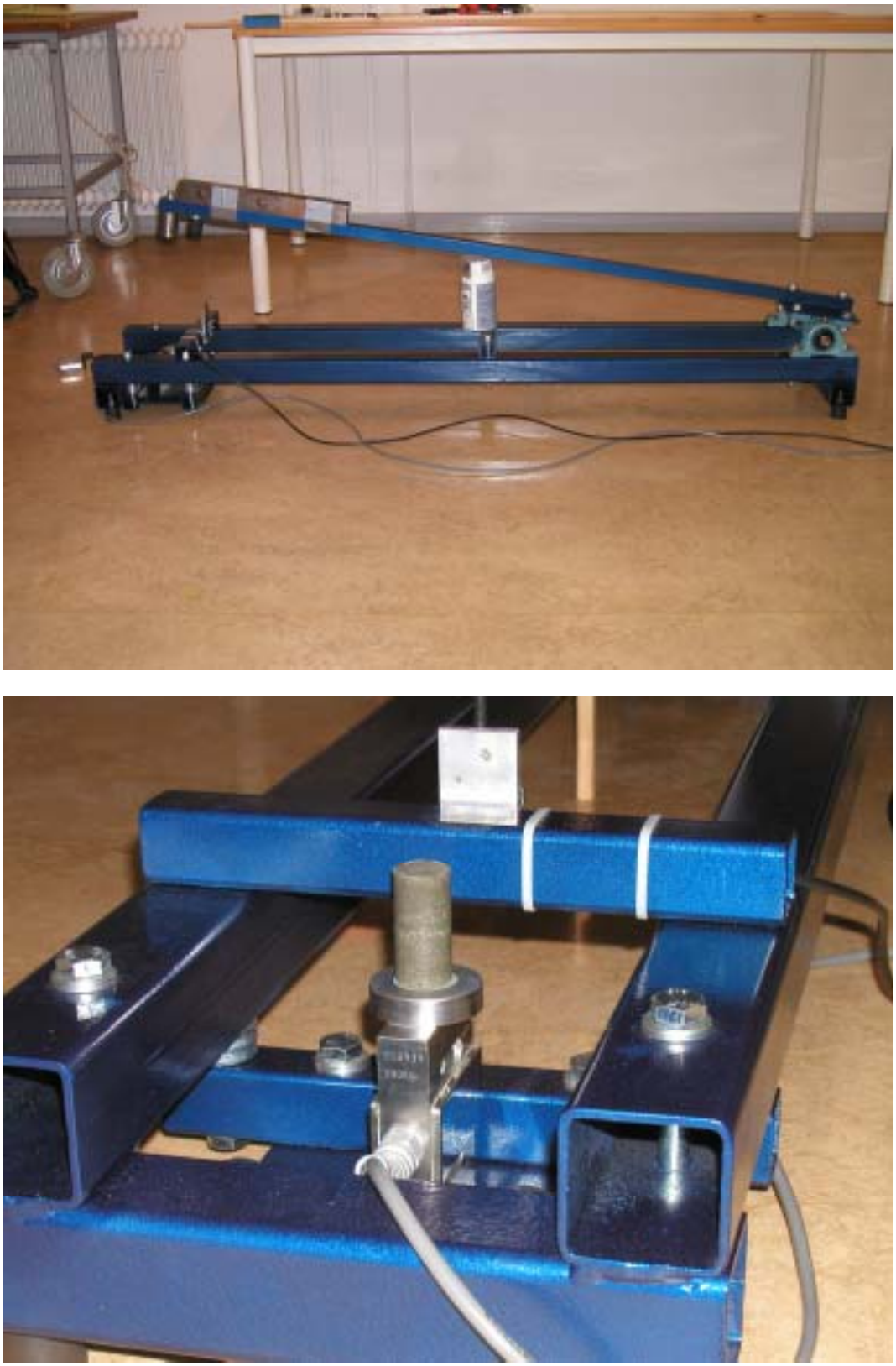

Figure 3-2. *Fall hammer device for shearing samples at very high rates. The upper picture shows the whole device with the pendulum arm attached to the frame (the can is placed on the frame for temporary support of the arm). The lower picture shows the sample placed on the pedestal and the force and displacement transducers.*

Before shearing, the samples were compacted to the intended densities and water saturated in oedemeters in confined conditions by wetting from the end faces of the samples. After completed shearing the density and water ratio of each sample were determined. The deformation and stress were plotted and the shear rate and shear strength evaluated. The shear strength (or actually the deviatoric stress at failure) is evaluated as the maximum force divided by the cross section area of the sample.

Figure 3-3 shows example of measured results from the two techniques. The difference in starting time of the displacement and stress for the test with the fall hammer depends on that the arm hits the displacement transducer before it hits the sample. In this example the shearing thus starts at the deformation 6 mm. Figure 3-4 shows the stress-strain relation with the strain evaluated as the deformation after start shearing divided to the height of the sample.

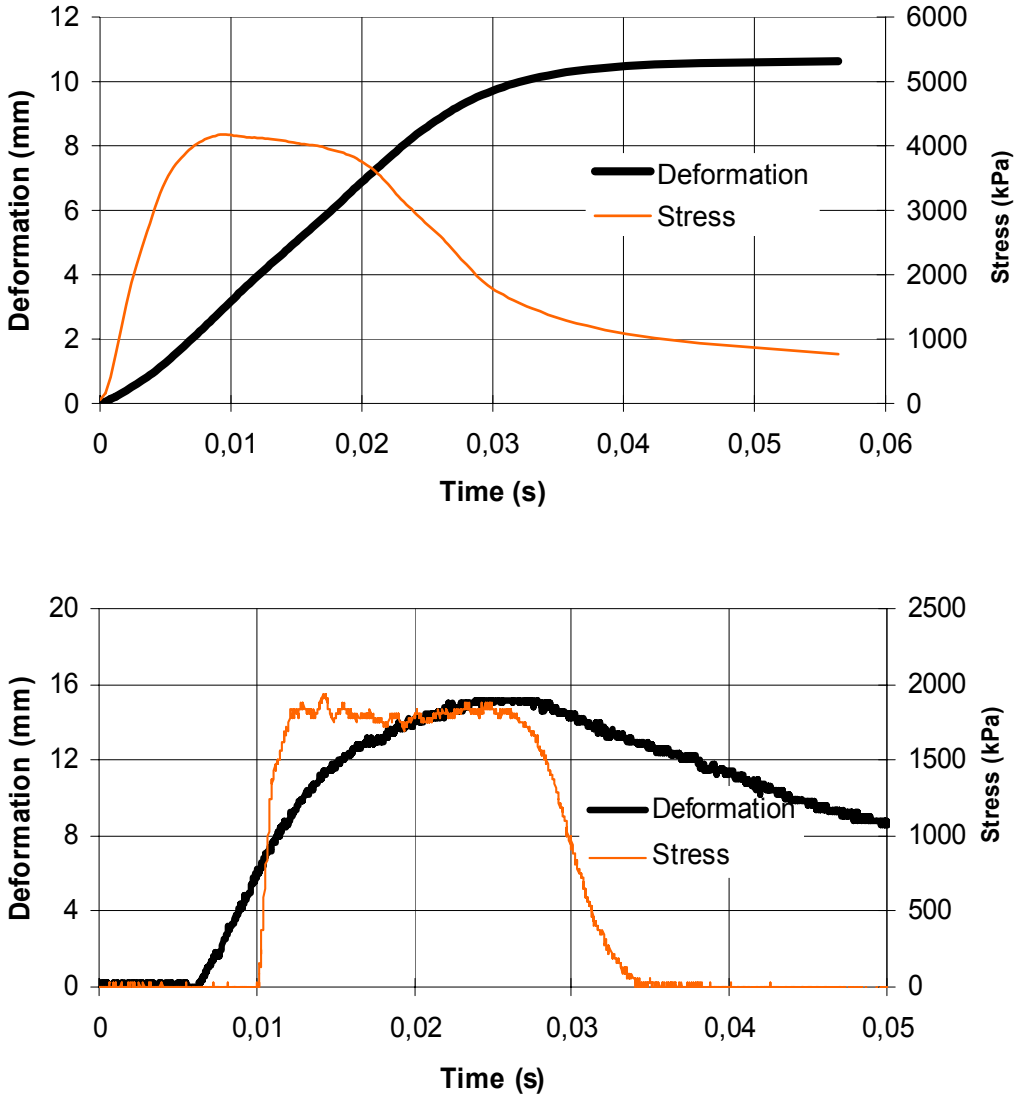

Figure 3-3. *Examples of measured results with the compression machine for test C6 (upper diagram) and with the fall hammer device for test A3 (lower).*

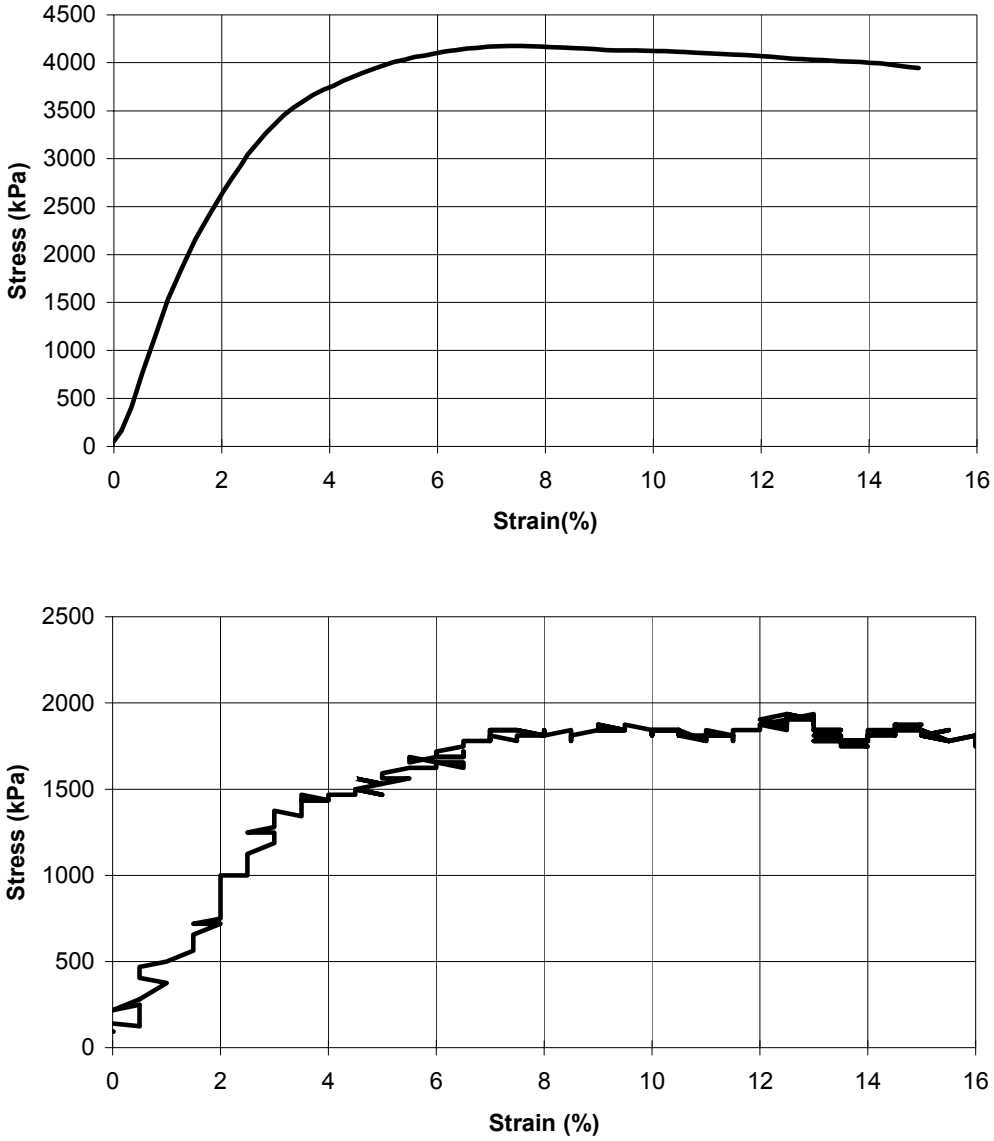

Figure 3-4. *Measured stress plotted as a function of measured strain for the tests in Figure 3-3 with the compression machine for test C6 (upper diagram) and with the fall hammer device for test A3 (lower).*

All test results are compiled in Table 3-3, which shows the water ratio (w) and density measured after the test, the calculated degree of water saturation (S_r) and void ratio (e) and the evaluated deformation rate and maximum deviatoric stress (q).

The results in Table 3-3 are compiled in Figure 3-5, which shows the deviatoric strength as a function of the shear rate. The results are plotted in a double logarithmic diagram that also includes the results from triaxial tests and the relation used for calculating the strength at the shear rate 1 m/s according to Equation 3-3 and Table 3-1. The comparison shows that values used for the shear rate 1 m/s in the modelling are in fair agreement with the measured results at that rate but also that the measured influence of the shear rate from the new tests seems to be lower than predicted by Equation 3-3 with the factor $n = 0.065$. The results should be further analyzed but for the present we merely state that the results confirm the values used for the shear rate 1 m/s rather well.

Table 3-3. Test results.

Test No	*w* (%)	Density (kg/m^3)	S_r	*e*	Def. rate (mm/s)	*q* (kPa)
A1	36.7	1890	1.01	1.01	3561.0	2373
A2	35.1	1872	0.97	1.01	2250.0	2123
A3	35.3	1889	0.99	0.99	1295.0	1936
A4	36.0	1880	0.99	1.01	345.2	1830
A5	35.6	1887	0.99	1.00	309.3	1792
A6	35.2	1890	0.99	0.99	85.4	1770
A7	35.3	1890	0.99	0.99	29.7	1550
A8	34.6	1883	0.97	0.99	10.0	1617
A9	34.4	1880	0.97	0.99	1.0	1524
A10	34.9	1891	0.99	0.98	0.1	1501
B1	29.5	1970	0.99	0.83	5948.0	3747
B2	28.2	1977	0.98	0.80	4847.4	3810
B3	30.3	1964	1.00	0.84	3625.0	3622
B4	28.3	1972	0.97	0.81	2521.0	3435
B5	28.8	1977	0.99	0.81	1808.8	2623
B6	29.6	1963	0.99	0.84	305.4	3163
B7	27.5	1981	0.97	0.79	301.1	3872
B8	28.7	1964	0.97	0.82	86.5	3261
B9	29.2	1945	0.96	0.85	29.1	2856
B10	28.6	1938	0.94	0.85	10.0	2952
B11	29.3	1962	0.98	0.83	3.0	2685
B12	28.8	1952	0.96	0.83	1.0	2791
B13	28.6	1970	0.98	0.81	0.1	2749
C1	27.3	2002	0.99	0.77	3669.7	4559
C2	26.4	1972	0.94	0.78	3412.3	4871
C3	26.0	1994	0.96	0.76	2500.0	4184
C4	27.2	1998	0.98	0.77	2268.5	4559
C5	25.7	2014	0.97	0.73	296.0	4770
C6	27.3	2006	0.99	0.76	312.3	4175
C7	25.1	2010	0.96	0.73	84.5	4794
C8	26.7	2006	0.98	0.76	29.0	3826
C9	25.8	2015	0.98	0.74	9.9	4110
C10	25.8	1999	0.96	0.75	1.0	3868
C11	25.0	2014	0.96	0.73	0.1	3826

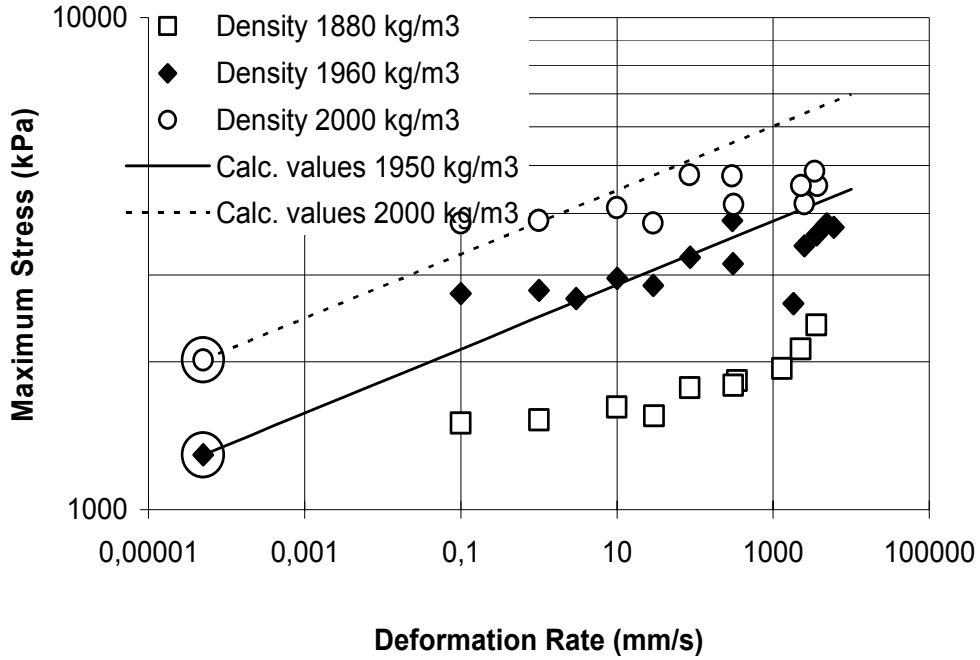

Figure 3-5. *Compilation of the laboratory test results with the maximum deviatoric stress plotted as a function of the shear rate and comparison with the values used for the densities 2000 kg/m^3 and 1950 kg/m^3. The encircled values are the basic results derived from triaxial tests.*

4 FEM model

4.1 General

The finite element code ABAQUS was used for the calculations. ABAQUS contains a capability of modelling a large range of processes in many different materials as well as complicated three-dimensional geometry. The code includes special material models for rock and soil and ability to model geological formations with infinite boundaries and in situ stresses by e.g. the own weight of the medium. Detailed information of the available models, application of the code and the theoretical background is given in the ABAQUS manuals /7/.

4.2 Finite element mesh

The finite element mesh consists of about 500 solid 3D elements. Figure 4-1 shows the entire model of the deposition hole and the three different parts (bentonite buffer, copper canister and cast iron insert). The rock is not modelled but assumed to be completely stiff. The model is symmetric along the axial plane that cuts the deposition hole into two halves. The insert is of the BWR type with 12 channels for fuel assemblies. The shear takes place in a plane perpendicular to the axis of the hole either in the centre or at the ¼ point. The dimensions are the following:

- Deposition hole: diameter 1.75 m and length 6.835 m.
- Copper canister: outer diameter 1.05 m and outer length 4.835 m.
- Copper wall thickness: 0.05 m.
- Cast iron insert: diameter 0.949 m and length 4.733 m.
- Wall thickness between fuel assemblies: 0.05 m.

The 0.5 mm slot between the copper canister and the cast iron insert is thus modelled.

Figure 4-2 shows the cast iron insert cut in the centre. Three elements are shown where results will be given.

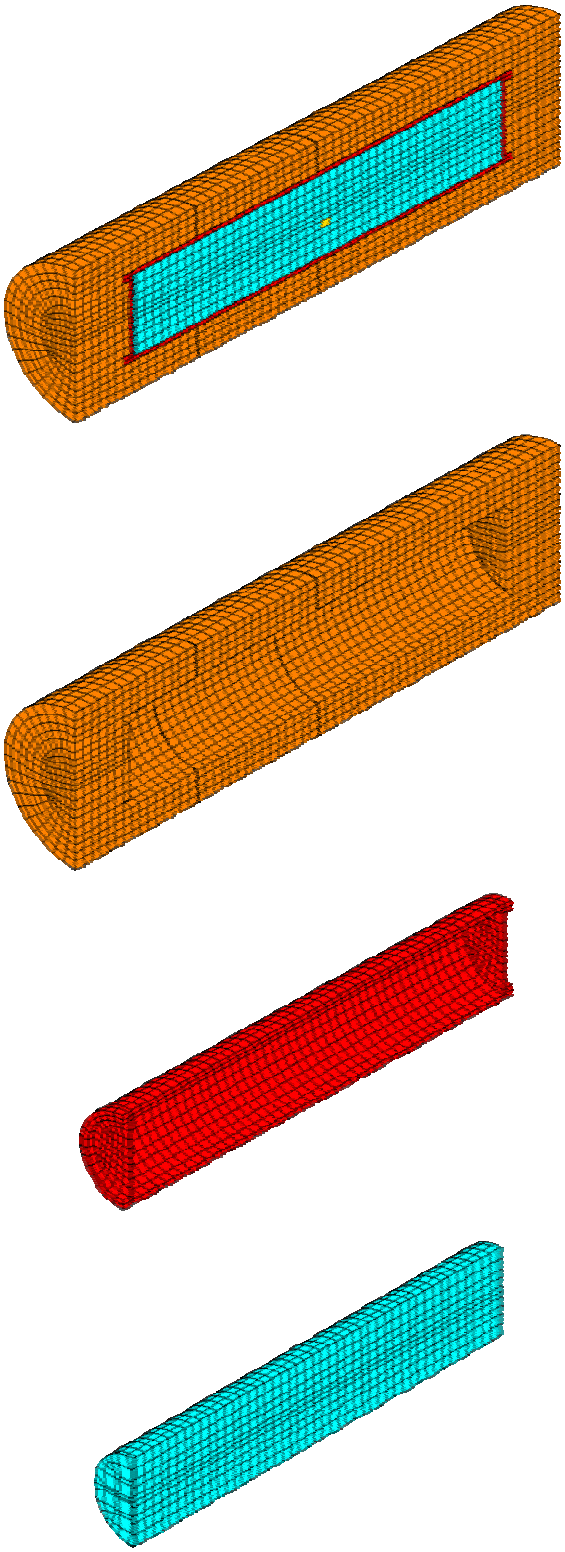

Figure 4-1. *Element mesh (from top to bottom) of the entire model, the bentonite buffer, the copper canister and the cast iron insert. The location of the shear planes are marked in the bentonite*

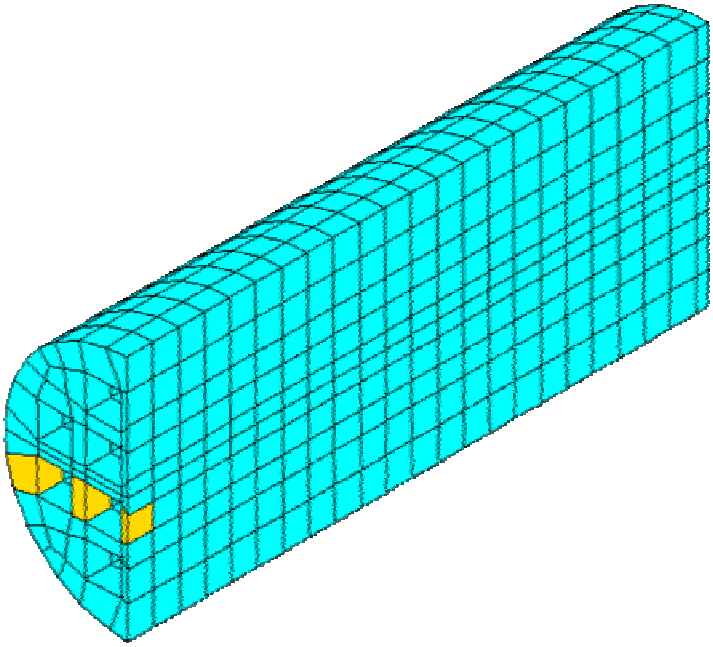

Figure 4-2. *Cross section of the cast iron insert with the elements where some results are presented (in yellow).*

4.3 Material models

Three materials have been modelled. The copper canister and the cast iron insert have properties mainly taken from /5/ and these properties are the same in all calculations. The properties of the bentonite buffer are taken from triaxial, shear tests /6/ and the laboratory tests showed in chapter 3.4. the shear strength varies with density and rate of shear according to Tables 3-1 and 3-2.

Bentonite buffer

The bentonite buffer is modelled using only total stresses that don't include the pore water pressure, the reason being the very fast compression and shear. The stress-strain relation is in ABAQUS described with von Mises stress σ_j that describes the "shear stress" or deviatoric stress in three dimensions according to Equation 4-1.

$$\sigma_j=(((\sigma_1-\sigma_3)^2+(\sigma_1-\sigma_2)^2+(\sigma_2-\sigma_3)^2)/2)^{1/2} \quad (4\text{-}1)$$

where

σ_1, σ_2 and σ_3 are the major principal stresses

The model includes an elastic part and a plastic part. Table 4-1 shows the elastic and plastic data for the four cases.

The relation between Mises stress and engineering strain for all four bentonite cases is shown in Figure 4-3.

Table 4-1. Elastic-plastic material data for the bentonite buffer.

Case No	Elastic part		Plastic part: von Mises stress σ_j (MPa) at the following plastic strains (ε_p)							
	E (MPa)	v	ε_p= 0	ε_p= 0.002	ε_p= 0.005	ε_p= 0.009	ε_p= 0.013	ε_p= 0.018	ε_p= 0.023	ε_p= 1.0
1	225	0.49	2.25	3.0	3.45	3.68	3.83	3.9	3.85	3.85
2	363	0.49	3.63	4.85	5.57	5.95	6.19	6.3	6.22	6.22
3	583	0.49	5.83	7.77	8.93	9.53	9.92	10.1	9.97	9.97
4	865	0.49	8.65	11.54	13.27	14.15	14.73	15.0	14.81	14.81

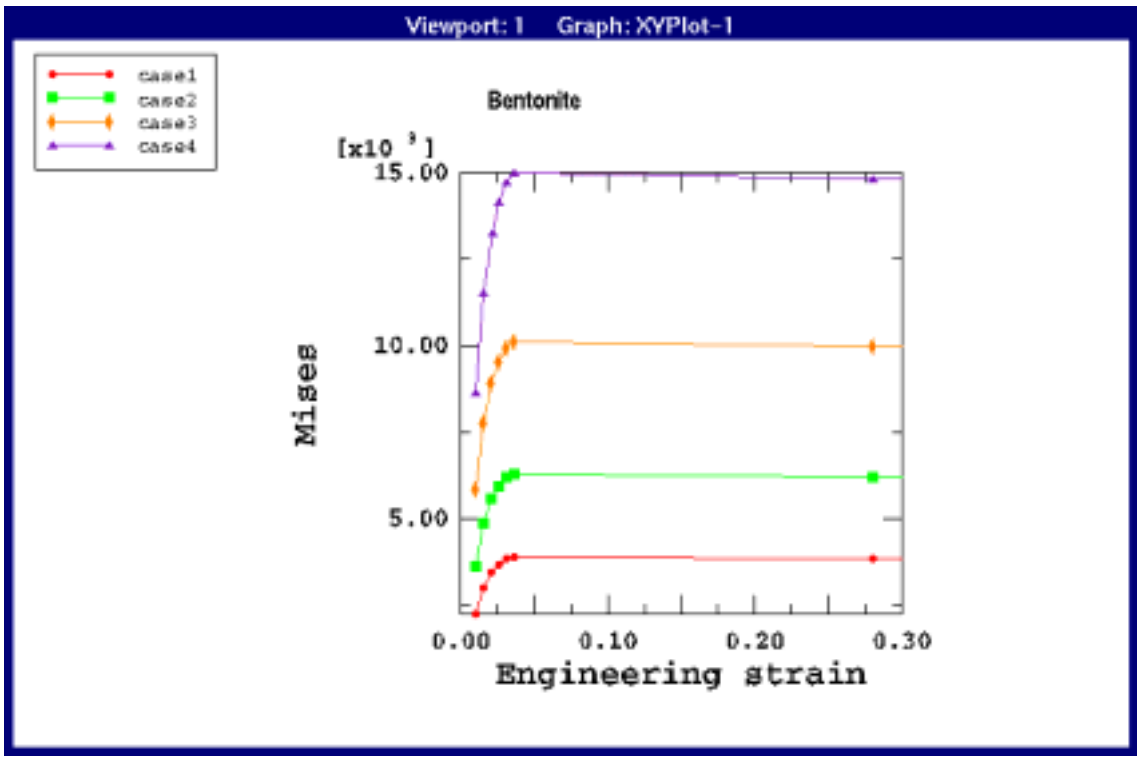

Figure 4-3. *Mises stress (kPa) as function of strain for the four cases of bentonite density and the shear rate 1 m/s.*

Cast iron and copper

The properties of the copper canister and the cast iron insert are also modelled with an elastic plastic model of the Mises stresses. Table 4-2 and Figure 4-4 show the relations.

Table 4-2. Elastic-plastic material data for the copper and cast iron.

Material	Elastic part		Plastic part: von Mises stress σ_j (MPa) at the following plastic strains (ε_p)			
	E (MPa)	v	ε_p= 0	ε_p= 0.2	ε_p= 0.5	ε_p= 1.0
Copper	$1.2 \cdot 10^5$	0.33	50	-	200	200
Cast iron	$1.5 \cdot 10^5$	0.32	260	400	-	400

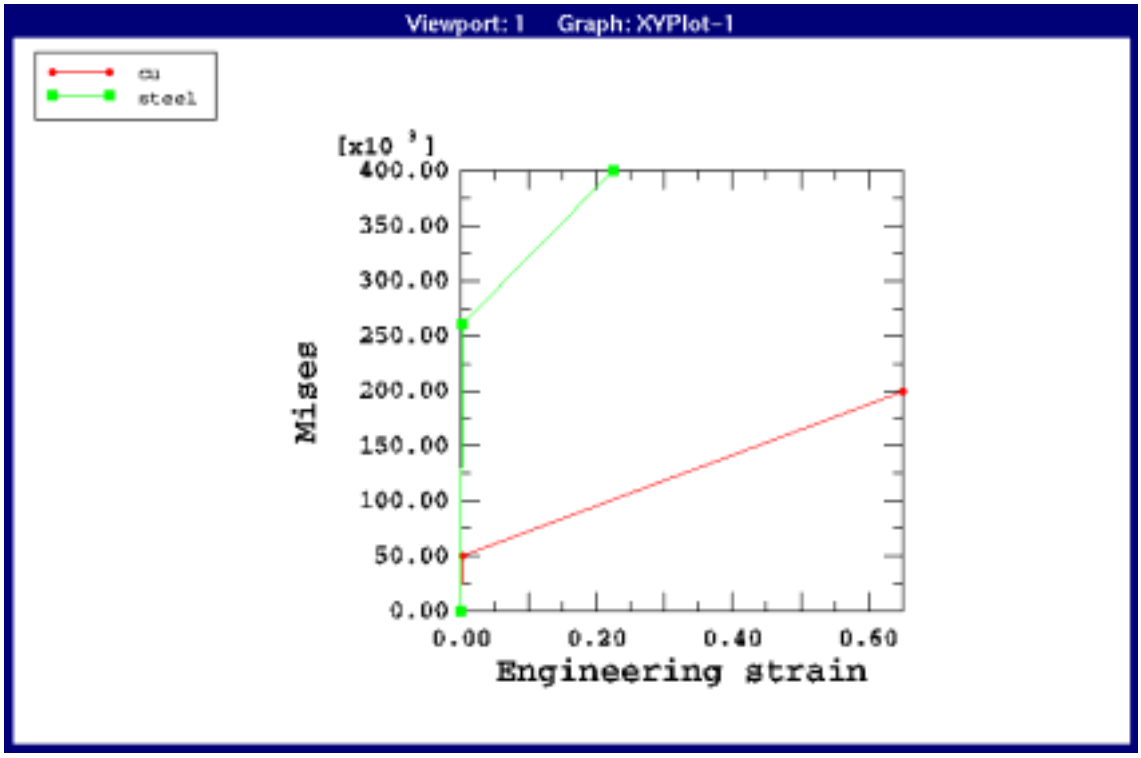

Figure 4-4. *Mises stress (kPa) as function of strain for copper and cast iron.*

4.4 Basic calculations

The calculations have been done in two steps. At first the swelling pressure has been applied, which mainly has resulted in a deformation of the copper canister due to the closure of the 1 mm gap between the copper and cast iron. Then the shear has started and continued until a total shear displacement of 20 cm. The applied swelling pressure does not influence the shear calculation in any other respect than the initial deformation and induced stresses.

Eight calculations have been performed; four with shear in the centre of the deposition hole and four with shear at the ¼ point. The shear planes are illustrated in Figure 4-1.

The calculations are named according to Table 4-3.

Table 4-3. Performed calculations and modelled densities at the shear rate 1 m/s.

Calculation	σ_m (kg/m^3)	Shear location
6b case1	1950	Eccentric
6b case2	2000	Eccentric
6b case3	2050	Eccentric
6b case4	2100	Eccentric
6c case1	1950	Centric
6c case2	2000	Centric
6c case3	2050	Centric
6c case4	2100	Centric

4.5 Additional calculation (*5b3_case2)*

As will be reported in chapter 5 very high tension stresses in the bentonite buffer on the passive side of the canister are achieved. The reason is mainly that the bentonite is modelled to be fixed to the canister by common nodes. In reality the contact can stand very little tension and there will be a gap between the canister and the buffer if high tension is received. In order to investigate the influence of the contact properties an alternative calculation has been performed. In this calculation the canister has been surrounded by contact elements that cannot withstand any tension. These elements will instead separate in the case of tension stresses. In case of compression the element have Mohr-Coloumb friction properties with the friction coefficient 0.1 (friction angle 5.7 degrees). Calculation *6b case2* (eccentric shear and the density 2000 kg/m^3) was repeated with this change (*5b3 case2*).

5 Results

5.1 Introduction

A large amount of results are derived from these 9 calculations. The results will be reported as displaced structures, contour plots of stresses and plastic strain after full shearing and as history plots of stresses and plastic strain in the most affected elements. In chapter 5.2 a number of results for one of the cases will be shown and commented, while the same results from the other cases will be included as appendices. In chapter 5.3 a comparison of the results for some interesting cases will be shown.

5.2 Results from calculation *6b_case2* (asymmetric shear at the density 2000 kg/m^3)

This case is used as reference case since it concerns the reference density after full saturation of the buffer (2000 kg/m^3) and the asymmetric shear case, which yields higher stresses in the canister than the symmetric shear at this density.

Deformed structure

Figure 5-1 shows the deformed structure after complete shearing and a part of the structure divided at the shear plane. A rather strong effect on the canister can be seen already in this figure.

Figure 5-2 shows the deformed copper canister while Figure 5-3 shows the same plot but with a magnification of the displacements with a factor 5 in order to enhance the effect. Figure 5-3 shows also the deformed cast iron insert with the same magnification.

Stresses in the cast iron insert

Figures 5-4, 5-5 and 5-6 show the stress and plastic strain in the cast iron insert. Figure 5-4 shows the plastic strain (PEEQ) on the outside of the cast iron structure. Since the shear plane is located 8 elements (about 0.8 m) from the bottom of the cast iron insert it is obvious that the largest strains are not located at the shear plane but about 1.0 m away towards the centre. Figure 5-5 shows the plastic strain in two cut sections, one with the cut perpendicular to the axis in the most stressed section and one with the cut parallel to the axis with the element boxes uncovered. Figure 5-6 shows plots of Mises stress and plastic strain as function of the rock shear displacement for three elements located in the most stressed section.

The figure reveals that the cast iron insert is deformed substantially and the largest plastic strain is about 4%.

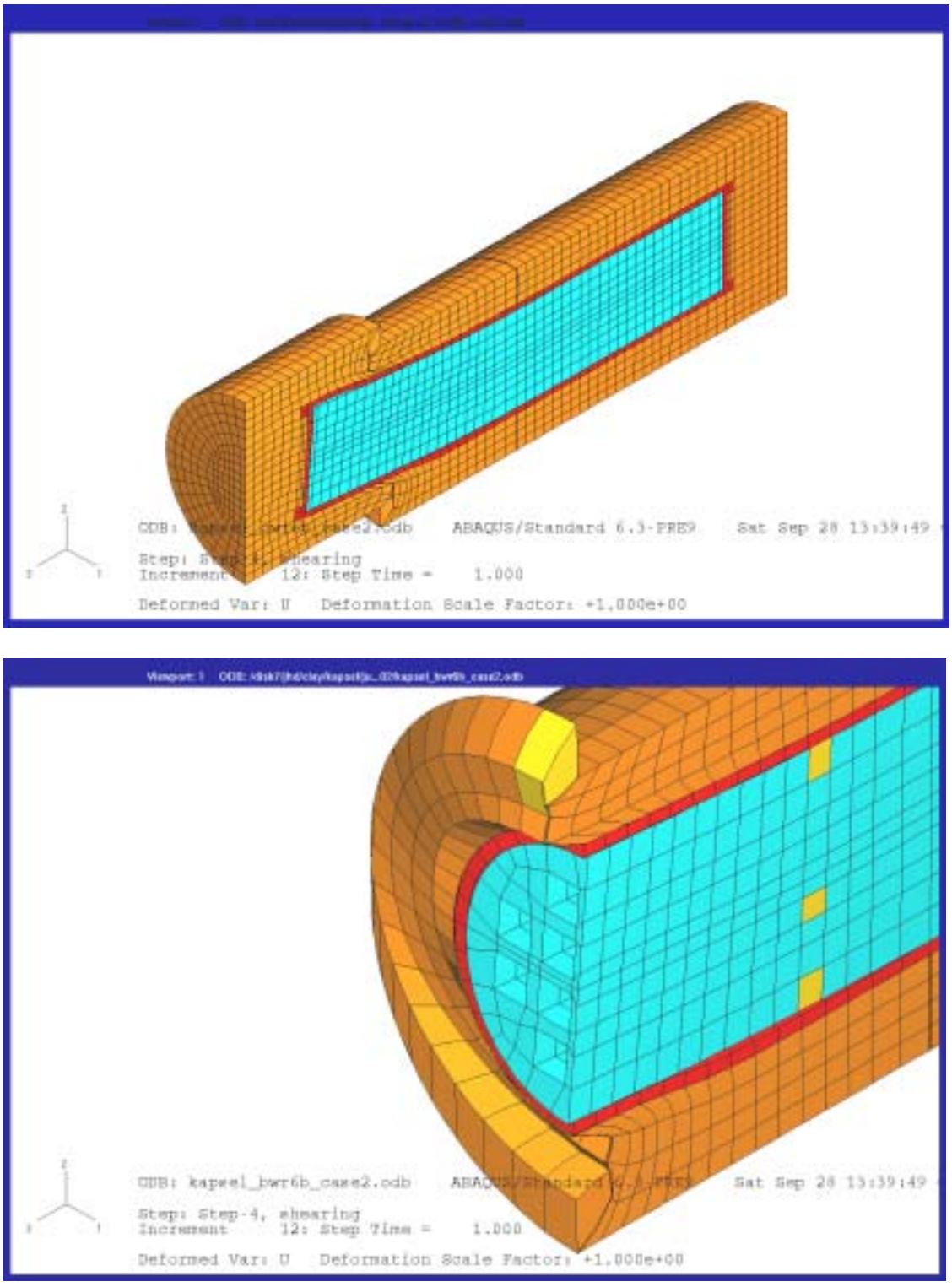

Figure 5-1. *Deformed structure after 20 cm rock displacement (upper) and a detail cut at the shear plane (lower). The three elements in the cast iron insert that are studied in more detail are marked yellow. The numbers are 744 (upper), 735 (central) and 747 (lower).*

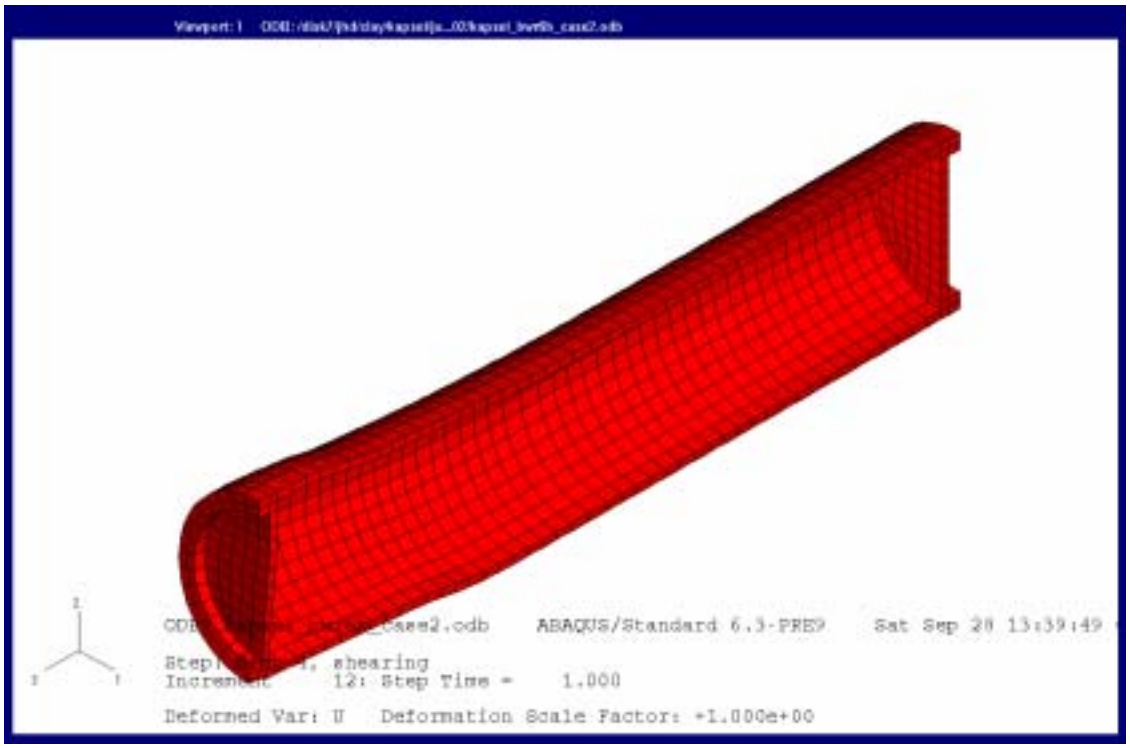

Figure 5-2. Deformed copper canister after 20 cm rock displacement.

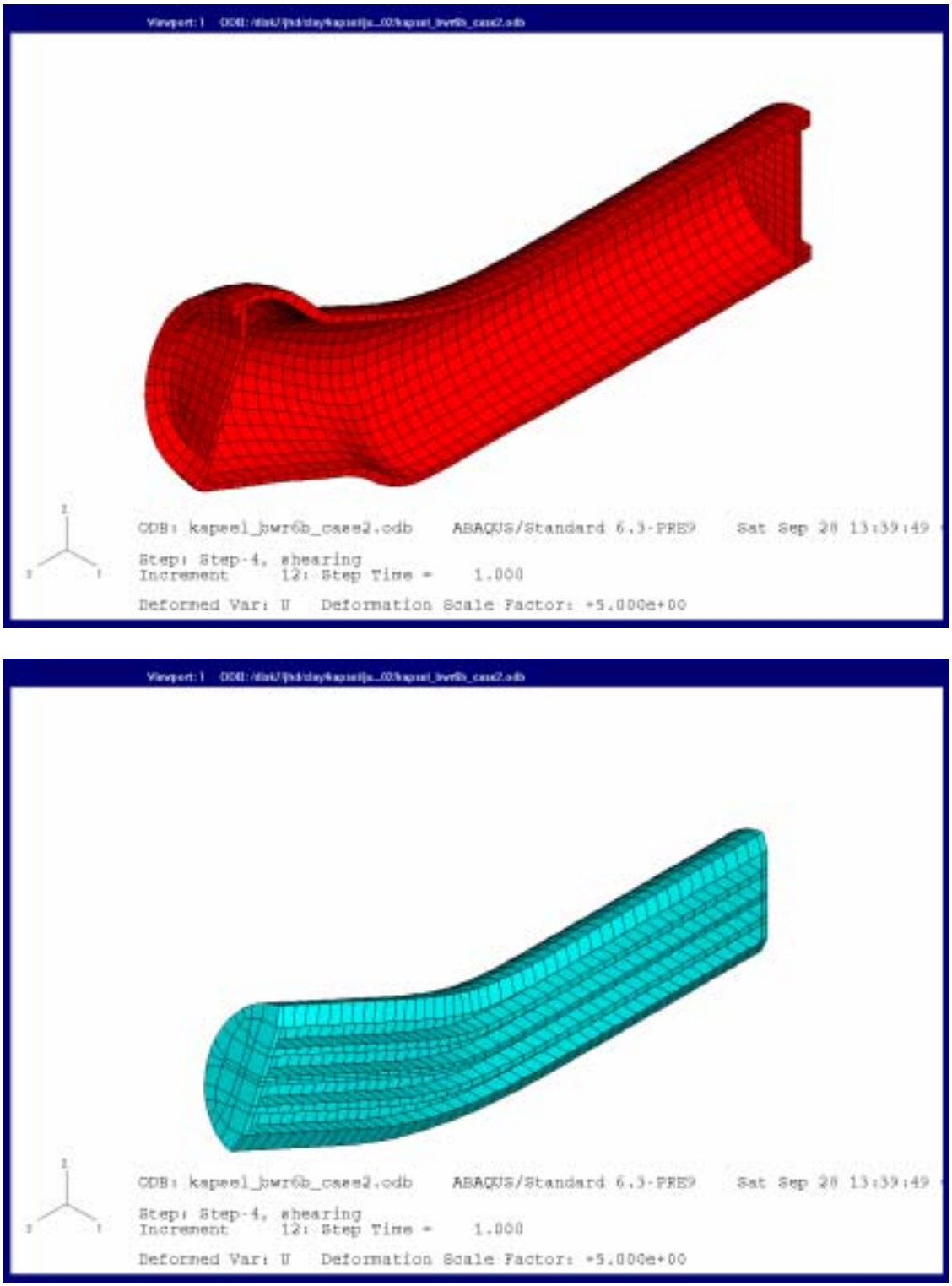

Figure 5-3. *Deformed copper canister (upper) and cast iron insert (lower) after 20 cm rock displacement with a deformation magnification factor of 5.*

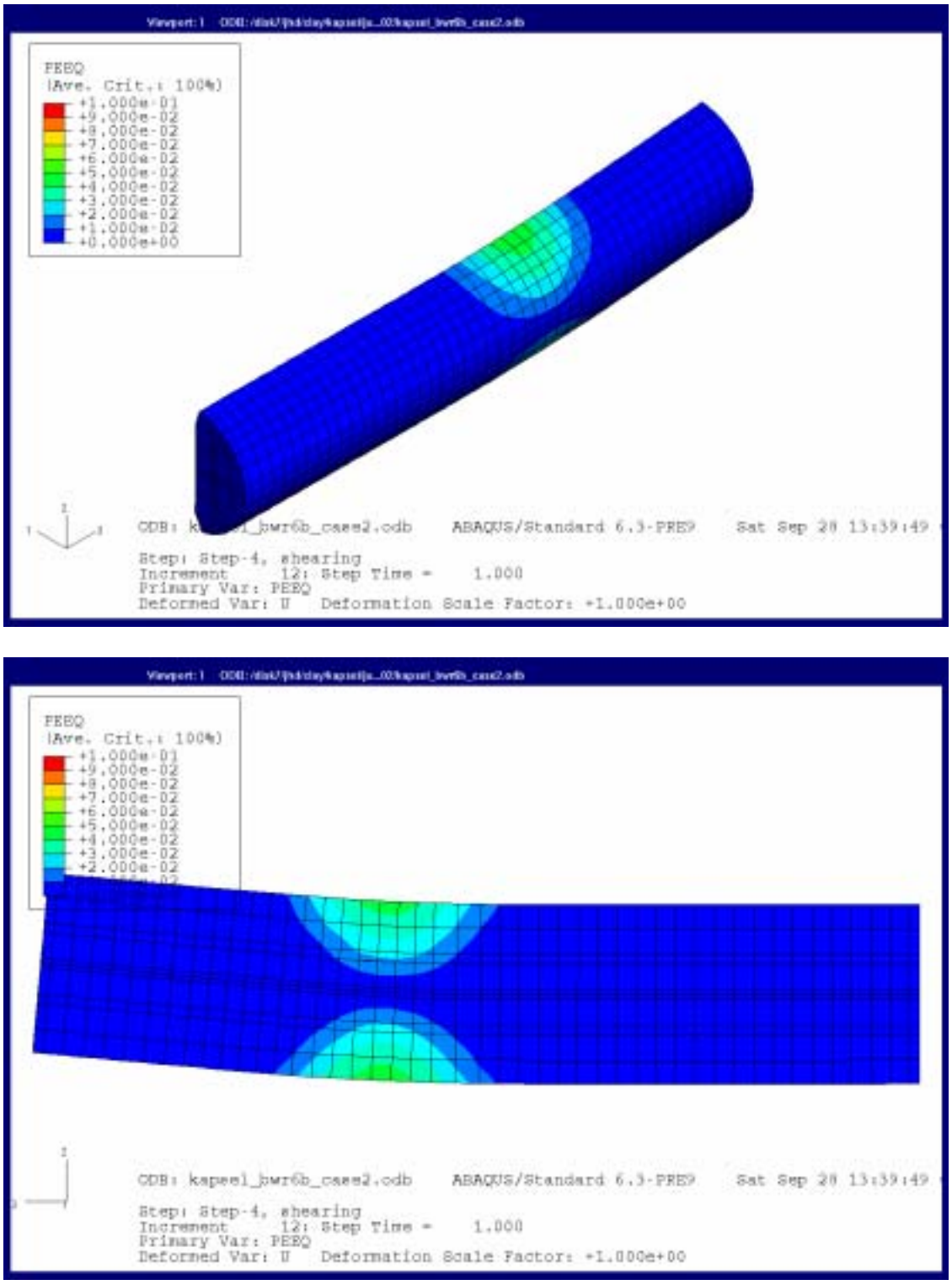

Figure 5-4. *Contour plots of the plastic strain in the cast iron insert seen from "behind" (upper) and straight "from the front" (lower) after 20 cm rock displacement. The shear plane is located 8 elements from the left side in the lower figure.*

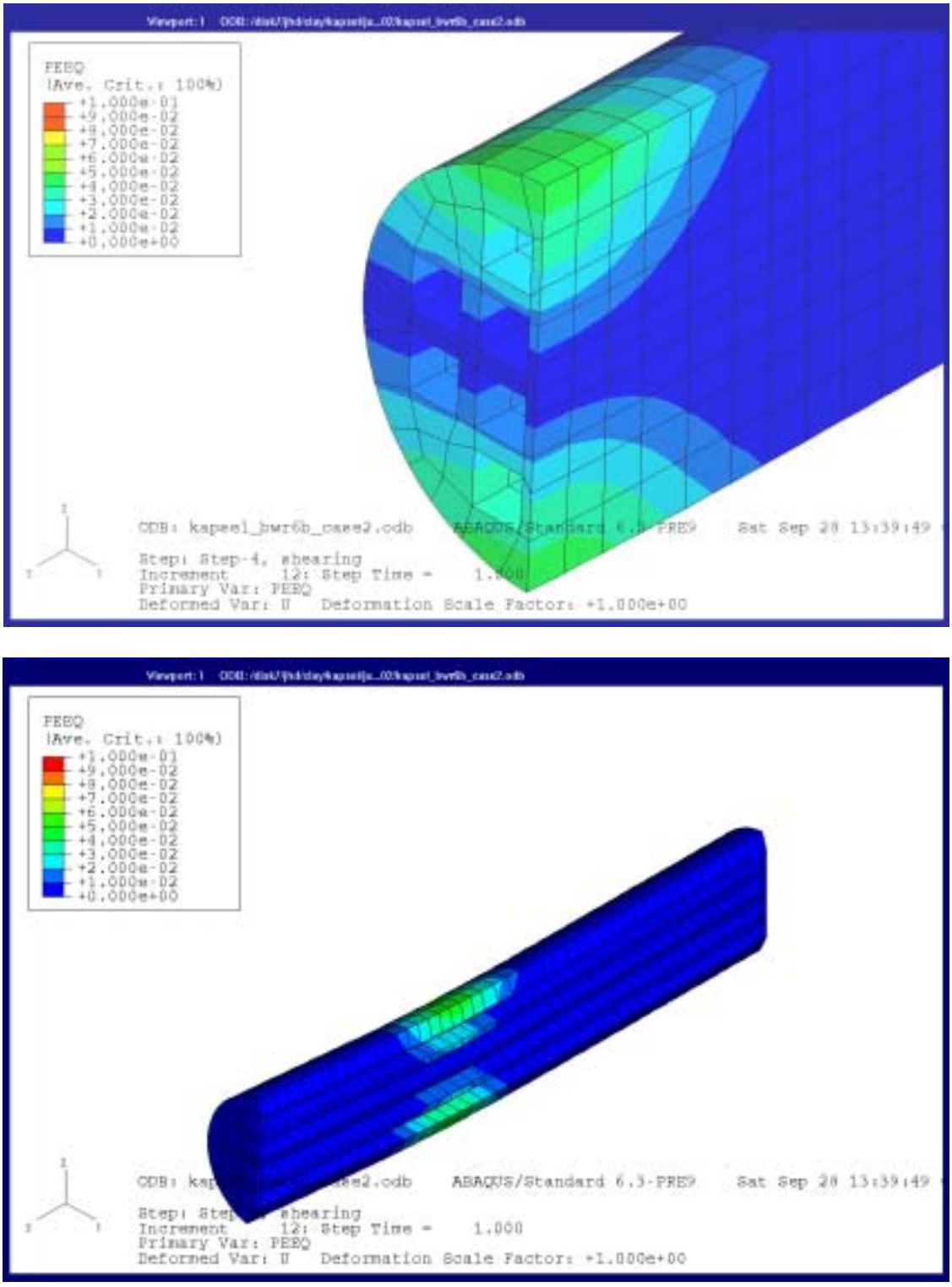

Figure 5-5. *Plastic strain in the cast iron insert after 20 cm rock displacement at a section cut perpendicular to the axis in the most stressed part (upper) and parallel to the axis (lower).*

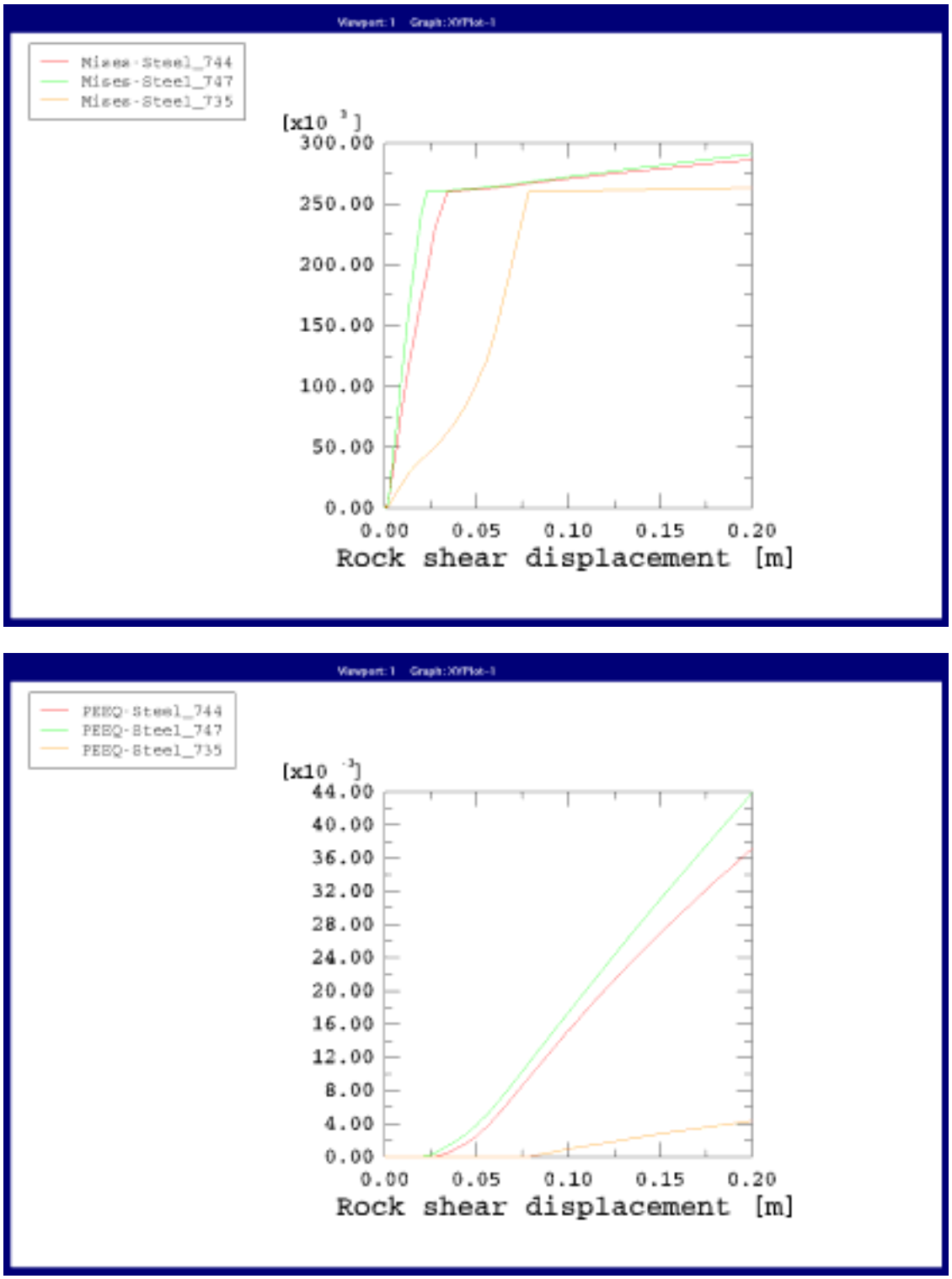

Figure 5-6. *Mises stress (kPa) (upper) and plastic strain (lower) as function of the rock shear displacement (m) for three elements located in the most stressed section. Elements 744 and 747 are located in the upper and lower periphery while element 735 is located in the centre (see Figure 5-1).*

Stresses in the copper canister

Figure 5-7 shows the plastic strain in the copper canister. The maximum plastic strain is about 8% on the canister envelope surface while it is locally much higher at the lid.

Stresses in the bentonite buffer

Figure 5-8 shows the plastic strain and the average stress (pressure) in the bentonite buffer. The figures show that a large part of the buffer is plasticized and that the plastic strain locally is several hundred percent. The buffer is also strongly pressurized on the active side of the canister while there is locally very strong tension on the passive side. The bentonite is modelled to be tied to the canister with no limitations in tension stresses, which may yield that kind of unrealistic results.

5.3 Results from the other basic calculations

The other 7 calculations are reported in Appendix 1–7, with identical figures and numberings as the reference calculation. Observe that the elements used to plot Mises stress and plastic strain as function of the rock shear displacement (in Figures A*X*–6) differ for the different calculations. The location of the elements is shown in Figures A*X*–1.

5.4 Results from additional calculation *5b3_case2* (contact element)

The additional calculation is reported in Appendix 8 for some results that are interesting for evaluating the influence of the contact properties.

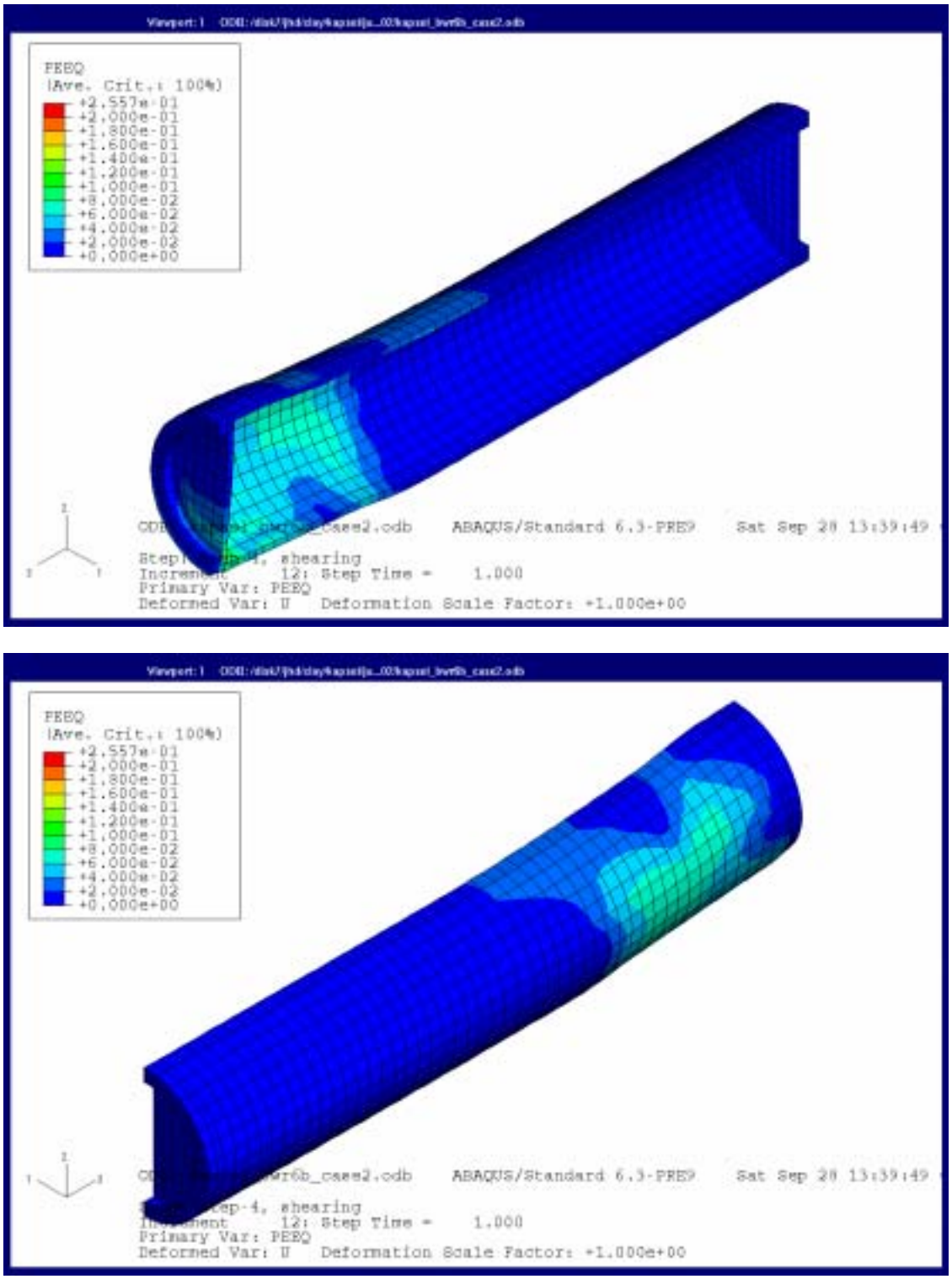

Figure 5-7. *Plastic strain in the copper canister after 20 cm rock displacement.*

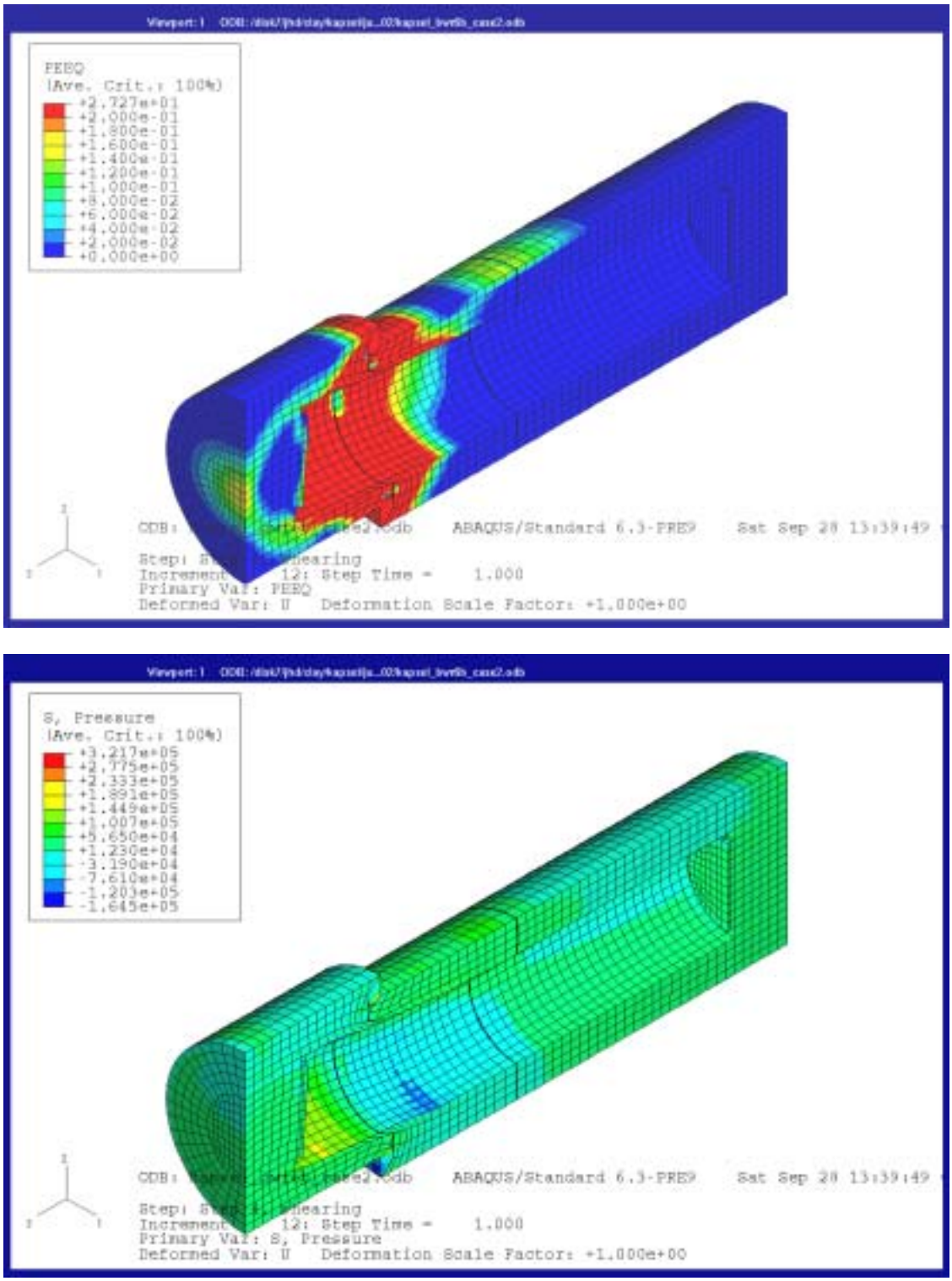

Figure 5-8. *Plastic strain (upper) and average stress (kPa pressure) (lower) in the bentonite buffer after 20 cm rock displacement.*

6 Comparison and evaluation of the results

It is interesting to compare the results from the different calculations in order to find out the influence of different factors. The influence of the bentonite density and the eccentricity of the shear plane, which are the two major differences between the calculation cases, will be analysed. Other interesting influences, which can be derived from the calculations, are the rate of shear and the magnitude of the rock shear displacement.

A summary of the results is given in Table 6-1. The table shows the maximum plastic strain ε_p in the copper tube (excluding the lid), the rock shear displacement δ_p when the plasticization of the cast iron insert starts and the maximum plastic strain ε_p at three different rock shear displacements (5, 10 and 20 cm).

Table 6-1. Calculated maximum plastic strain ε_p in the copper envelope surface and cast iron insert at different rock displacement δ (ec=eccentric shear, c=centric shear, δ_p =start plasticization).

Shear plane location/ Density (kg/m^3)	Copper tube Max ε_p (%)	Cast iron insert δ_p (cm)	ε_p (%) at δ=5 cm	ε_p (%) at δ=10 cm	ε_p (%) at δ=20 cm
ec*/1950	6	3	0.1	0.7	2.7
ec/2000	8	2	0.4	1.6	4.4
ec/2050	15	2	0.8	2.4	6.2
ec/2010	24	2	1.2	4.1	10
c*/1950	4	-	0	0	0
c/2000	6	4	0.01	0.08	0.17
c/2050	16	3	0.5	3.6	11
c/2010	26	2	3	9	19

Influence of bentonite density

As shown in Table 4-1 and Figure 4-3 the stiffness of the buffer is strongly influenced by the density with an increased stiffness of almost a factor 4, at an increased density from 1950 kg/m^3 to 2100 kg/m^3. The strong effect of the buffer density is illustrated by Figures 6-1 to 6-3 and Table 6-1.

Figure 6-1 shows the deformed cast iron insert with plastic zones at different densities after 20 cm centric rock shear at the density 2000 kg/m^3 (6c case1-4). At the two lower densities there is no visible plasticization and the cast iron insert is just tilting, while there are plastic zones with plasticization of more than 10% and the cast iron insert is obviously bent at the higher densities.

The same pattern is noted in Figure 6-2, which shows the deformed copper canister at the same calculations. Since the canister is modelled with a slot between the copper and the cast iron, the copper will be deformed also at the lower densities. The cast iron is needed for supporting the copper.

The influence of the buffer density is also clearly seen in Table 6-1.

It is also interesting to compare the plasticization of the bentonite buffer at the different densities. Figure 6-3 shows that the plasticization is very widespread over a large part of the buffer and almost identical for the two lower densities while it is reduced at the density 2050 kg/m^3 and concentrated to the vicinity of the shear plane at the density 2100 kg/m^3. After a plastic strain of 3–4% the bentonite becomes ideally plastic with no further increase in shear resistance. The canister can thus move rather unhindered at the two lower densities, which explains that the cast iron insert only tilts and does not become bent.

Influence of shear plane location

The influence of the location of the shear plane is a little surprising. Figure 6-4 shows the plastic zones in the cast iron insert after 20 cm rock shear for both the eccentric and centric shear cases at the two lower densities. The centric shear results in no bending or plasticization (see also Figure 6-1) while the eccentric shear results in a plasticization of up to 5%.

The reason for this surprising difference is mainly the difference in plasticization of the bentonite buffer, which in turn depends on the difference in canister length counted from the shear plane. Figure 6-5 shows the plastic zones in the buffer for the two shear cases at the buffer density 2000 kg/m^3. For centric shear the buffer is widely plasticized with more than 4% plastic strain, while for eccentric shear a large part of the buffer along the longer side of the canister is widely unplasticized. It seems as the grip on that side of the canister from the buffer is strong enough to keep that end of the canister fixed in the initial position without tilting, while the canister in the centric shear can tilt. The strains in the canister thus seem to be dependent on the canister length. If the "free" length of the canister measured from the shear plane is long enough no tilting is allowed and the canister will instead be deformed.

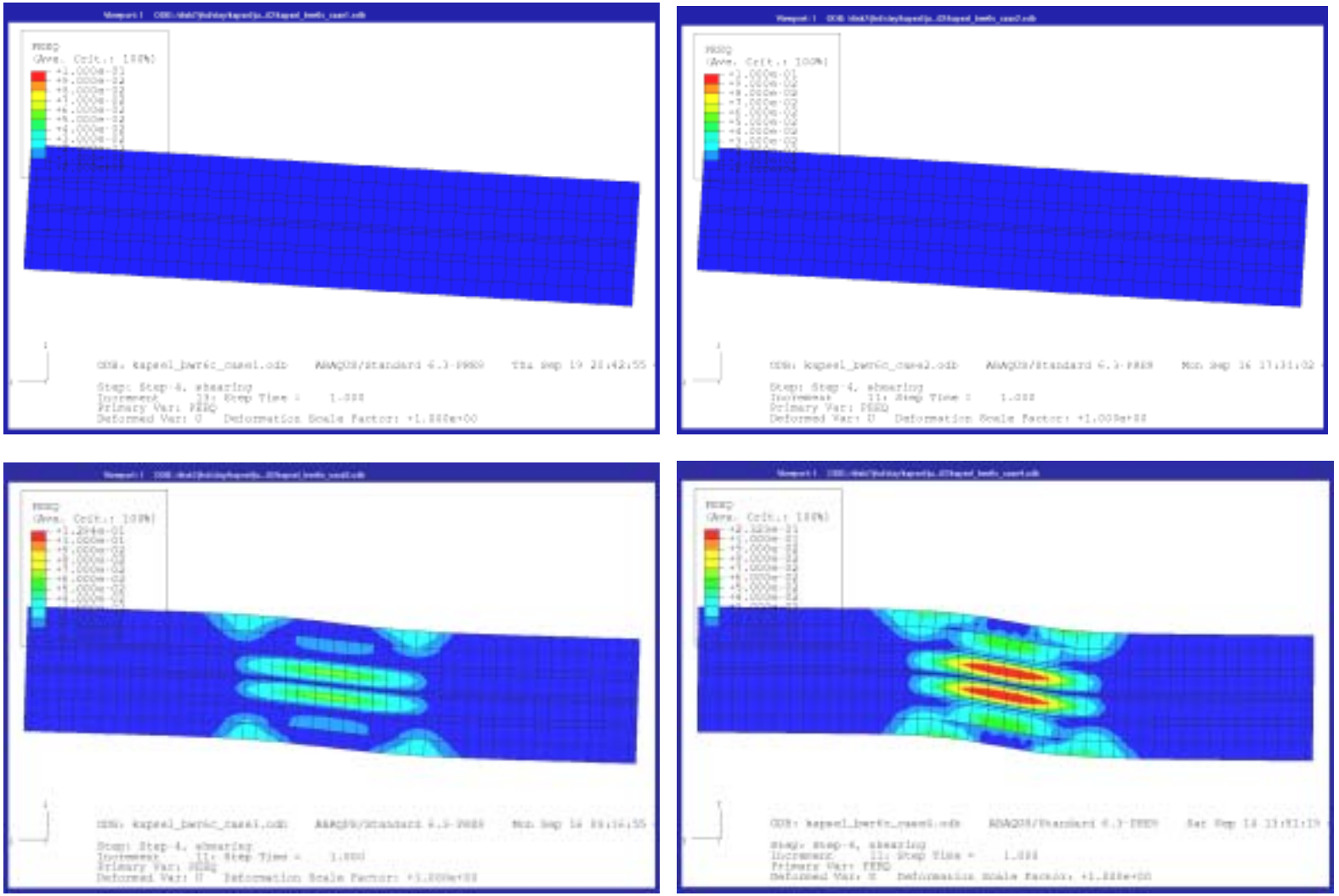

Figure 6-1. *Influence of buffer density. Plastic strain and deformed structure of the cast iron insert after 20 cm centric rock shear. Density 1950 kg/m^3 (upper left), 2000 kg/m^3 (upper right), 2050 kg/m^3 (lower left) and 2100 kg/m^3 (lower right).*

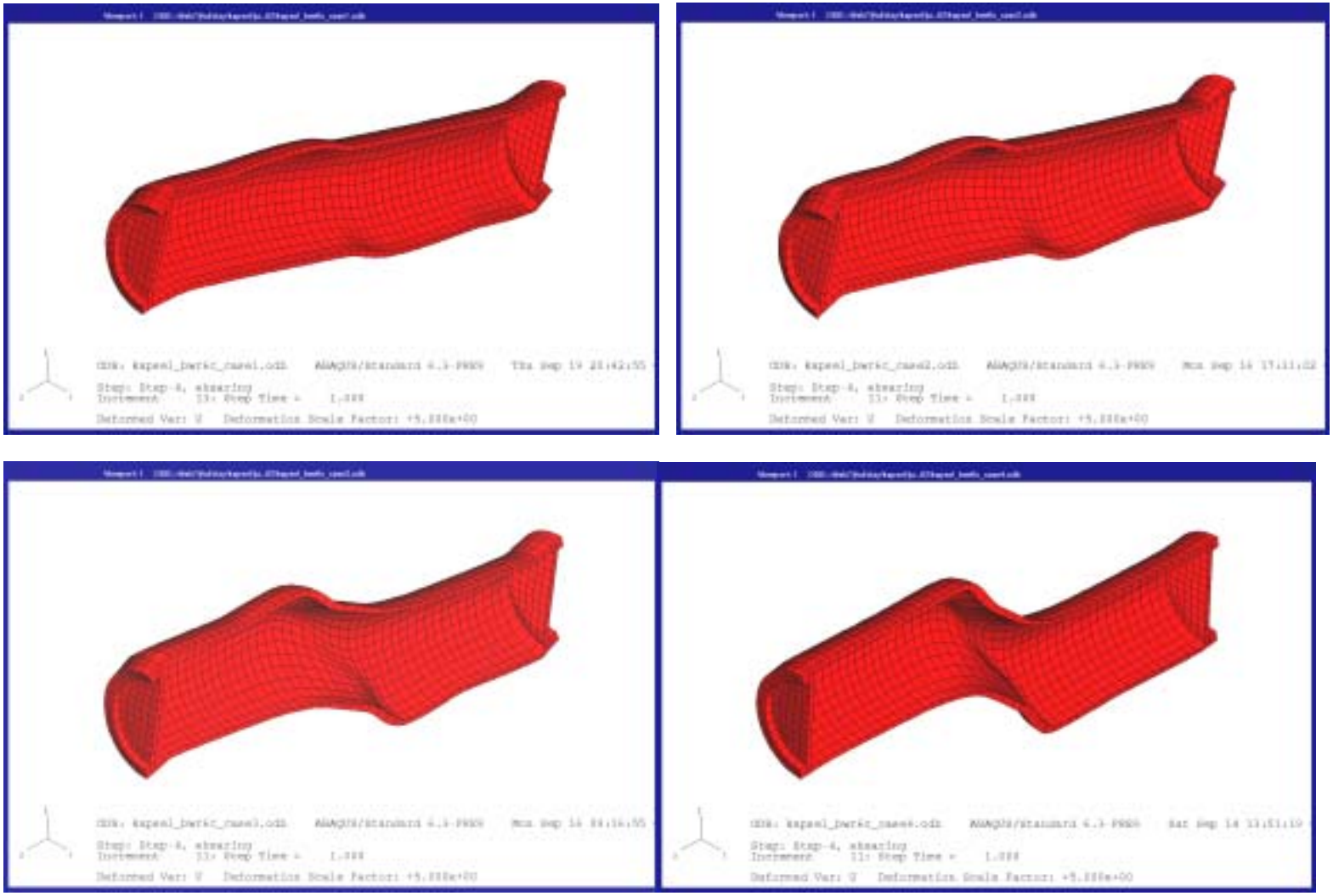

Figure 6-2. *Deformed structure of the copper canister with a deformation magnification factor of 5 after 20 cm centric rock shear. Density 1950 kg/m^3 (upper left), 2000 kg/m^3 (upper right), 2050 kg/m^3 (lower left) and 2100 kg/m^3 (lower right).*

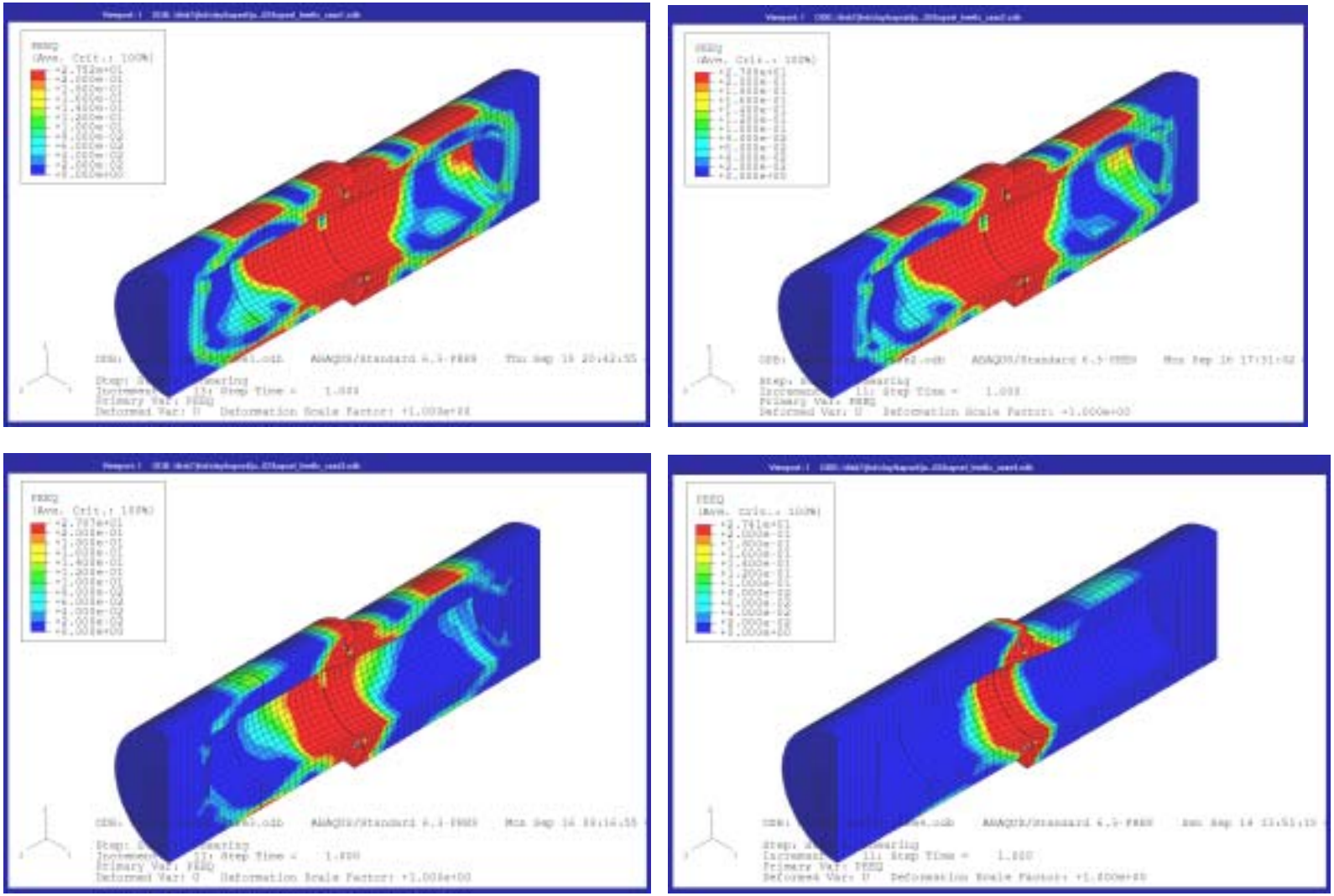

Figure 6-3. *Plastic strain in the bentonite buffer after 20 cm centric rock shear. Density 1950 kg/m^3 (upper left), 2000 kg/m^3 (upper right), 2050 kg/m^3 (lower left) and 2100 kg/m^3 (lower right).*

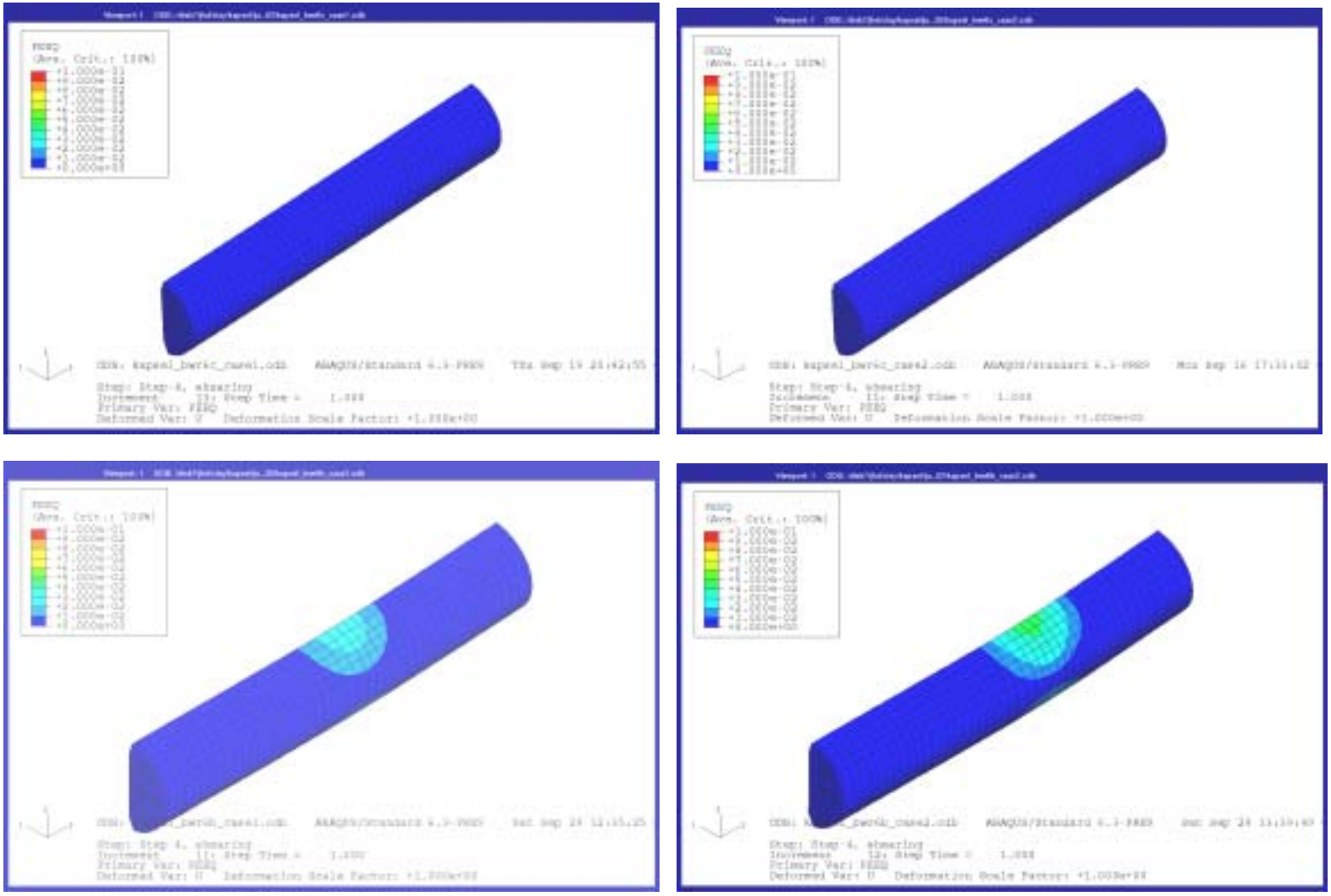

Figure 6-4. *Influence of shear location. Plastic strain and deformed structure of the cast iron insert after 20 cm rock shear. Centric shear at density 1950 kg/m^3 (upper left) and, 2000 kg/m^3 (upper right). Eccentric shear at density 1950 kg/m^3 (lower left) and 2000 kg/m^3 (lower right).*

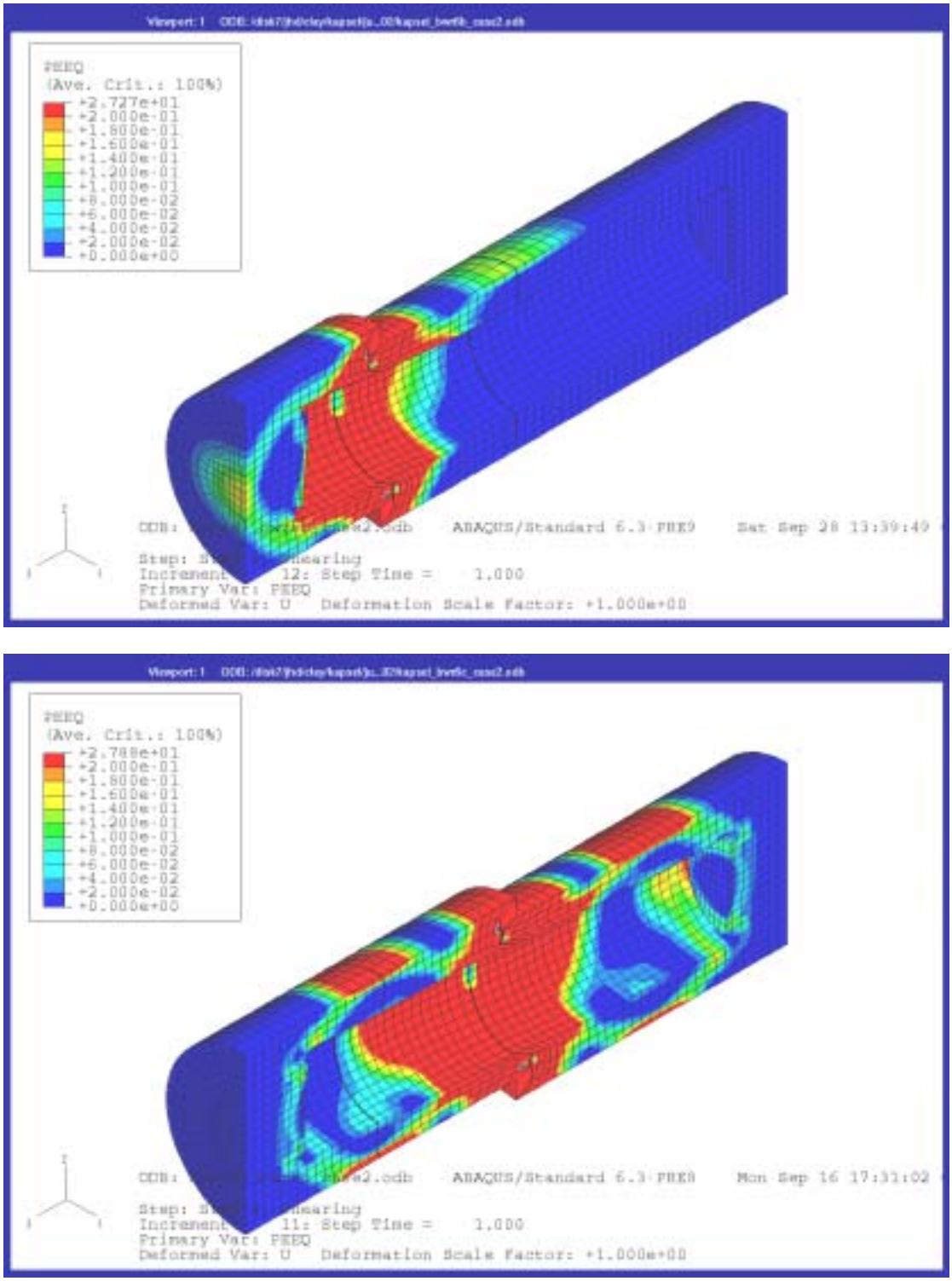

Figure 6-5. *Comparison of plastic zones of the bentonite buffer after 20 cm rock shear at the buffer density 2000 kg/m^3 for eccentric shear (upper) and centric shear (lower).*

It is interesting to note from Table 6-1 that the influence of the shear plane location is very little affecting the plastic strain in the copper canister but strongly the plastic strain in the cast iron insert. The eccentric shear is more serious for the cast iron insert at low densities but the centric shear is more serious at high densities. The reason is thus that at low density a long free length from the shear plane is required to prevent the canister to tilt and this requirement can be fulfilled for one part of the canister at the eccentric shear and not for any part at the centric shear. At high densities, however, the required free length is not so long, which means that both ends of the canister are prevented to tilt at the centric shear, while at the eccentric shear the shorter side of the canister (in relation to the shear plane) will still tilt.

Influence of rate of shear

The influence of the rate of shear is guided by Equation 3-3, which shows that the shear strength increases with a factor proportional to the shear rate raised 0.065. This means that an order of magnitude (factor of 10) increase in shear rate increases the strength with a factor 1.16. This factor can be compared with the influence of an increase in buffer density. In order to reach the same influence on the buffer shear strength as a ten times increase in shear rate the density must be increased with about 15 kg/m^3 or 0.75% (evaluated from Table 3-1). The influence of the shear rate is thus rather small compared to the influence of the density. An increase in density with 0.75% has the same influence on the stresses in the canister as an increase in shear rate with 1000%.

In spite of the low influence it is of vital importance to take the shear rate into account since the very fast rate that is expected at an earthquake is several orders of magnitude higher than the standard shear rates used at soil testing.

The similarity in behaviour allows us thus to play with density and shear rate in order to evaluate other combinations as shown in Table 3-2. For example: A centric shear at the density 2050 kg/m^3, which causes a maximum plasticization of 11% of the cast iron insert at the shear rate 1 m/s and shear displacement 20 cm (case 6b3), will hardly cause any plasticization if the shear rate is 0.7 mm/s, since this corresponds to case 6b2.

Influence of the magnitude of the rock shear displacement

For most cases the plastic strain in the cast iron insert is strongly affected by the magnitude of the shear displacement. This is clearly shown by Table 6-1, where the maximum plastic strain is given for different rock shear displacements. The only cases, where the magnitude of the shear displacement is unessential, are centric shear at the densities 1950 kg/m^{3}and 2000 kg/m^3, where there is practically no plasticization at all of the cast iron. The reason is, as mentioned earlier, that the bentonite buffer is largely plasticized at an early stage, which means that the canister can tilt and be displaced without further increase in shear resistance.

Influence of the properties of the canister/bentonite contact

Calculation *5b3 case2*, which has a contact element with no tension strength between the canister and the bentonite buffer, can be compared to the identical calculation *6b case2*, which has fixed contact. Figure 6-6 shows the plastic strain in the cast iron insert after 20 cm shear displacement for both cases. The figure clearly shows that the difference is small. The plastic strain is slightly smaller when the contact element is included. In Figure 6-7 the average stress in the buffer in the two calculations is compared. As expected all tension stresses noted in the basic case has disappeared when the contact elements are included.

The largest effect of the contact element is seen in the copper canister. In the calculation with the contact element the maximum plastic strain in the envelop surface is not more than in the cast iron insert i.e. about 3% while in the calculation without contact element the maximum plastic strain is almost 8%. The reason is that the copper is directly affected by tension stresses in the contact between the copper and the buffer while the 0.5 mm gap between the cast iron insert and the copper tube prevents those stresses from reaching the cast iron insert in the same way as the contact element functions for the copper tube. As s can be seen in Figure A8-1 in Appendix 8 a gap is formed between the copper tube and the bentonite on the passive sides of the canister.

Thus a contact element with no tension strength affects the stresses in the cast iron insert very little since there is a gap between the cast iron insert and the copper tube that is included in the model.

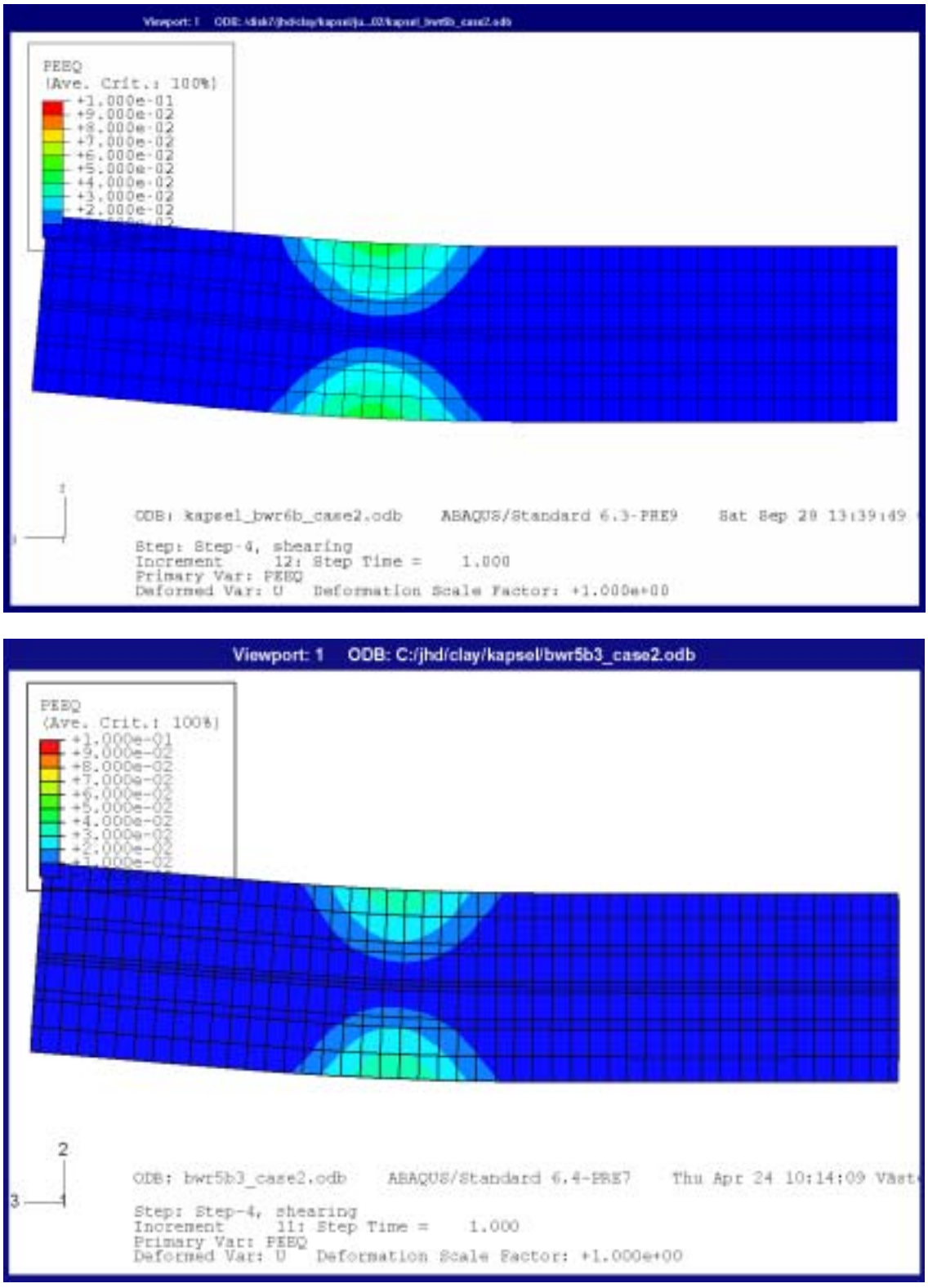

Figure 6-6. *Comparison of plastic strain in the cast iron insert when the contact between the canister and the bentonite buffer is fixed (upper) and released (lower) for eccentric shear at the density 2000 kg/m^3.*

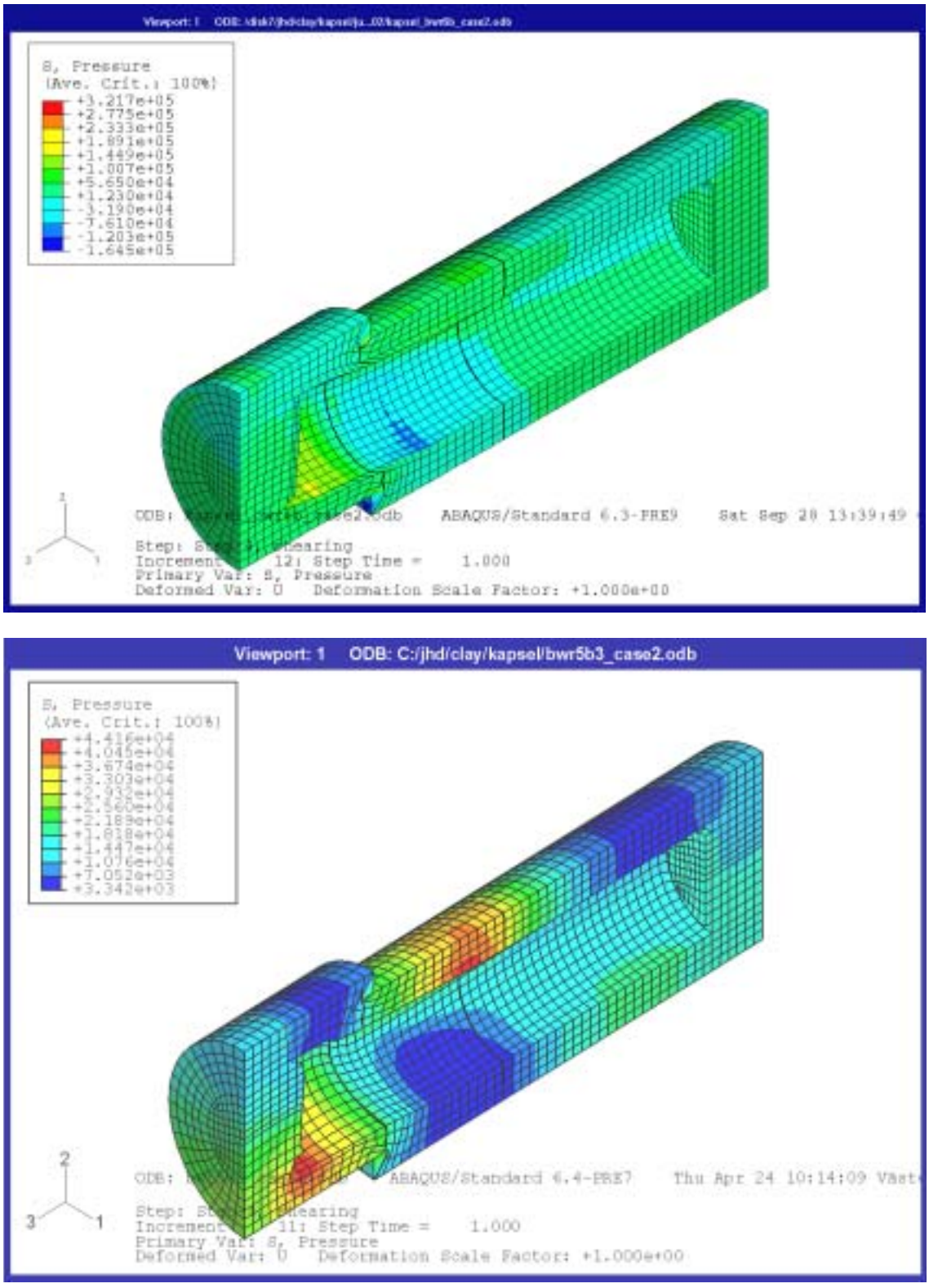

Figure 6-7. *Comparison of average stress (kPa) in the bentonite beuffer when the contact between the canister and the bentonite buffer is fixed (upper) and released (lower) for eccentric shear at the density 2000 kg/m^3.*

7 Conclusions

The effect of an earthquake induced rock shear through a deposition hole has been investigated by nine finite element calculations. The influence of bentonite buffer density, shear rate, shear displacement magnitude and shear plane location has been investigated. The influence of the properties of the contact between canister and buffer has also been checked. The following conclusions were drawn:

The *influence of shear rate* on the bentonite properties was investigated by very fast laboratory shear tests. These tests confirmed the values of the shear strength at the shear rate 1 m/s for some of the densities. The values were originally derived from very slow triaxial test results that were extrapolated with the assumption that the shear strength increases with shear rate in a logarithmic way according to Equation 3-3. The increase is in average a factor of 1.16 at every 10 times increase in shear rate.

The influence of the bentonite buffer density is much stronger and in order to reach the same influence on the buffer shear strength as a ten times increase in shear rate the density must be increased with about 15 kg/m^3 or 0.75%.

The calculations were done with an assumed shear rate of 1.0 m/s at the buffer densities 1950, 2000, 2050 and 2100 kg/m^3. At the *reference case* (density 2000 kg/m^3 and eccentric shear) the plastic strain in the cast iron insert starts after 2 cm shear and increases to 4.4% plastic strain after 20 cm shear displacement. The corresponding maximum plastic strain in the copper is about 8% on the canister envelope surface while it is locally much higher at the lid.

The *influence of buffer density* is very strong and an increase in density from the reference case (eccentric shear) 2000 kg/m^3 to 2100 kg/m^3 yields an increase in plastic strain after 20 cm displacement to from 4.4% to 10%, while a reduction in density to 1950 yields a reduction in plastic strain to 2.7%.

There is also a surprisingly strong *influence of the shear plane location*. For centric shear at the buffer densities 1950 and 2000 kg/m^3 there is practically no plasticization of the cast iron insert, while at the higher densities 2050 and 2100 kg/m^3 the plastic strain is 11% and 19% respectively. The influence of buffer density is thus much stronger at centric shear than at eccentric shear. The reason is judged to be that at low density a long part of the canister is needed for keeping it in a firm grip strong enough to prevent tilting, which means that one side of the canister is prevented from tilting at the eccentric shear while the whole canister tilts at centric shear. The reverse is the case at high density where the length of the canister is enough to keep both ends in a firm grip at centric shear and prevent both end from tilting, while the shorter part of the canister still can tilt at the eccentric shear.

The *influence of the magnitude of the shear displacement* logically seems to be rather strong when the canister is prevented from tilting with a plastic strain that usually is more than doubled at an increase in shear displacement from 10 cm to 20 cm. However, when the buffer plasticities at a shear strength that is not high enough to prevent tilting the magnitude of the shear displacement has no effect, since the canister just continues to tilt as in a liquid with high viscousity.

The *copper canister* is strongly plasticized according to these calculations especially at the high densities. In contrast to the cast iron insert the copper is not affected by the shear plane location. However, the copper is strongly influenced by the tension stresses on the passive sides. When a more realistic model with contact elements was used the plasticization of the copper was reduced to the same magnitude as in the cast iron insert for the reference case.

The plastic strain in the cast iron was, in contrary to the copper, not affected by *introducing contact elements* around the copper canister due to the slot between the copper and the cast iron, which has the same effect for the cast iron as the contact elements for the copper.

References

/1/ **Börgesson L, Hökmark H, Karnland O, 1988.** Rheological properties of sodium smectite clay. SKB TR 88-30.

/2/ **Börgesson L, 1986.** Model shear tests of canisters with smectite clay envelopes in deposition holes. SKB TR 86-26.

/3/ **Börgesson L, 1988.** Modelling of buffer material behaviour. Some examples of material models and performance calculations. SKB TR 88-29.

/4/ **Börgesson L, 1992.** Interaction between rock, bentonite buffer and canister. FEM calculations of some mechanical effects on the canister in different disposal concepts. SKB TR 92-30.

/5/ **Andersson C-G, 2002.** Development of fabrication technology for copper canisters with cast inserts. Status report in August 2001. SKB TR-02-07.

/6/ **Börgesson L, Johannesson L-E, Sandén T, Hernelind J, 1995.** Modelling of the physical behaviour of water saturated clay barriers. Laboratory tests, material models and finite element application. SKB TR-95-20.

/7/ **ABAQUS Manuals.** ABAQUS Inc.

Appendix 1

Calculation *6b_case1*
Asymmetric shear at the buffer density 1950 kg/m^3

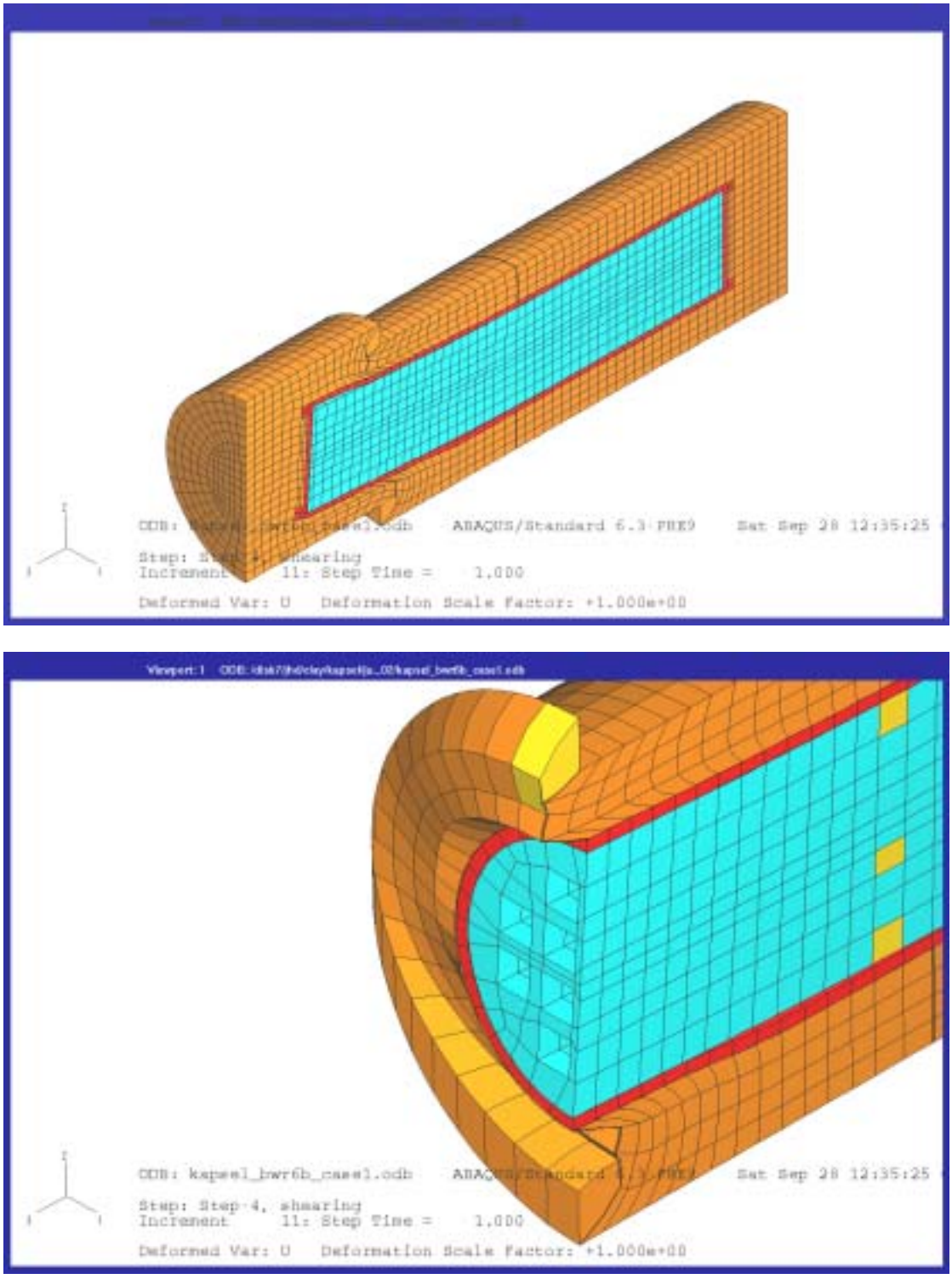

Figure A1-1. *Deformed structure after 20 cm rock displacement (upper) and a detail cut at the shear plane (lower). The three elements in the cast iron insert that are studied in more detail are marked yellow. The numbers are 870 (upper), 861 (central) and 873 (lower).*

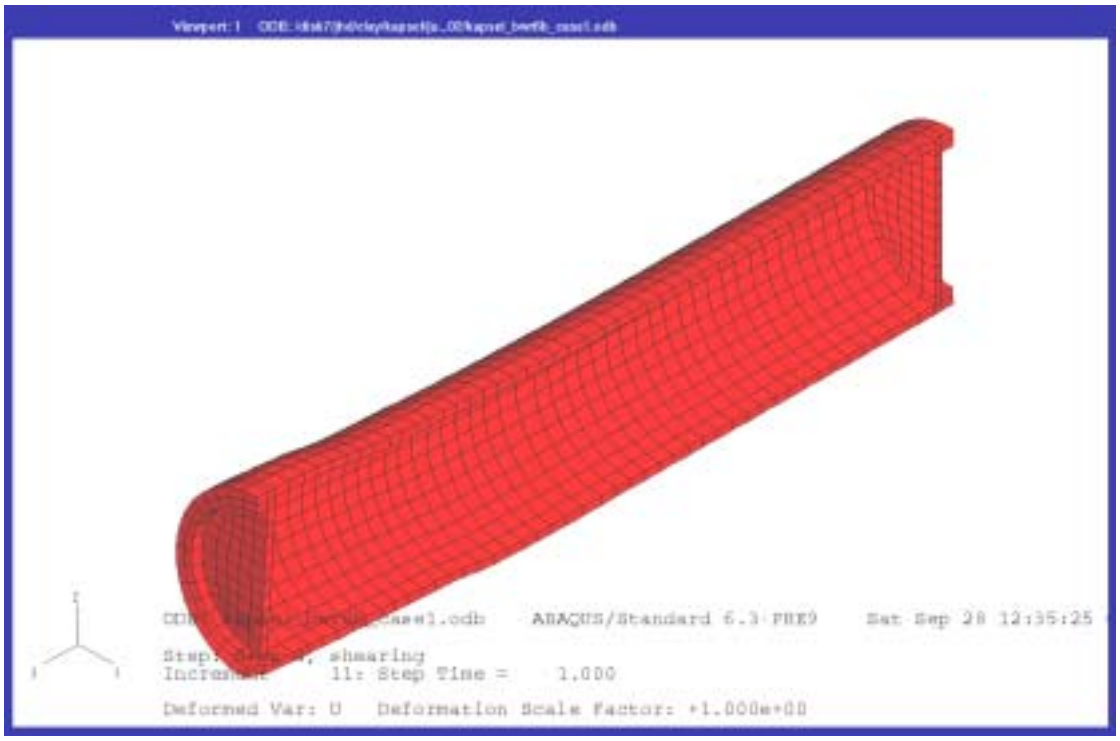

Figure A1-2. *Deformed copper canister after 20 cm rock displacement.*

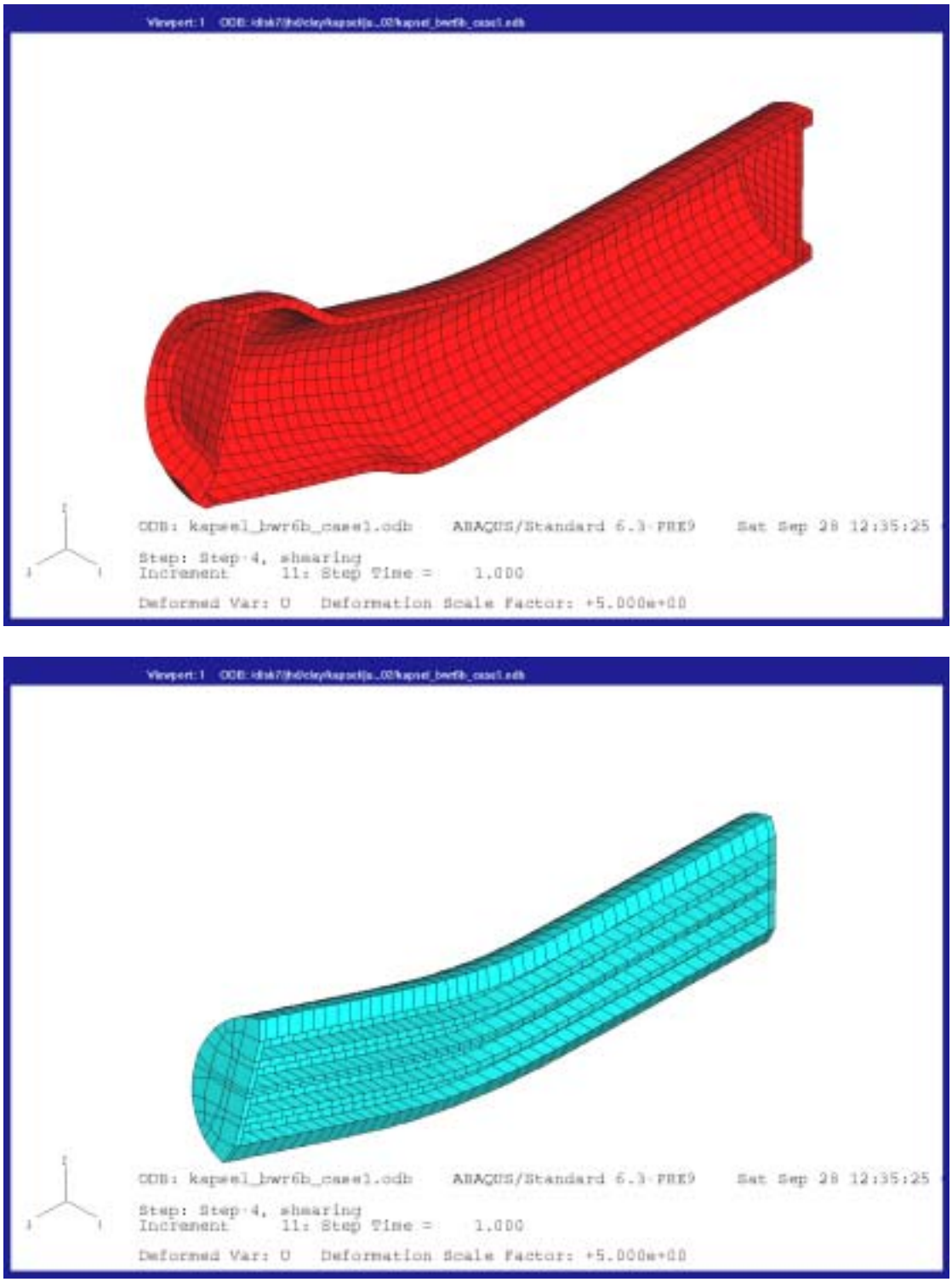

Figure A1-3. *Deformed copper canister (upper) and cast iron insert (lower) after 20 cm rock displacement with a deformation magnification factor of 5.*

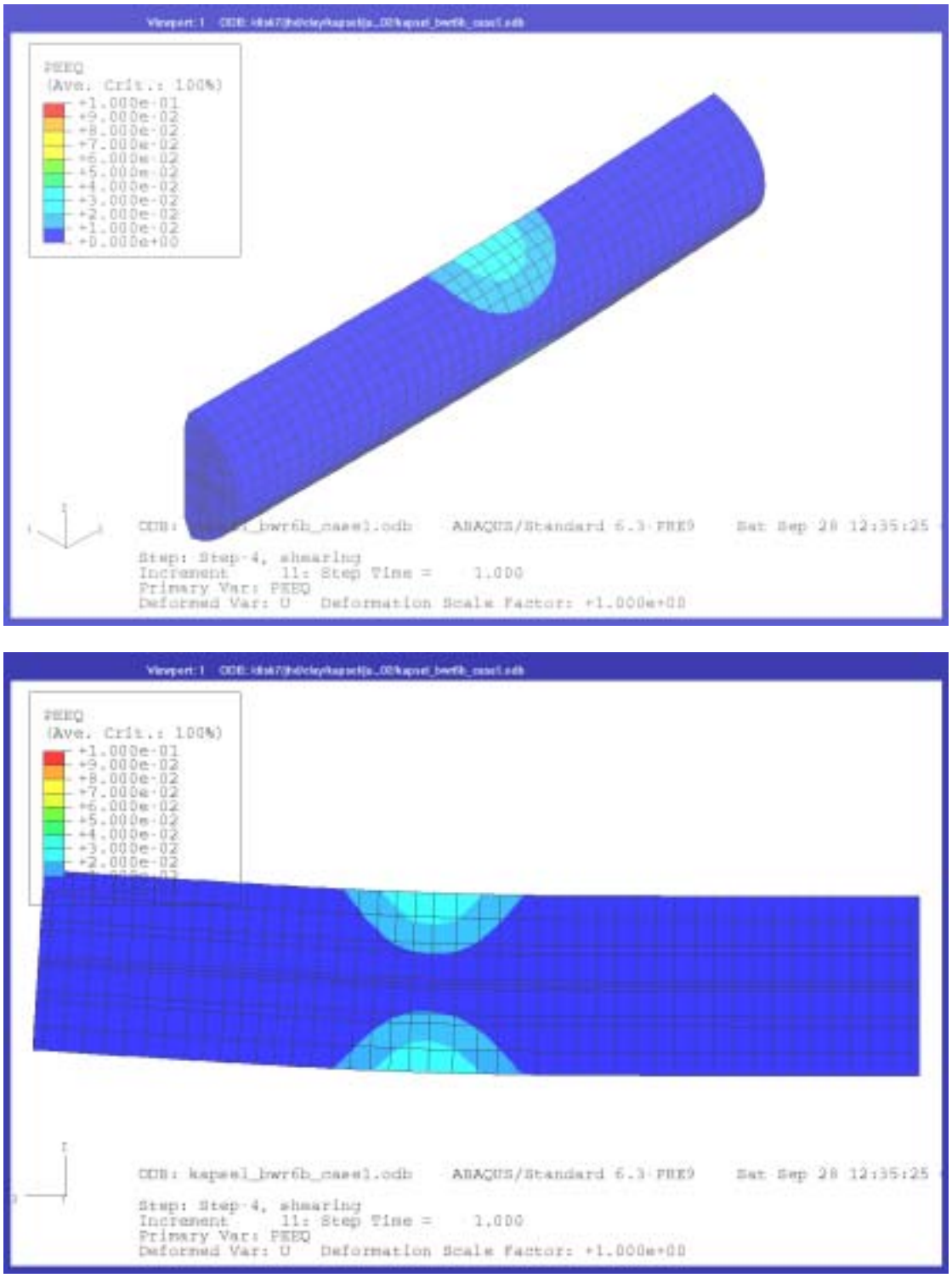

Figure A1-4. *Contour plots of the plastic strain in the cast iron insert seen from "behind" (upper) and straight "from the front" (lower) after 20 cm rock displacement. The shear plane is located 8 elements from the left side in the lower figure.*

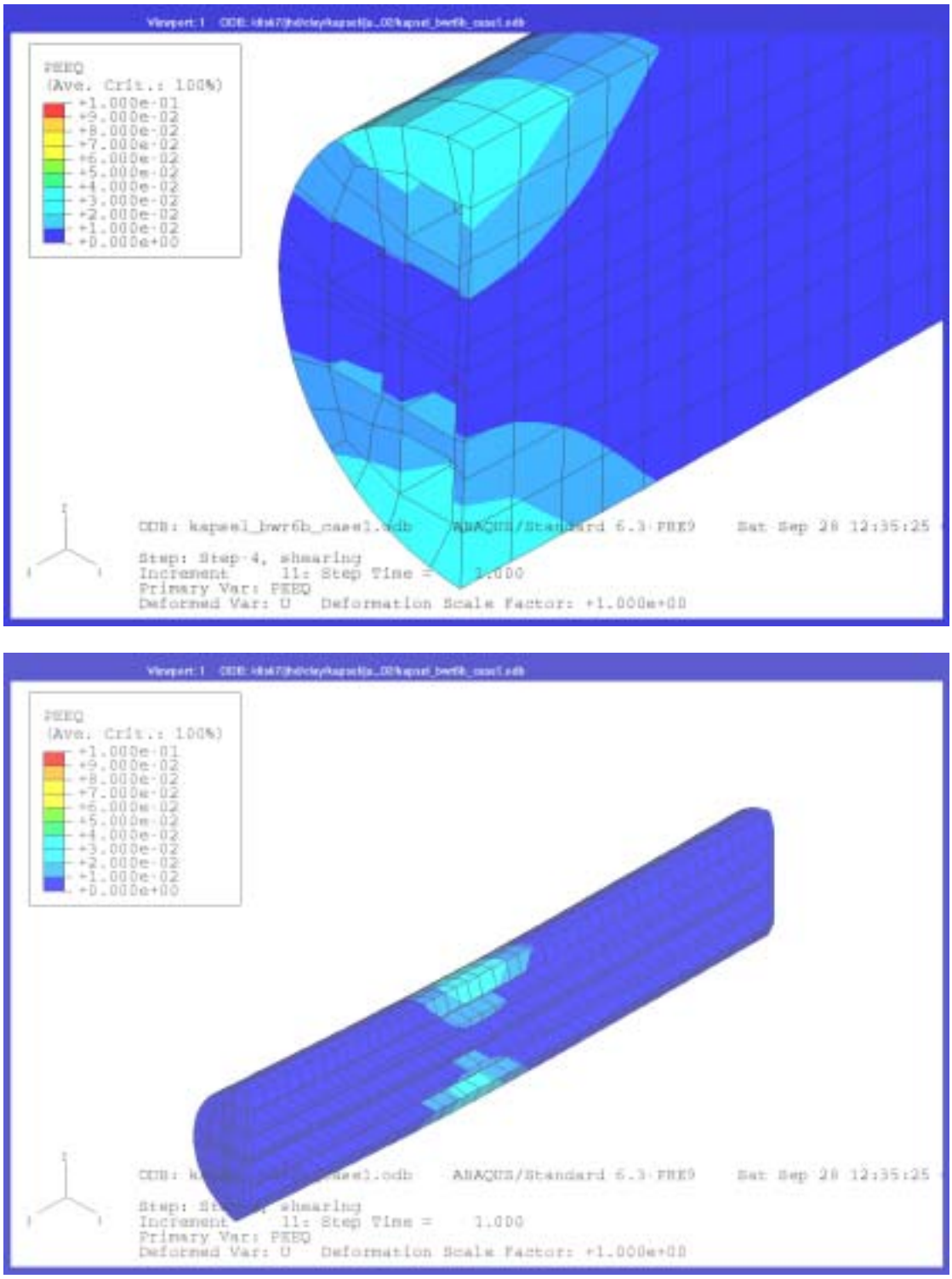

Figure A1-5. *Plastic strain in the cast iron insert after 20 cm rock displacement at a section cut perpendicular to the axis in the most stressed part (upper) and parallel to the axis (lower).*

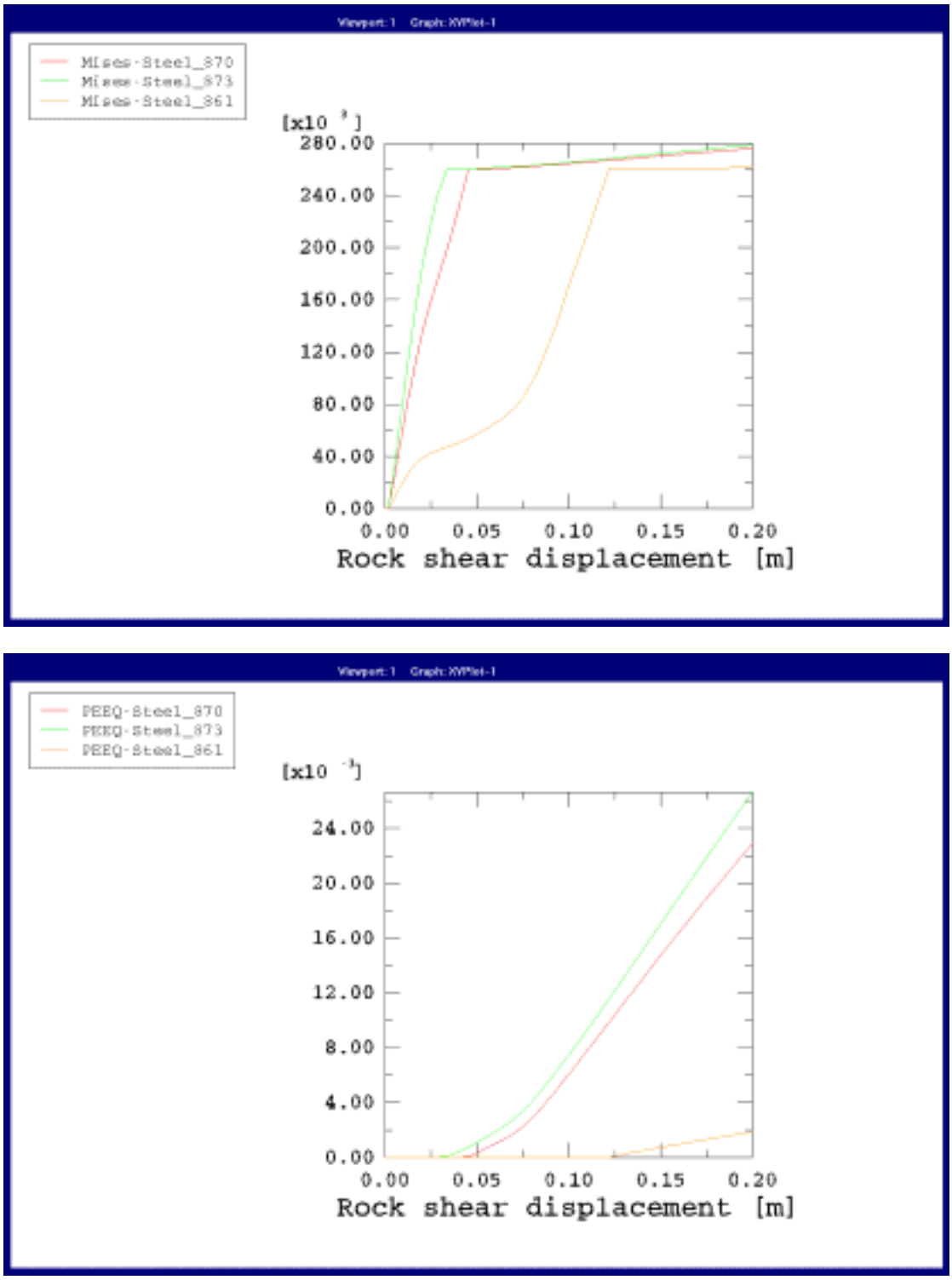

Figure A1-6. *Mises stress (kPa) (upper) and plastic strain (lower) as function of the rock shear displacement (m) for three elements located in the most stressed section. Elements 870 and 873 are located in the upper and lower periphery while element 861 is located in the centre (see Figure A1-1).*

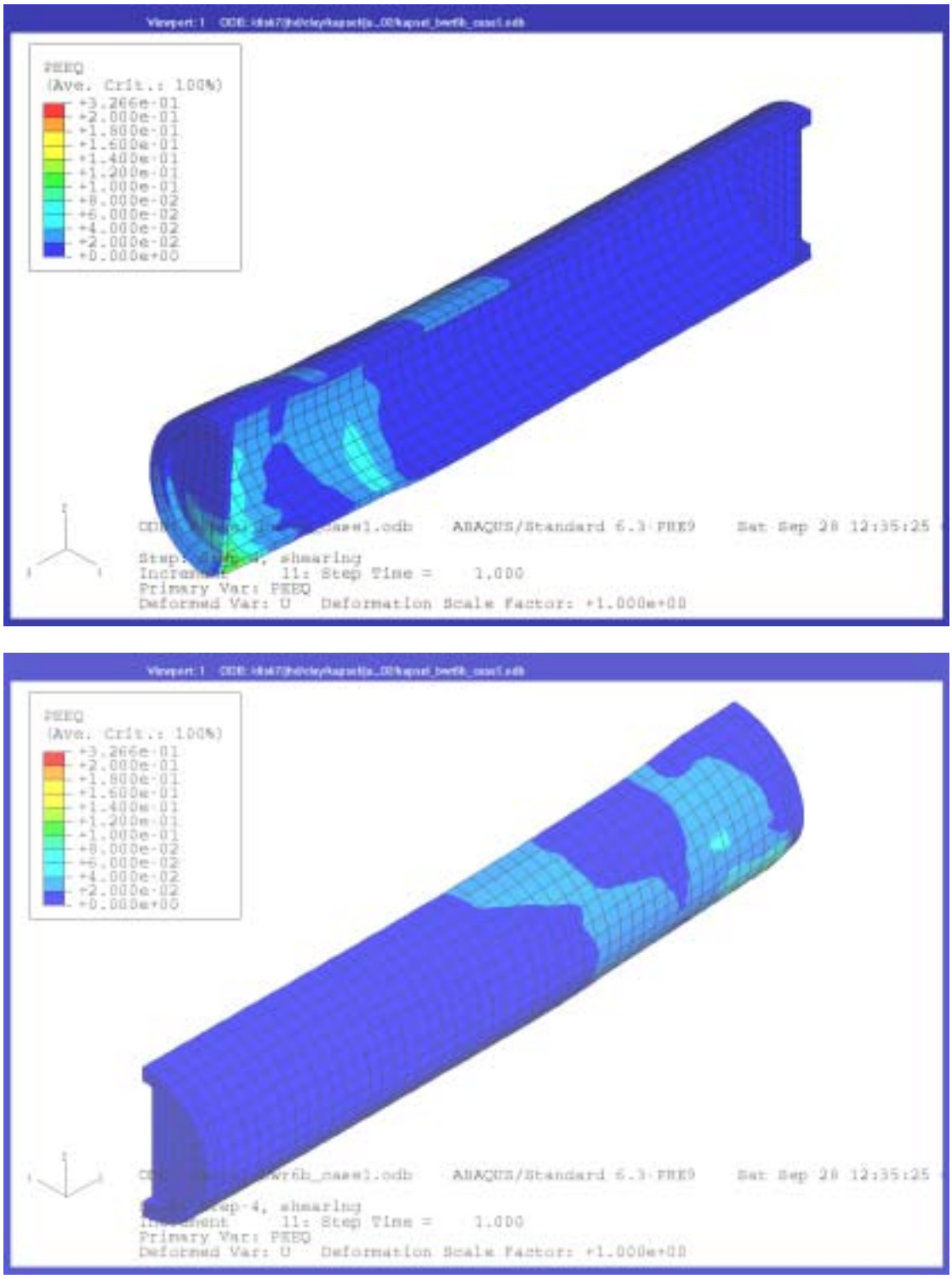

Figure A1-7. *Plastic strain in the copper canister after 20 cm rock displacement.*

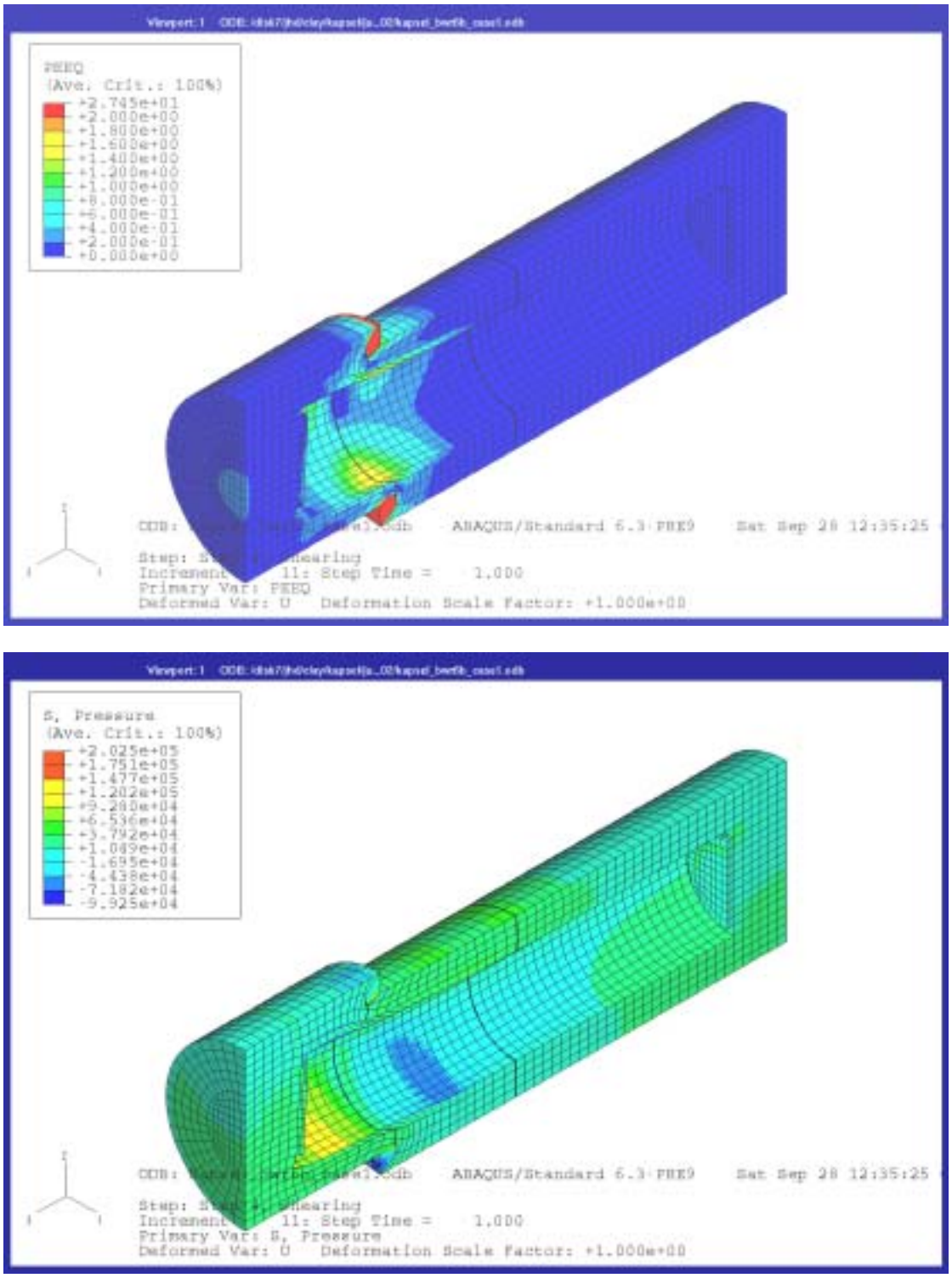

Figure A1-8. *Plastic strain (upper) and average stress (kPa pressure) (lower) in the bentonite buffer after 20 cm rock displacement.*

Appendix 2

Calculation *6b_case3*
Asymmetric shear at the buffer density 2050 kg/m^3

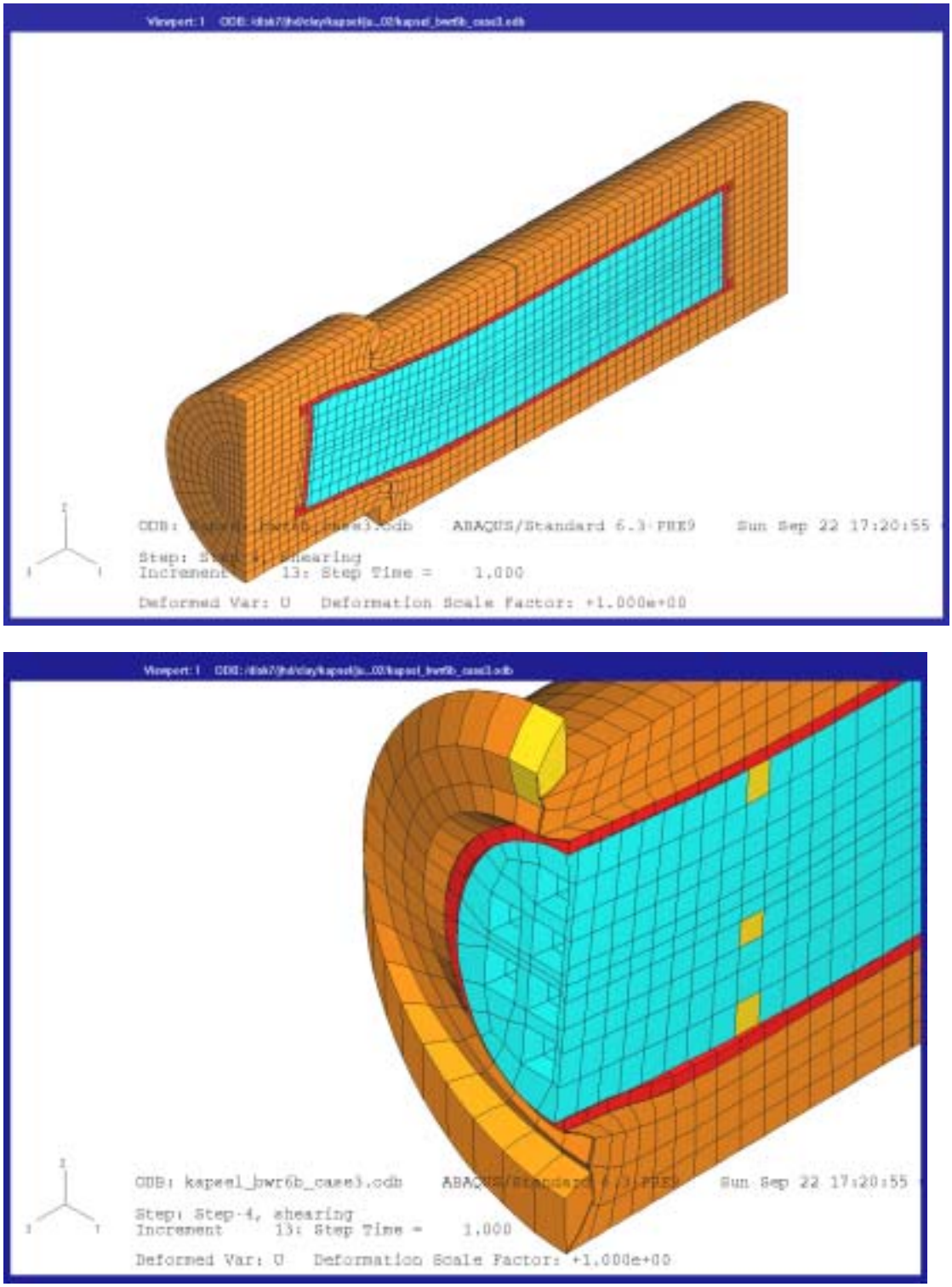

Figure A2-1. *Deformed structure after 20 cm rock displacement (upper) and a detail cut at the shear plane (lower). The three elements in the cast iron insert that are studied in more detail are marked yellow. The numbers are 660 (upper), 651 (central) and 663 (lower).*

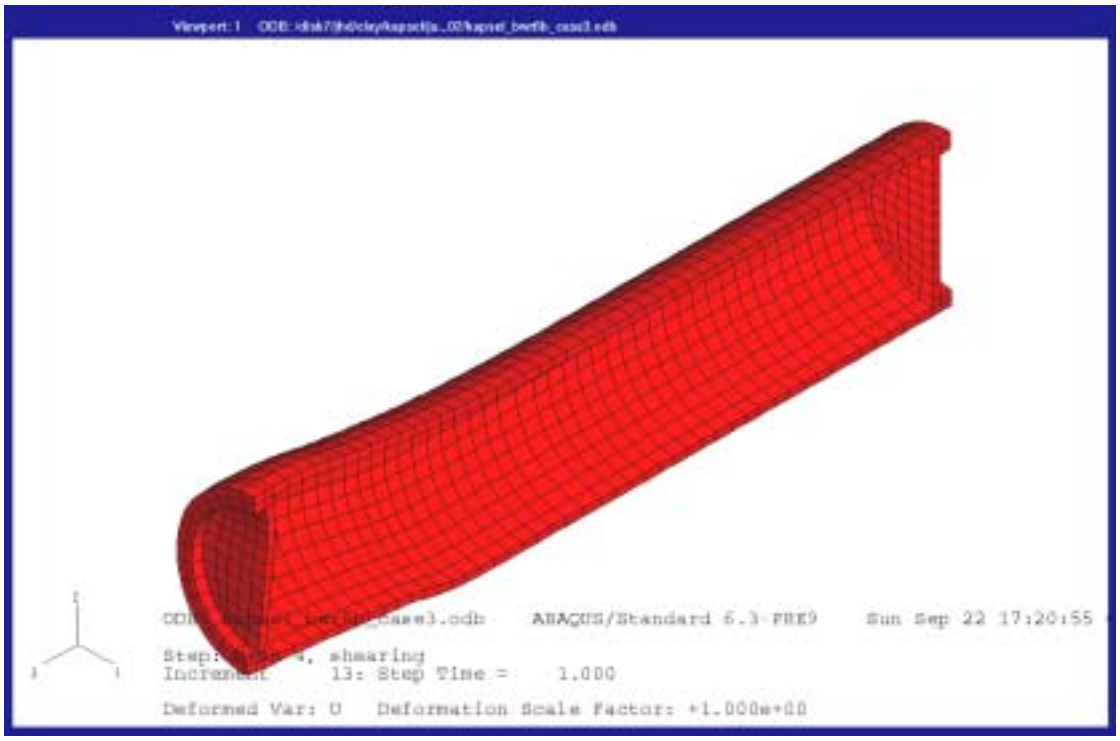

Figure A2-2. *Deformed copper canister after 20 cm rock displacement.*

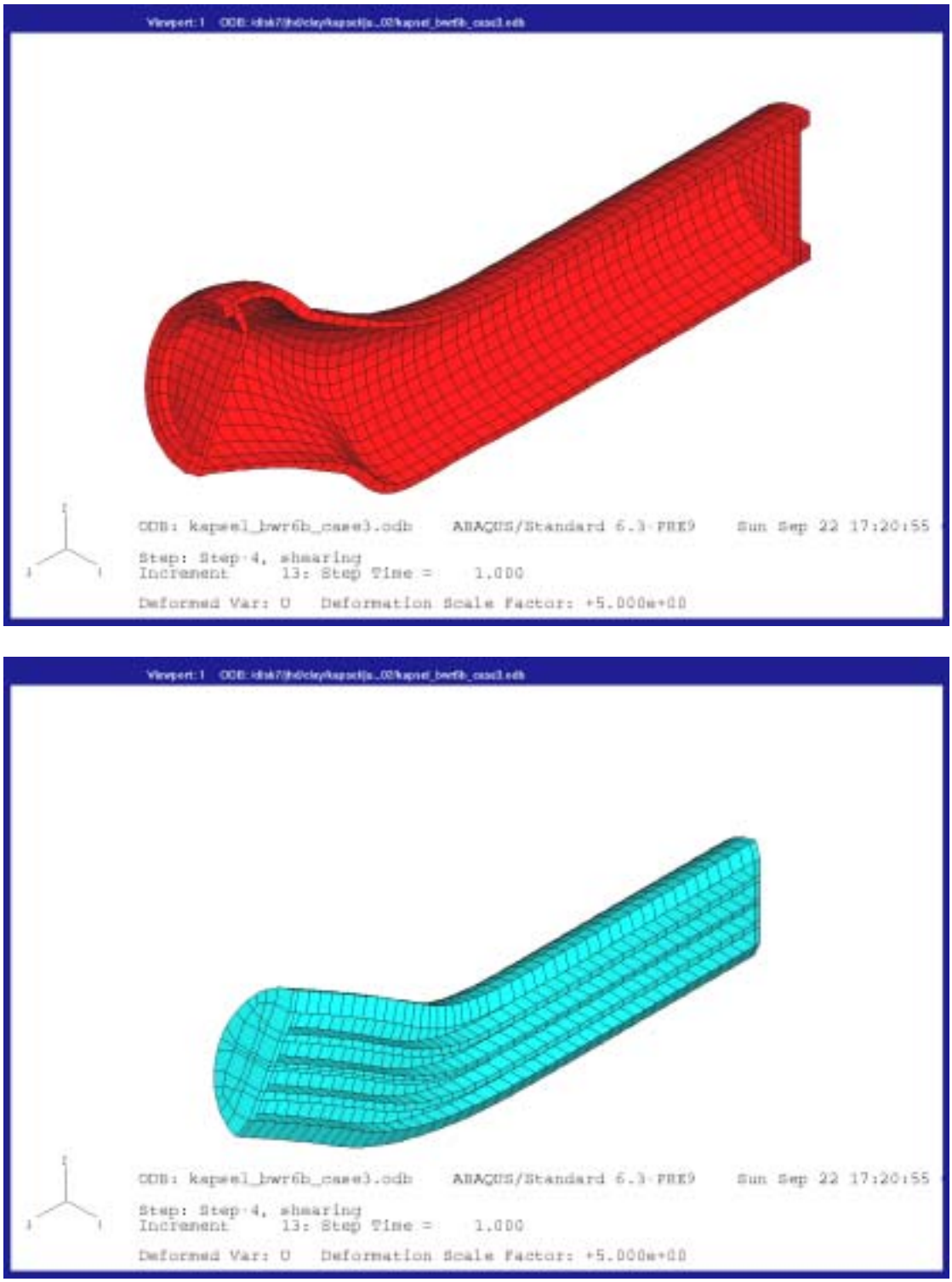

Figure A2-3. *Deformed copper canister (upper) and cast iron insert (lower) after 20 cm rock displacement with a deformation magnification factor of 5.*

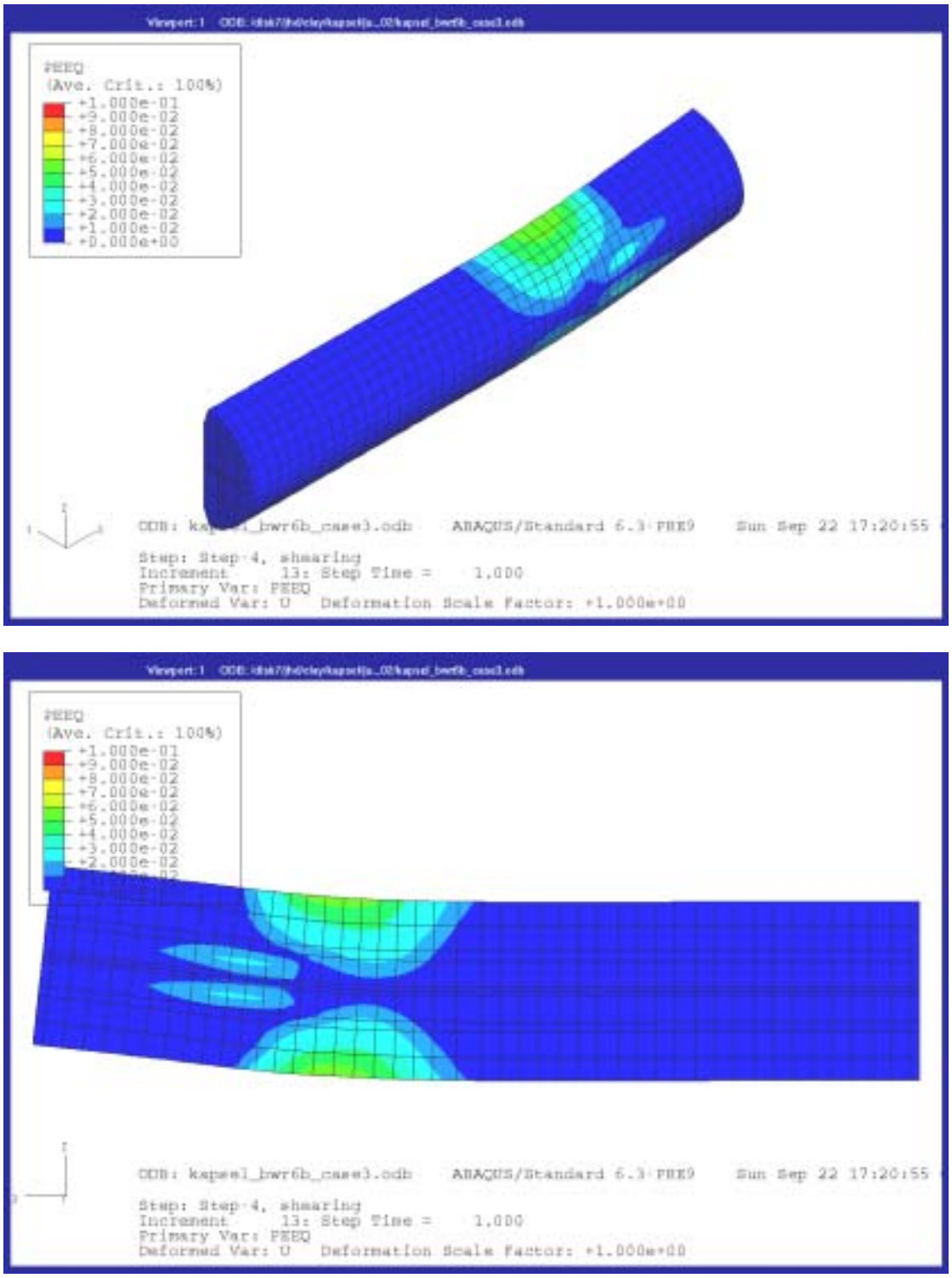

Figure A2-4. *Contour plots of the plastic strain in the cast iron insert seen from "behind" (upper) and straight "from the front" (lower) after 20 cm rock displacement. The shear plane is located 8 elements from the left side in the lower figure.*

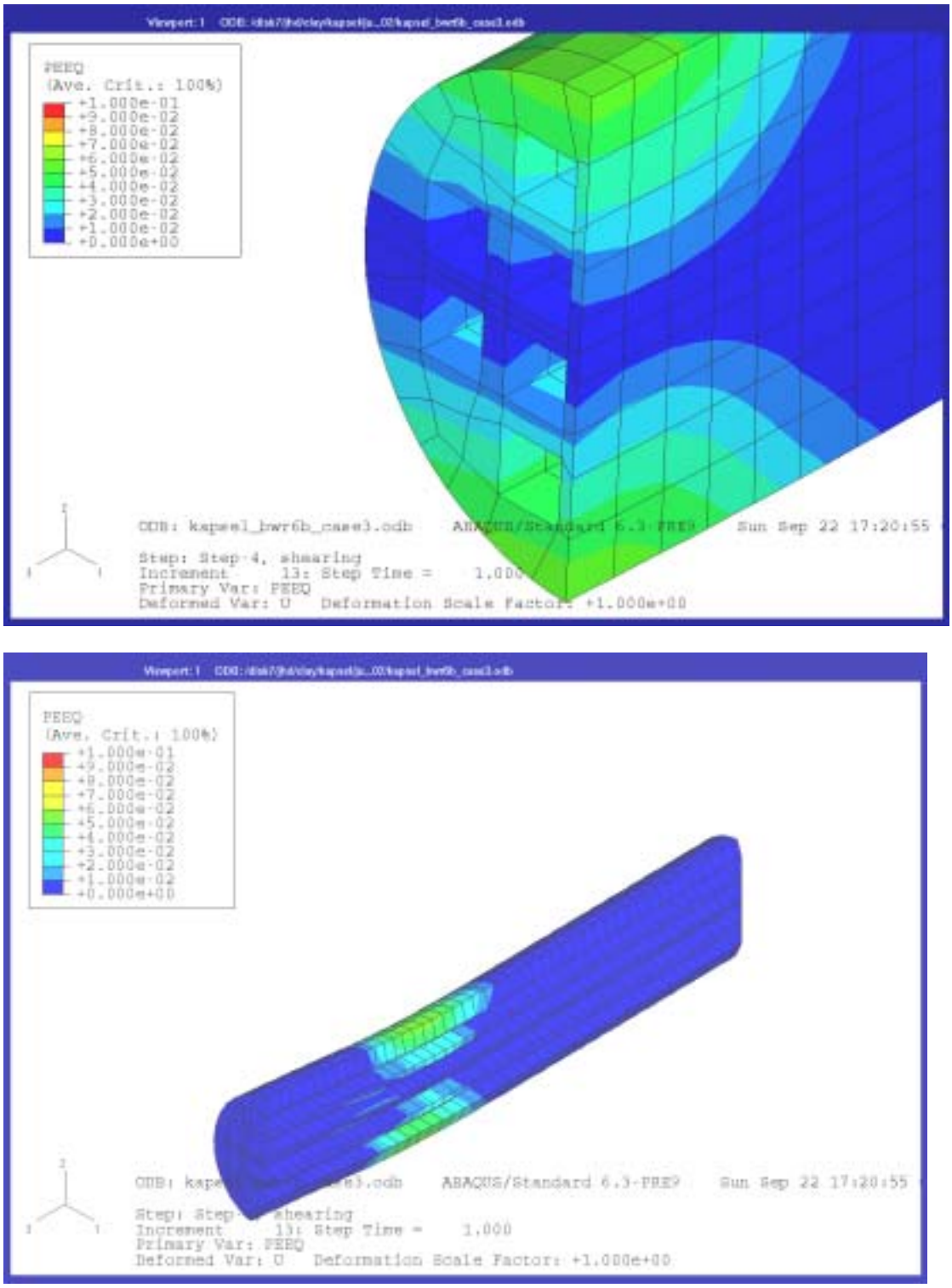

Figure A2-5. *Plastic strain in the cast iron insert after 20 cm rock displacement at a section cut perpendicular to the axis in the most stressed part (upper) and parallel to the axis (lower).*

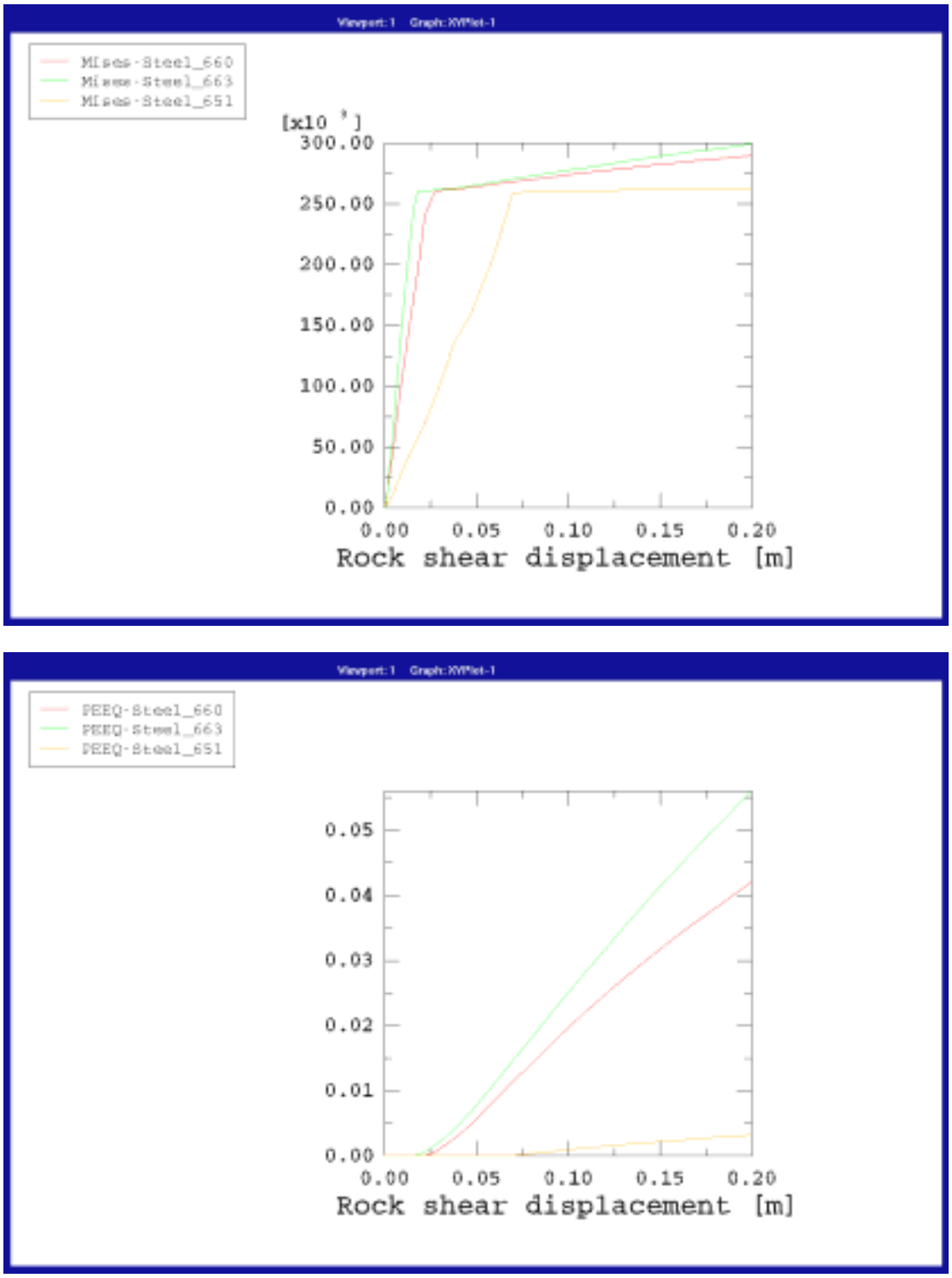

Figure A2-6. *Mises stress (kPa) (upper) and plastic strain (lower) as function of the rock shear displacement (m) for three elements located in the most stressed section. Elements 660 and 663 are located in the upper and lower periphery while element 651 is located in the centre (see Figure A2-1).*

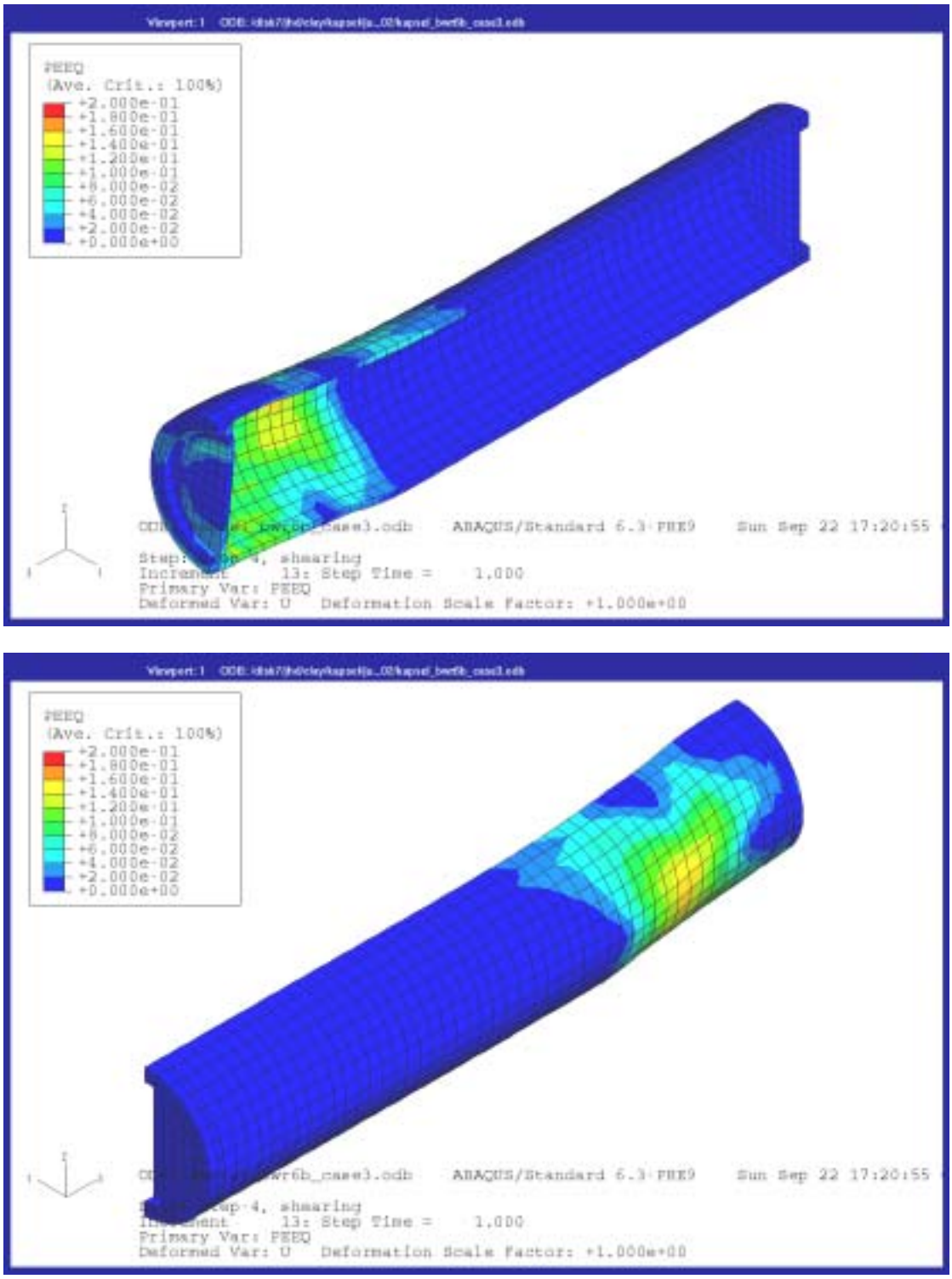

Figure A2-7. *Plastic strain in the copper canister after 20 cm rock displacement.*

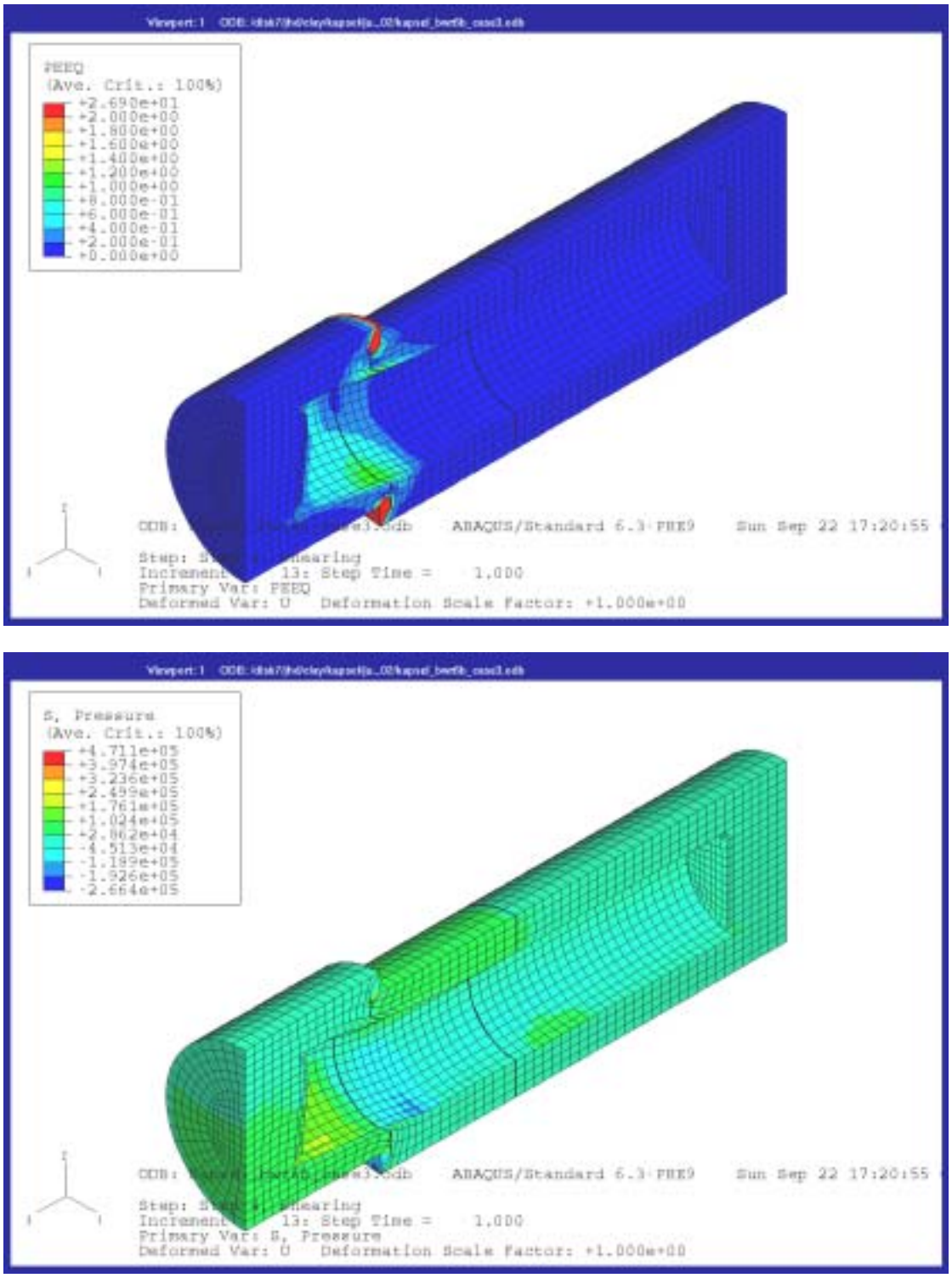

Figure A2-8. *Plastic strain (upper) and average stress (kPa pressure) (lower) in the bentonite buffer after 20 cm rock displacement.*

Appendix 3

Calculation *6b_case4*
Asymmetric shear at the buffer density 2100 kg/m^3

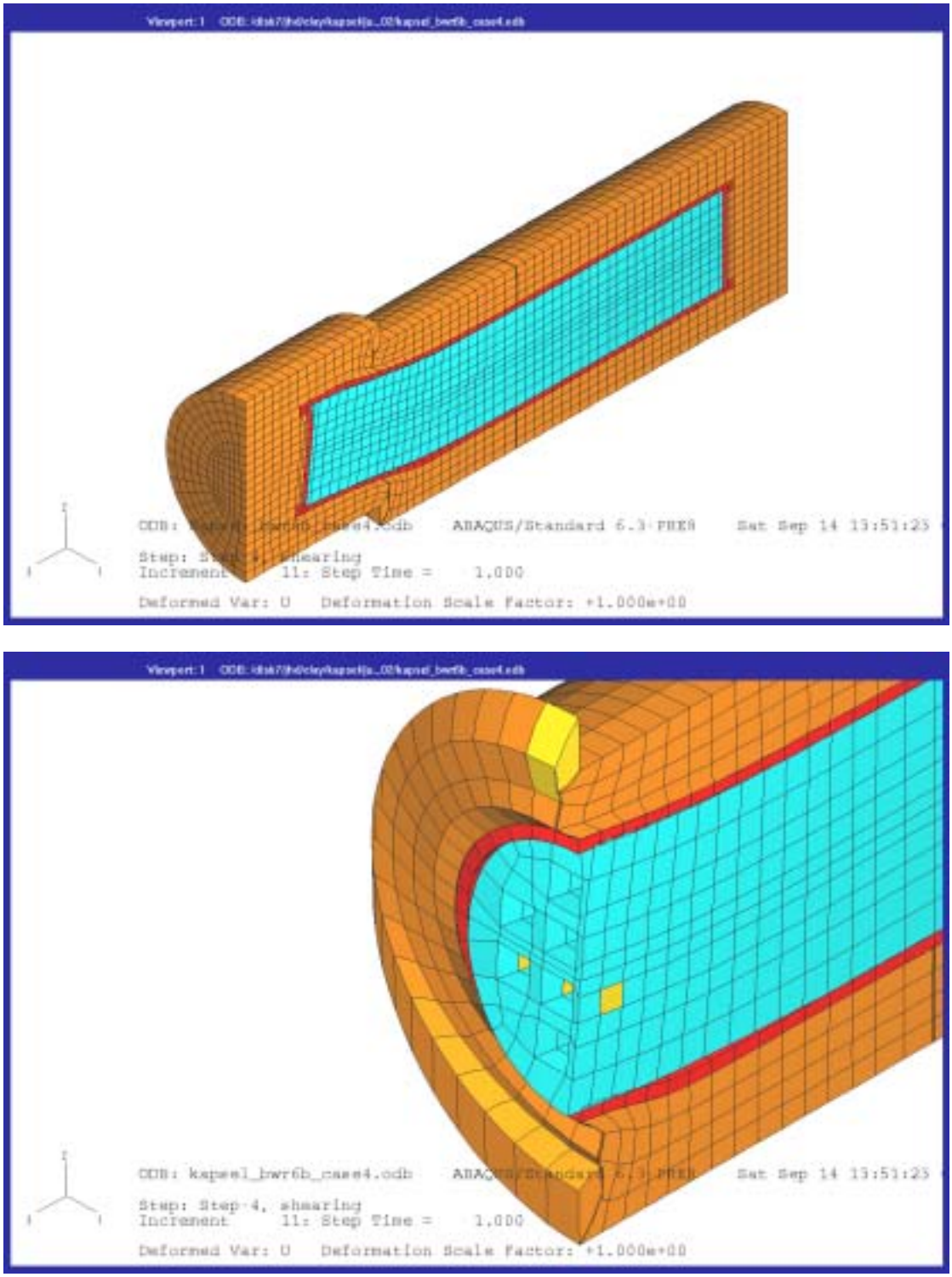

Figure A3-1. *Deformed structure after 20 cm rock displacement (upper) and a detail cut at the shear plane (lower). The three elements in the cast iron insert that are studied in more detail are marked yellow. The numbers are 357 (front element), 360 (central) and 361 (furthest element).*

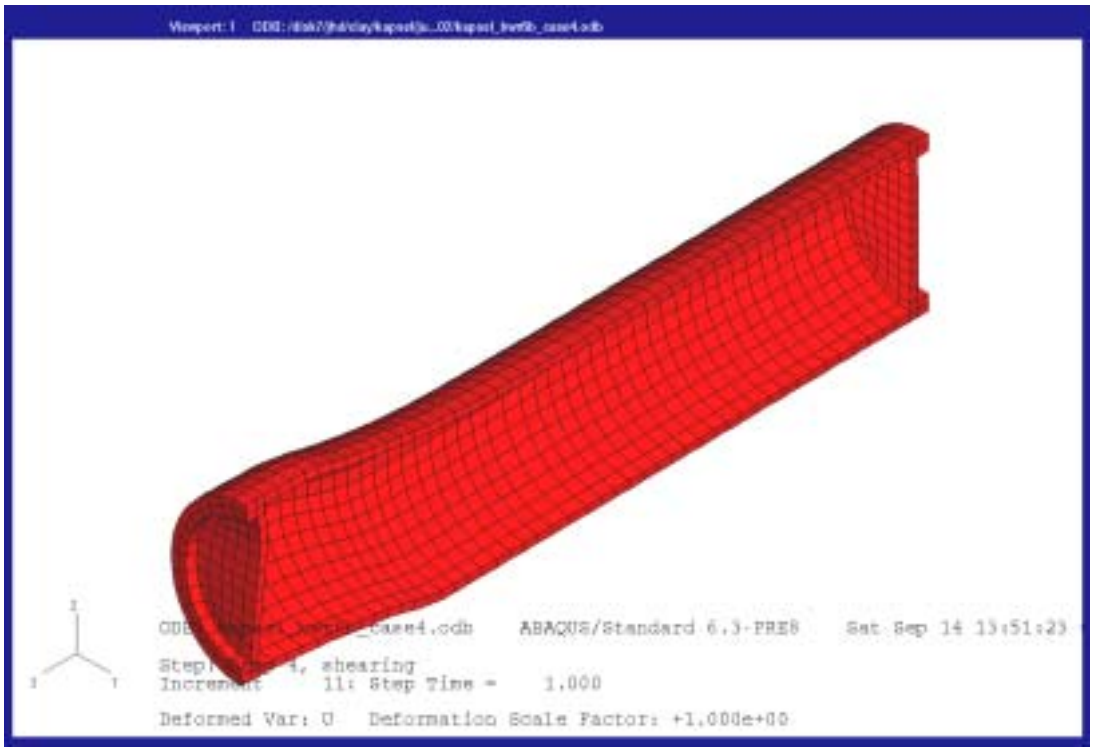

Figure A3-2. *Deformed copper canister after 20 cm rock displacement.*

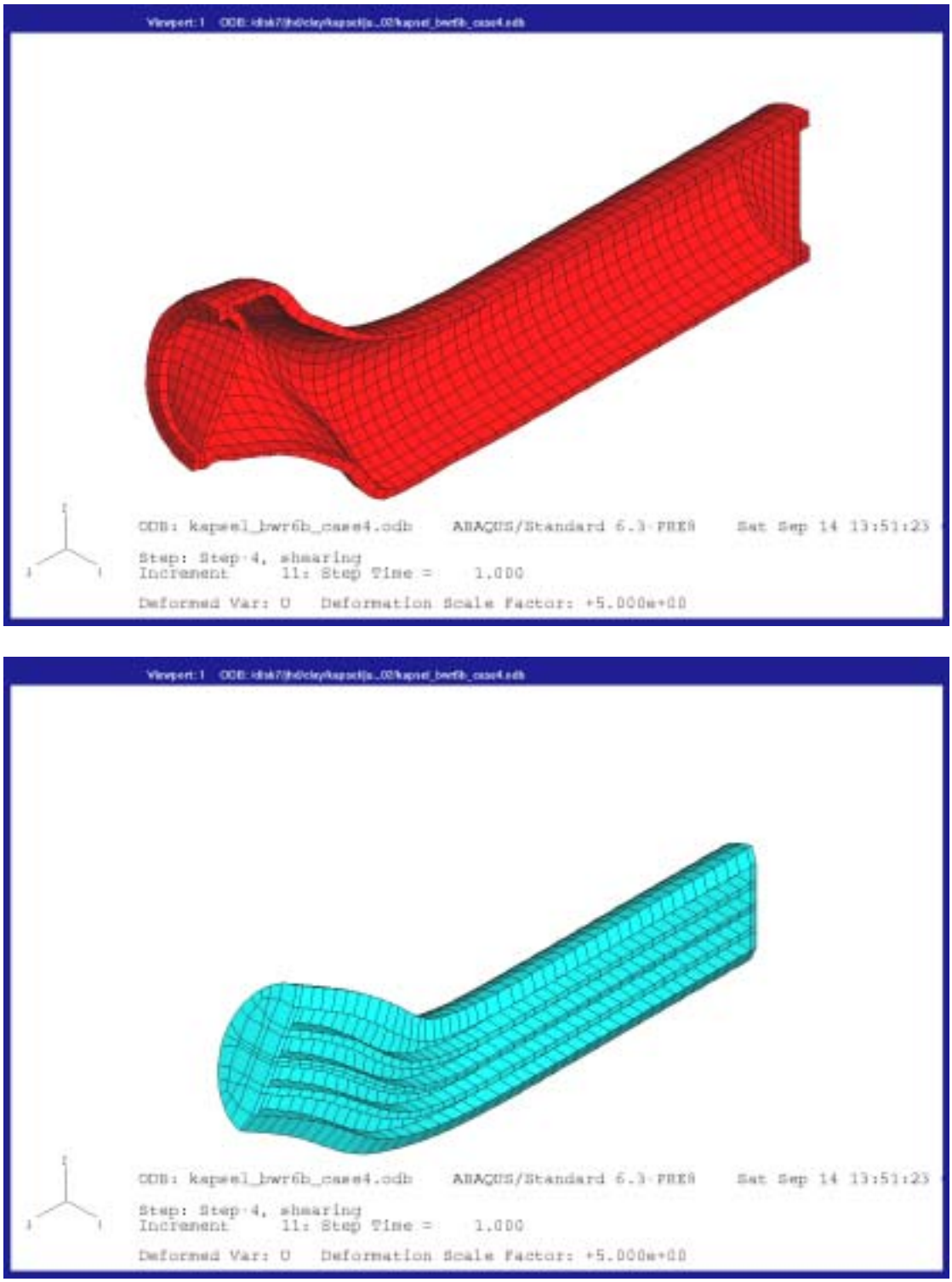

Figure A3-3. *Deformed copper canister (upper) and cast iron insert (lower) after 20 cm rock displacement with a deformation magnification factor of 5.*

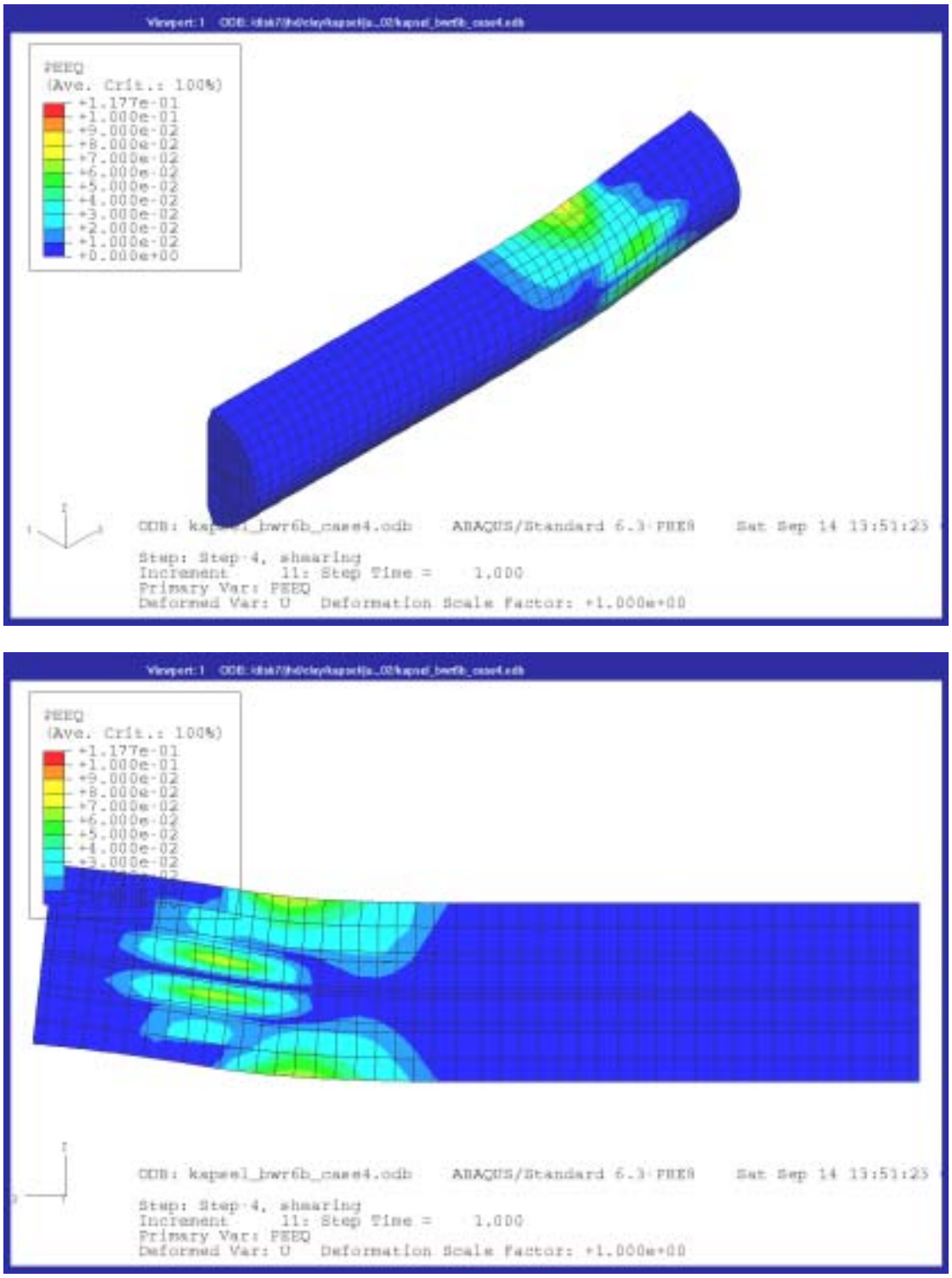

Figure A3-4. *Contour plots of the plastic strain in the cast iron insert seen from "behind" (upper) and straight "from the front" (lower) after 20 cm rock displacement. The shear plane is located 8 elements from the left side in the lower figure.*

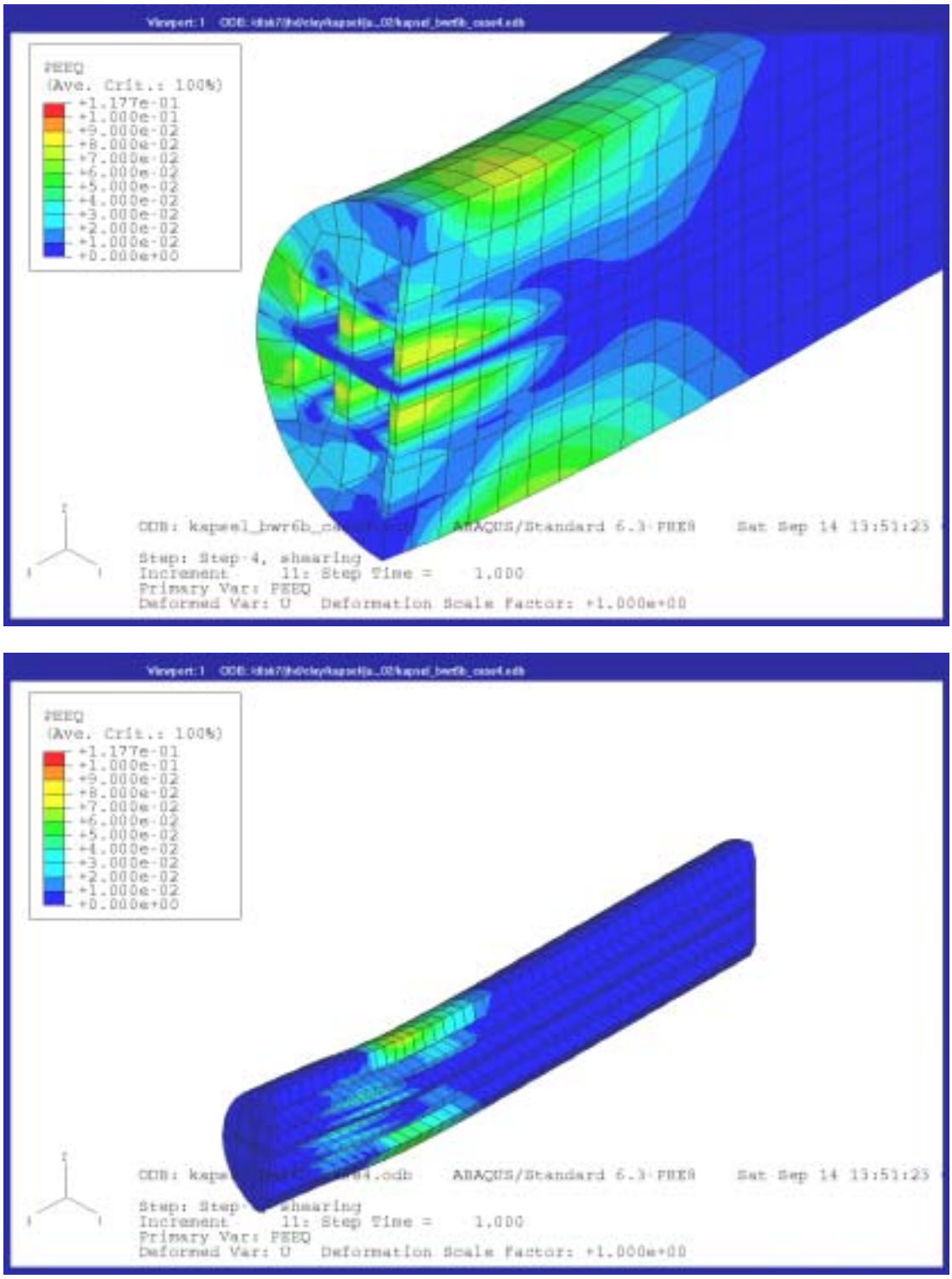

Figure A3-5. *Plastic strain in the cast iron insert after 20 cm rock displacement at a section cut perpendicular to the axis in the most stressed part (upper) and parallel to the axis (lower).*

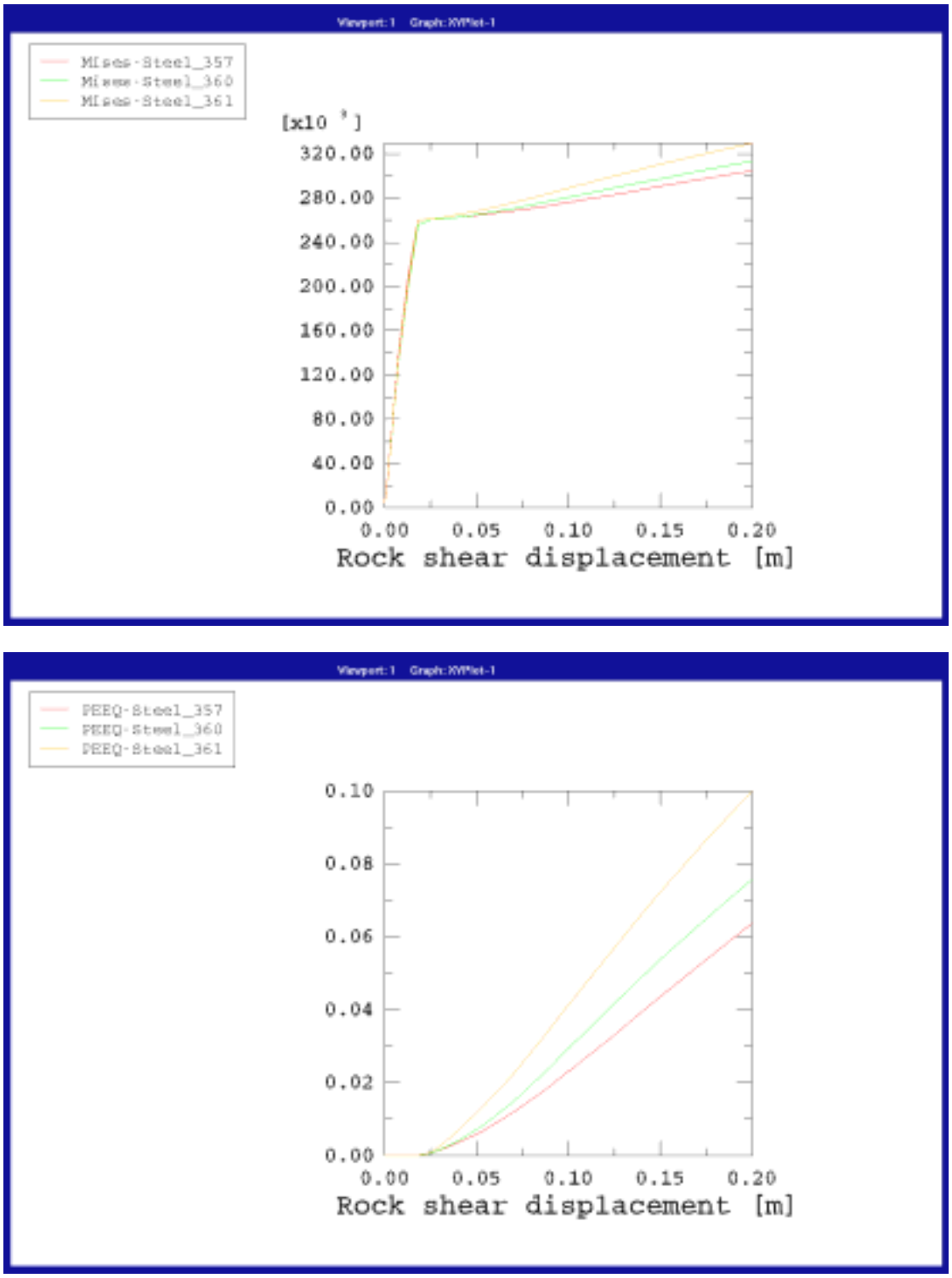

Figure A3-6. *Mises stress (kPa) (upper) and plastic strain (lower) as function of the rock shear displacement (m) for three elements located in the most stressed section. Element 357 is located in the axial symmetry plane while elements 360 and 361 are located in more peripheral parts (see Figure A3-1).*

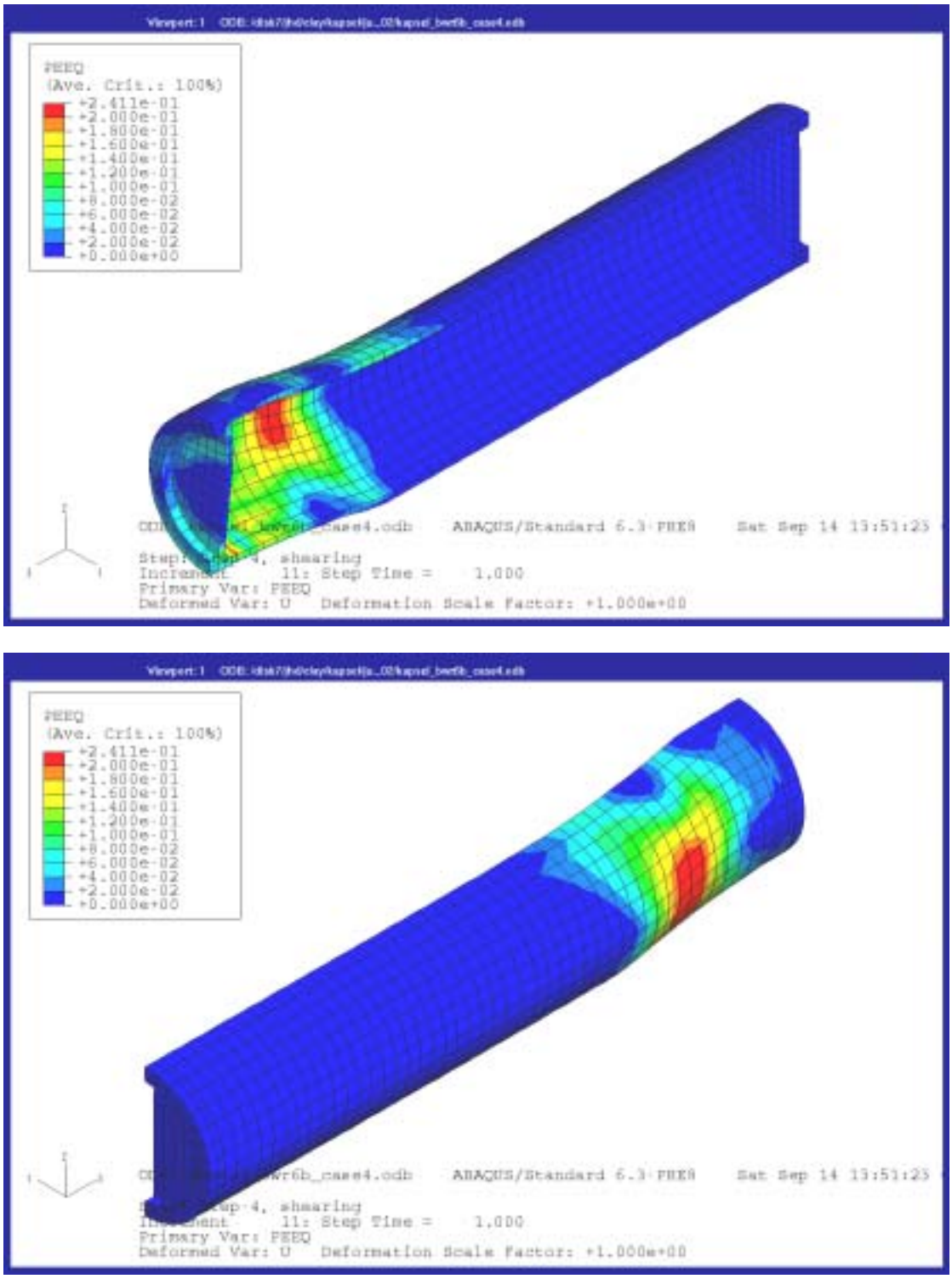

Figure A3-7. *Plastic strain in the copper canister after 20 cm rock displacement.*

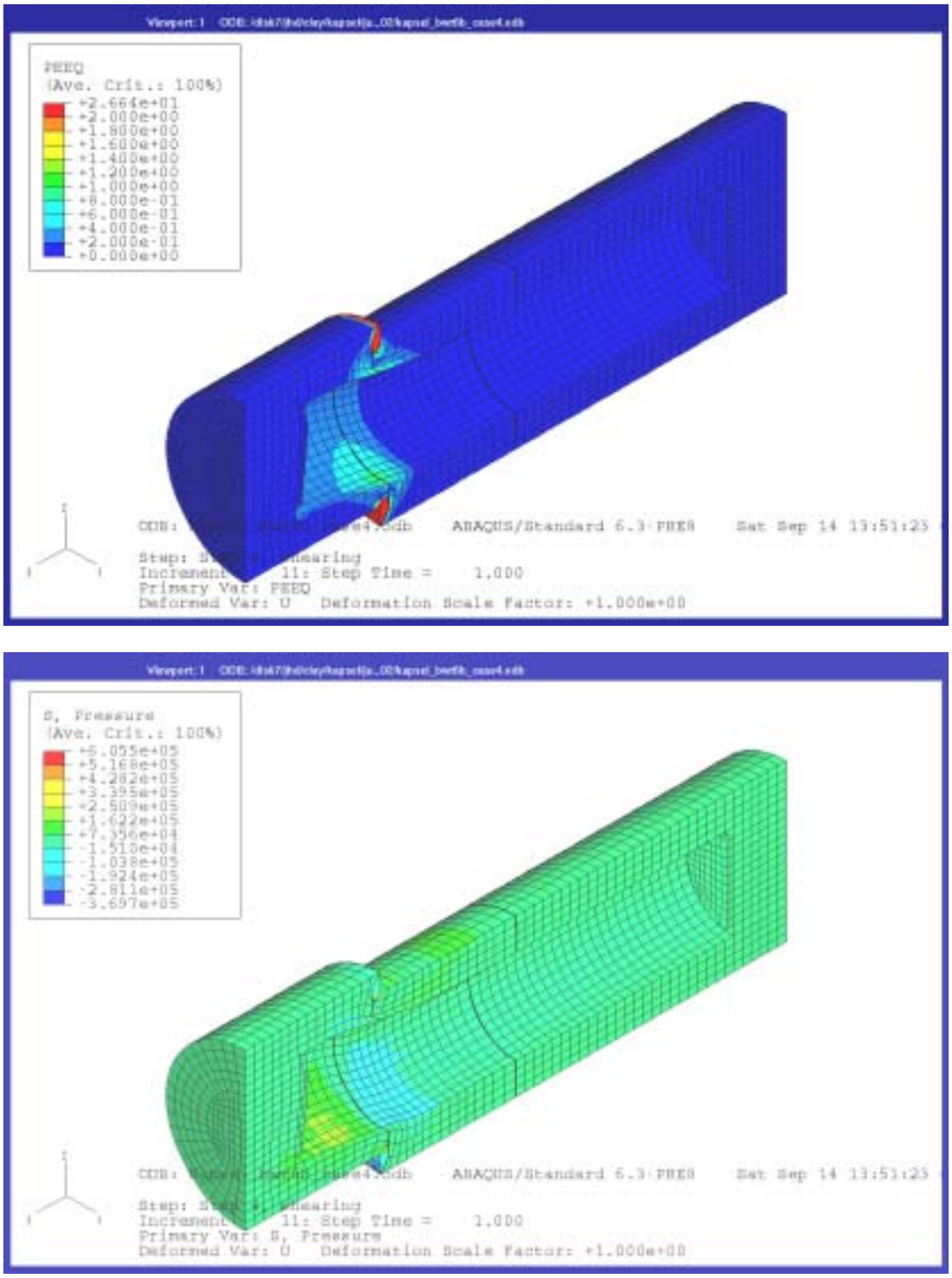

Figure A3-8. *Plastic strain (upper) and average stress (kPa pressure) (lower) in the bentonite buffer after 20 cm rock displacement.*

Appendix 4

Calculation *6c_case1*
Symmetric shear at the buffer density 1950 kg/m^3

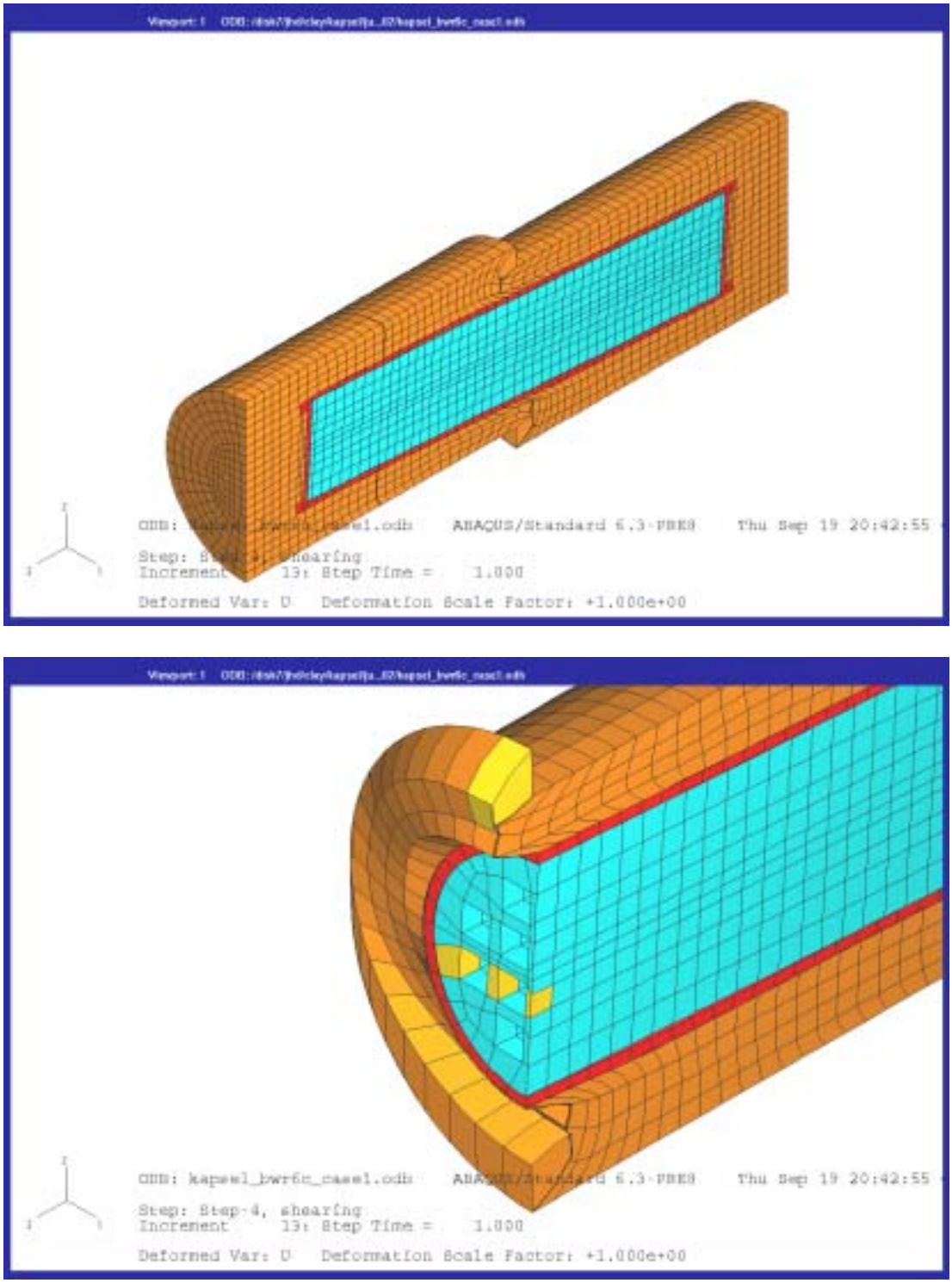

Figure A4-1. *Deformed structure after 20 cm rock displacement (upper) and a detail cut at the shear plane (lower). The three elements in the cast iron insert that are studied in more detail are marked yellow. The numbers are 945 (front element), 948 (central) and 949 (furthest element).*

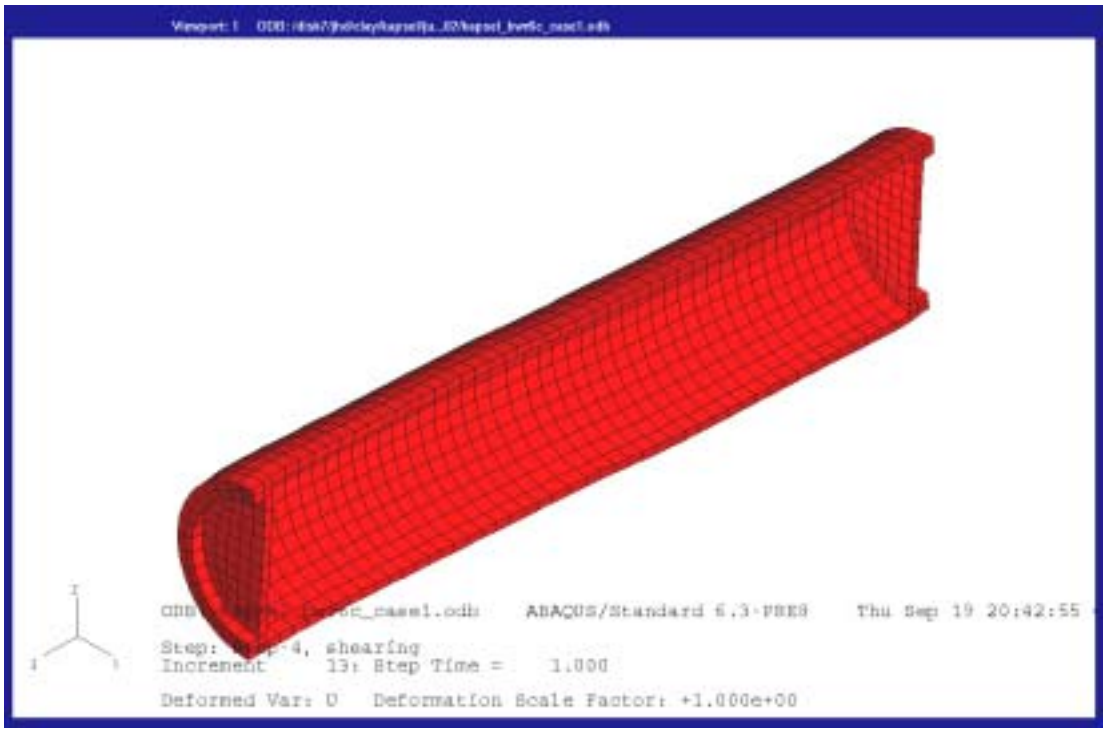

Figure A4-2. *Deformed copper canister after 20 cm rock displacement.*

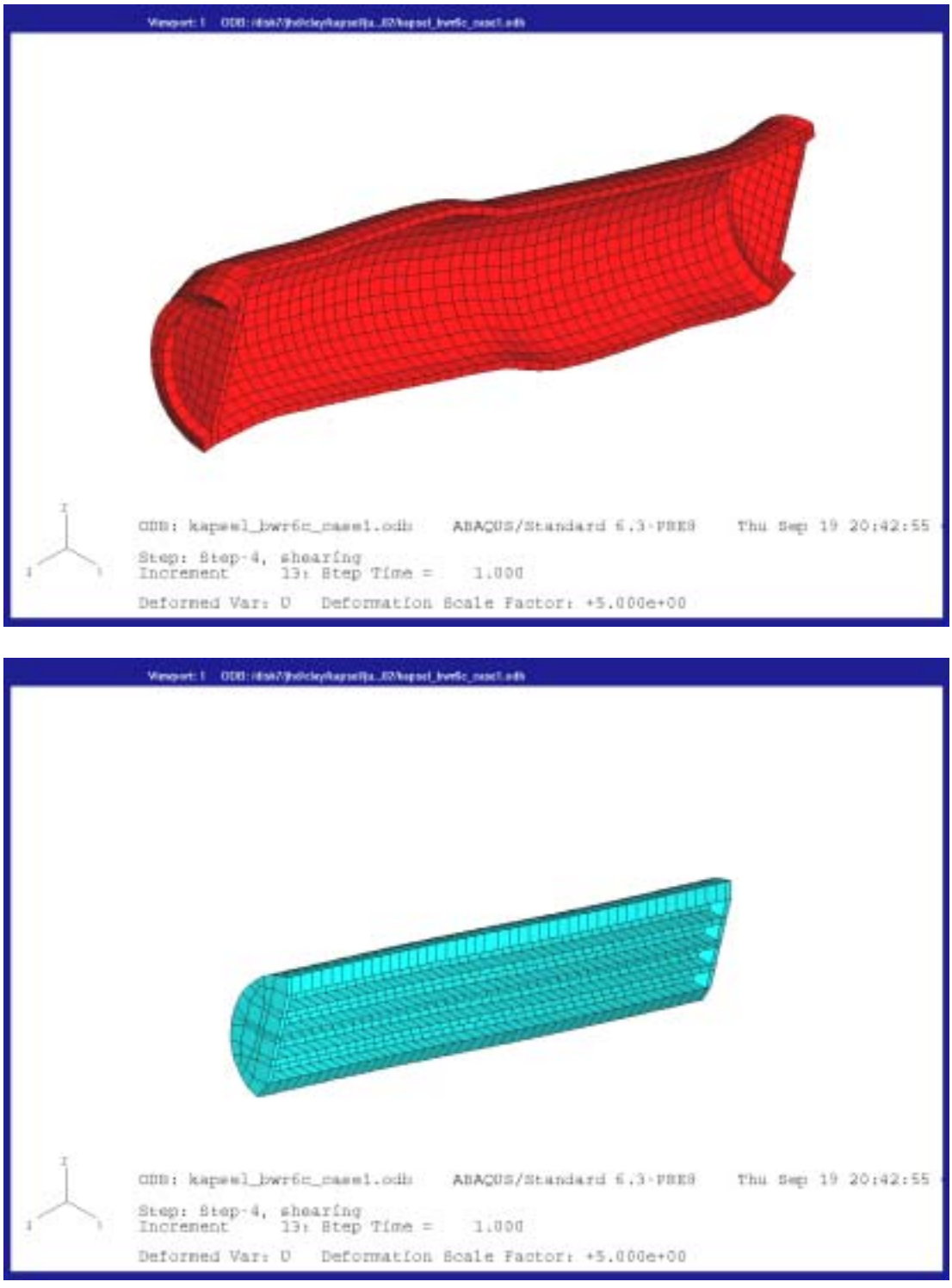

Figure A4-3. *Deformed copper canister (upper) and cast iron insert (lower) after 20 cm rock displacement with a deformation magnification factor of 5.*

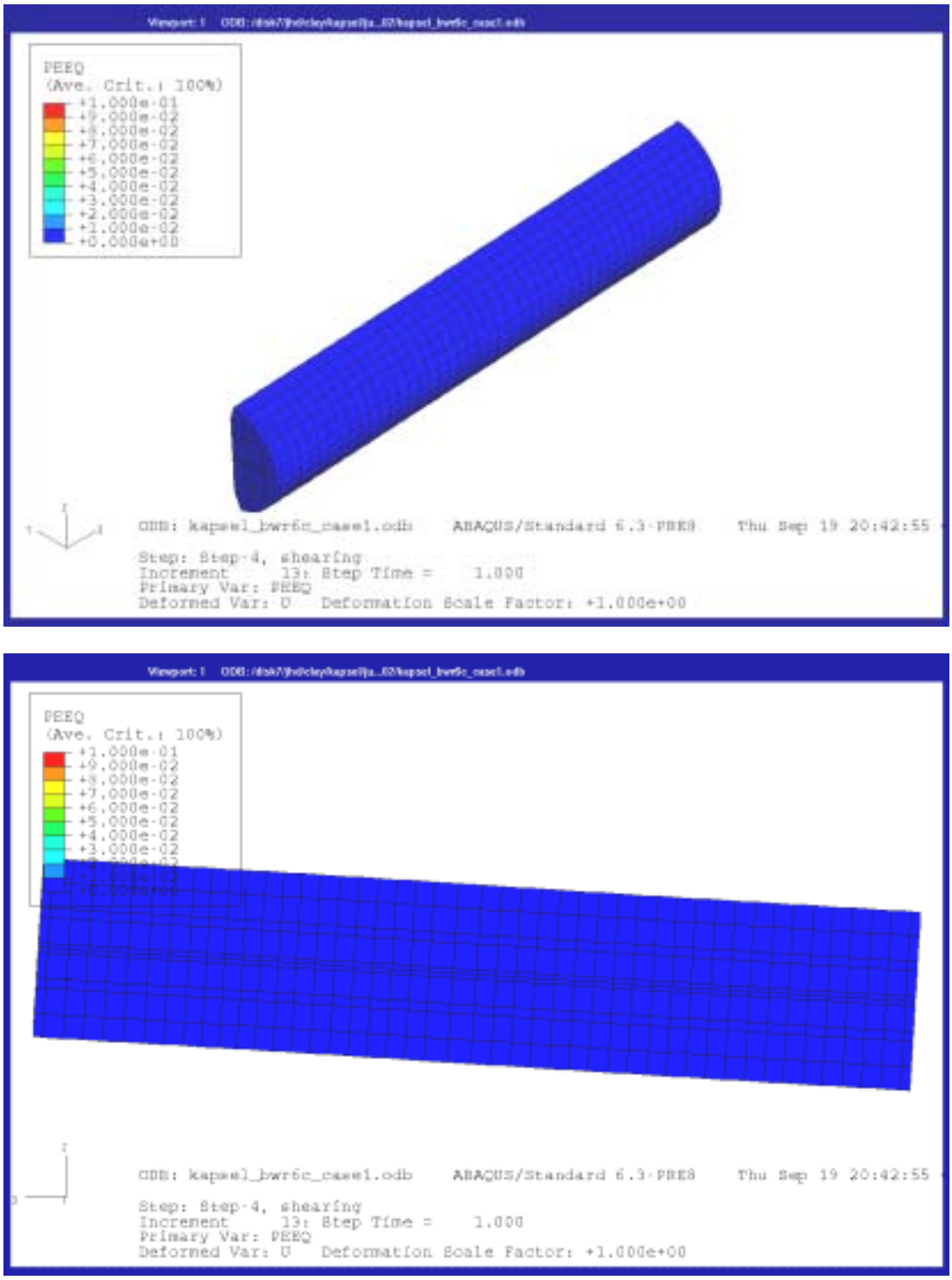

Figure A4-4. *Contour plots of the plastic strain in the cast iron insert seen from "behind" (upper) and straight "from the front" (lower) after 20 cm rock displacement. The shear plane is located 8 elements from the left side in the lower figure.*

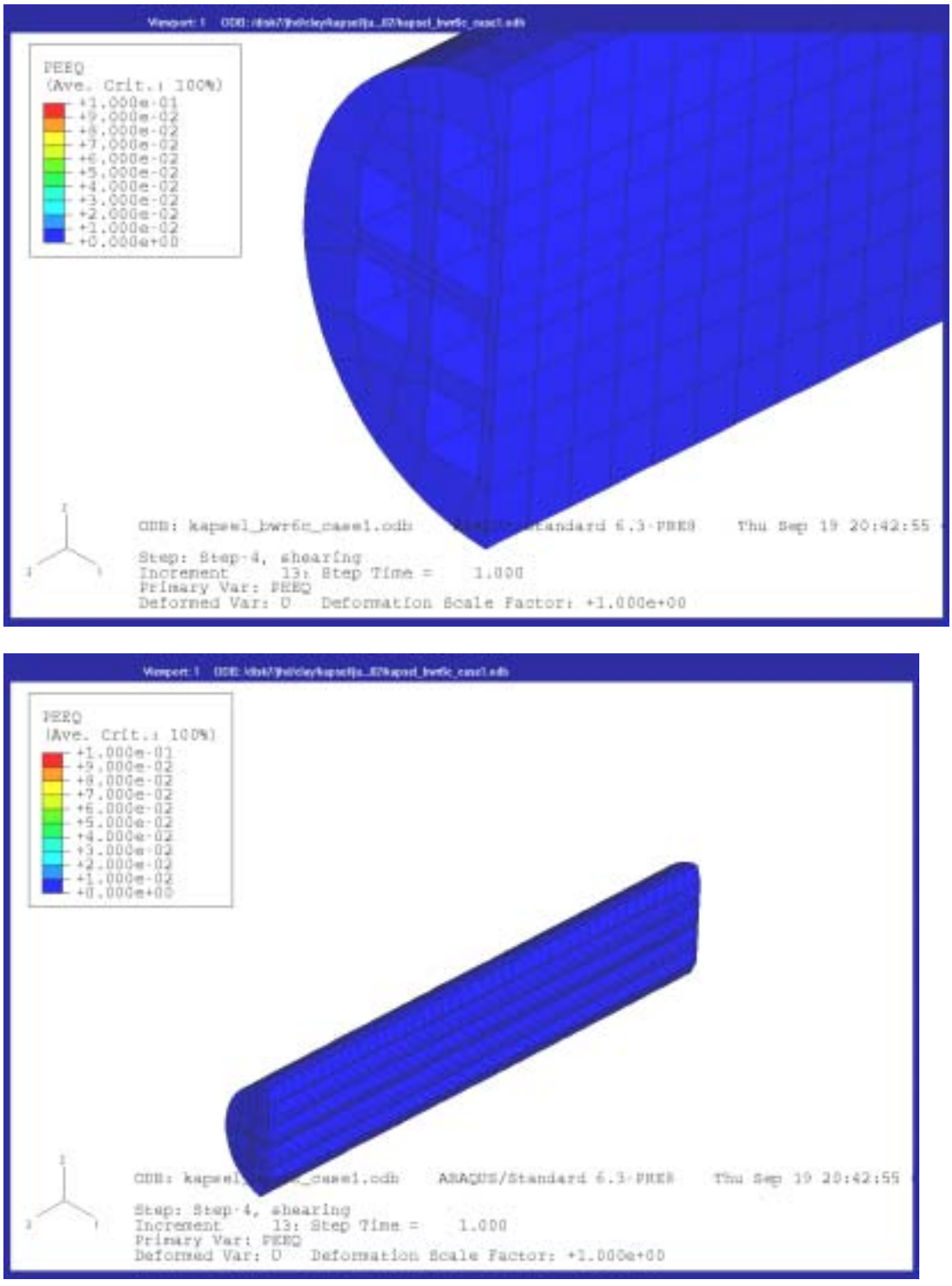

Figure A4-5. *Plastic strain in the cast iron insert after 20 cm rock displacement at a section cut perpendicular to the axis in the most stressed part (upper) and parallel to the axis (lower).*

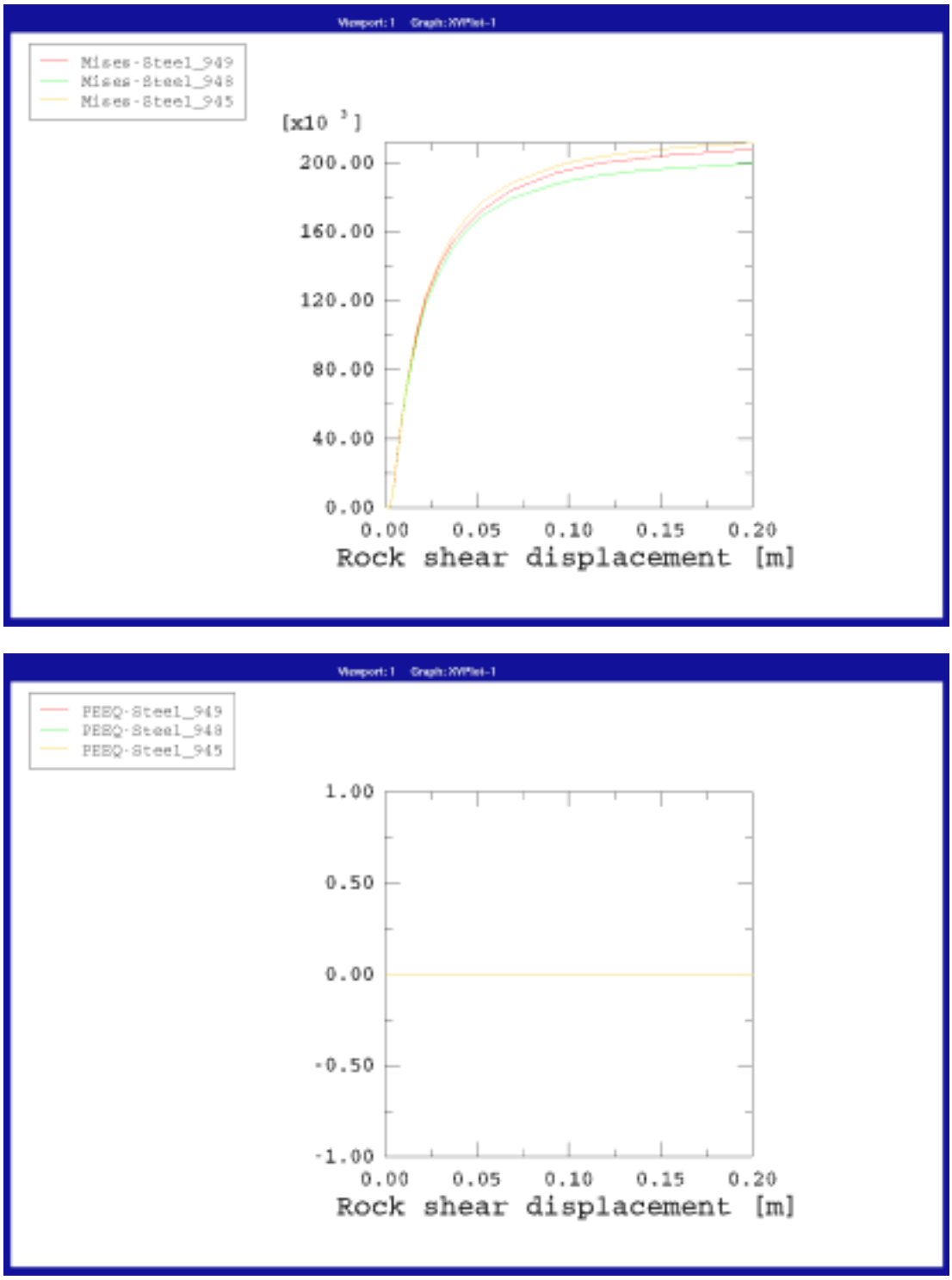

Figure A4-6. *Mises stress (kPa) (upper) and plastic strain (lower) as function of the rock shear displacement (m) for three elements located in the most stressed section. Element 945 is located in the axial symmetry plane while elements 948 and 949 are located in more peripheral parts (see Figure A4-1).*

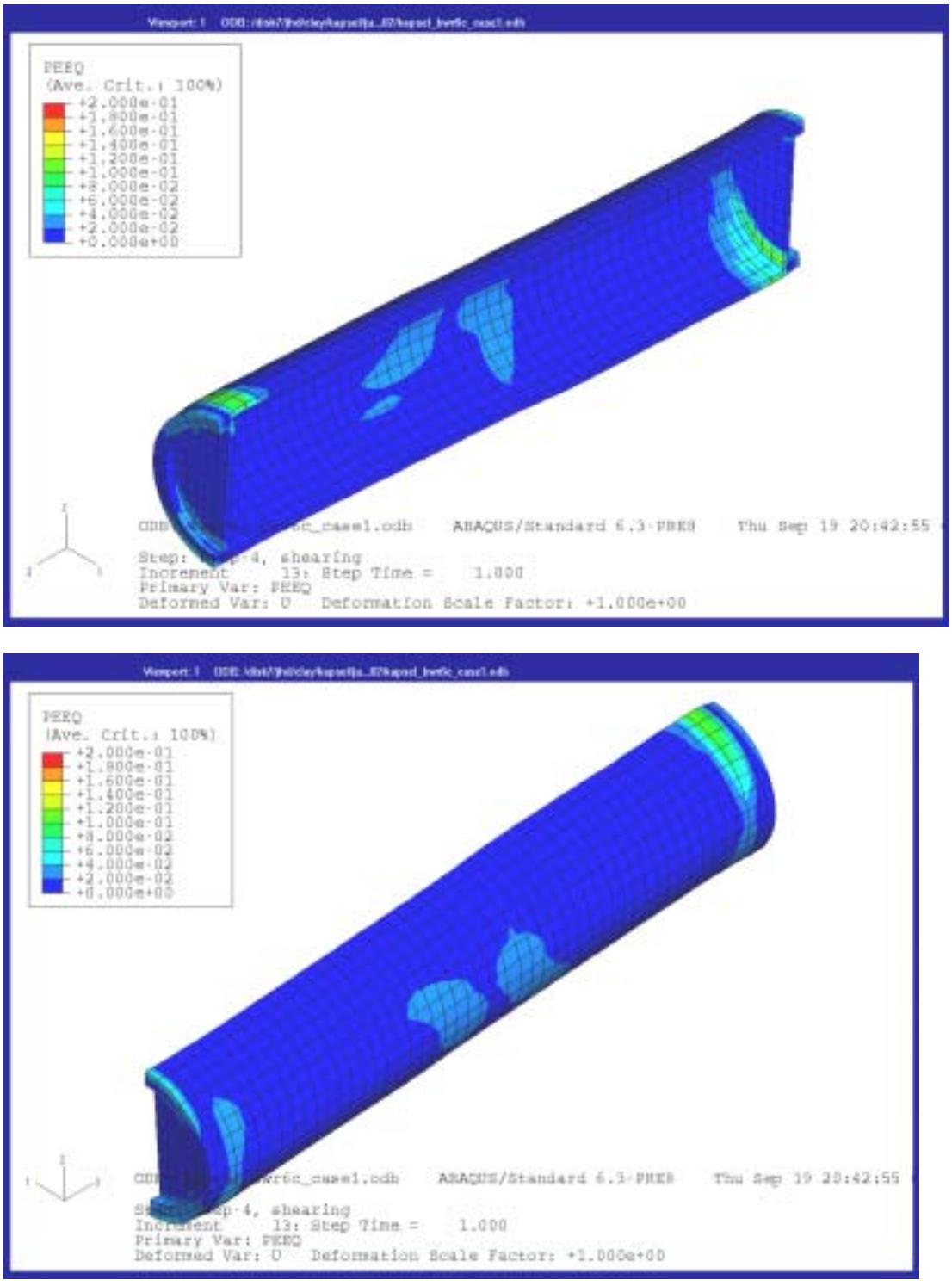

Figure A4-7. *Plastic strain in the copper canister after 20 cm rock displacement.*

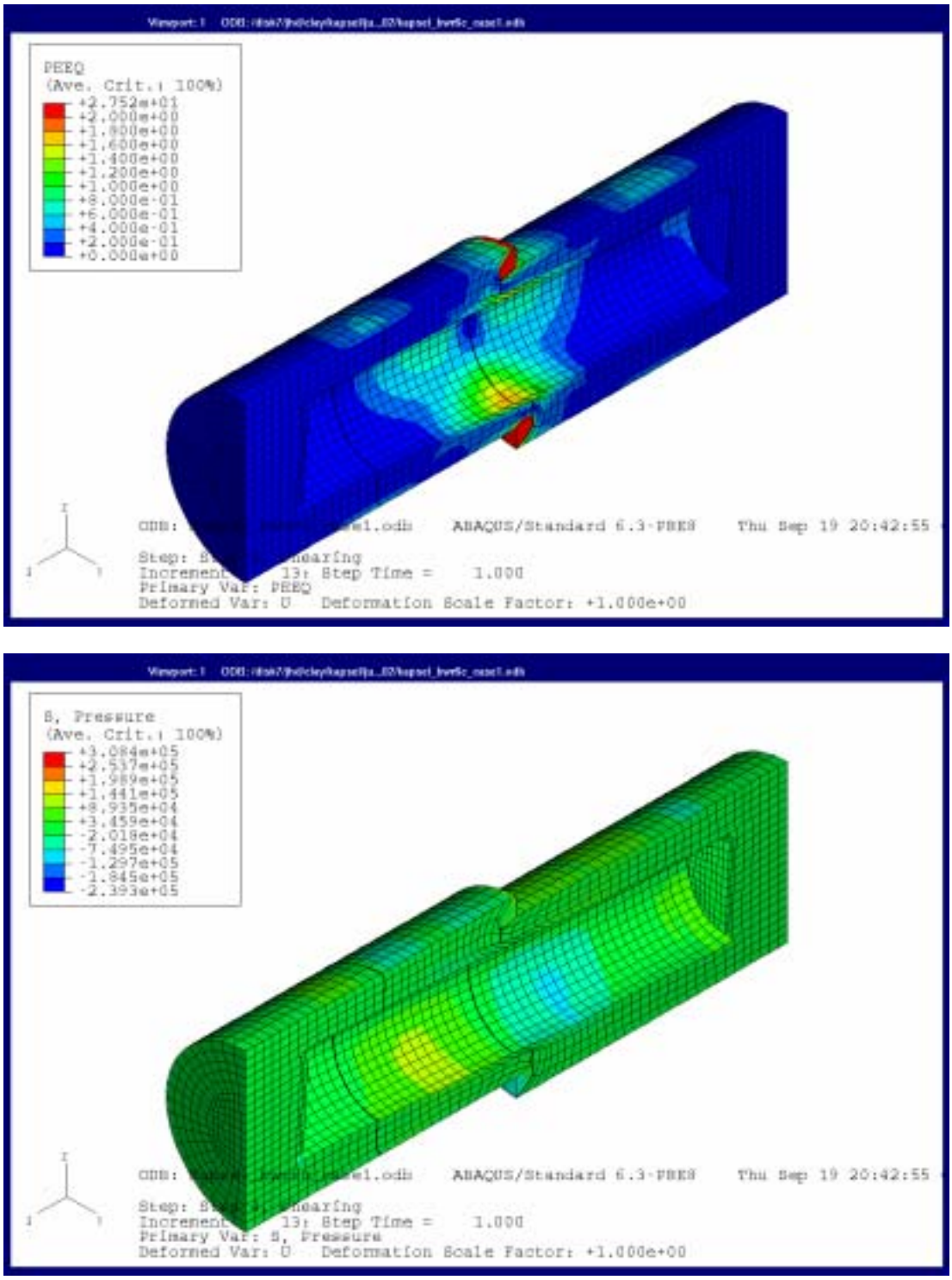

Figure A4-8. *Plastic strain (upper) and average stress (kPa pressure) (lower) in the bentonite buffer after 20 cm rock displacement.*

Appendix 5

Calculation *6c_case2*
Symmetric shear at the buffer density 2000 kg/m^3

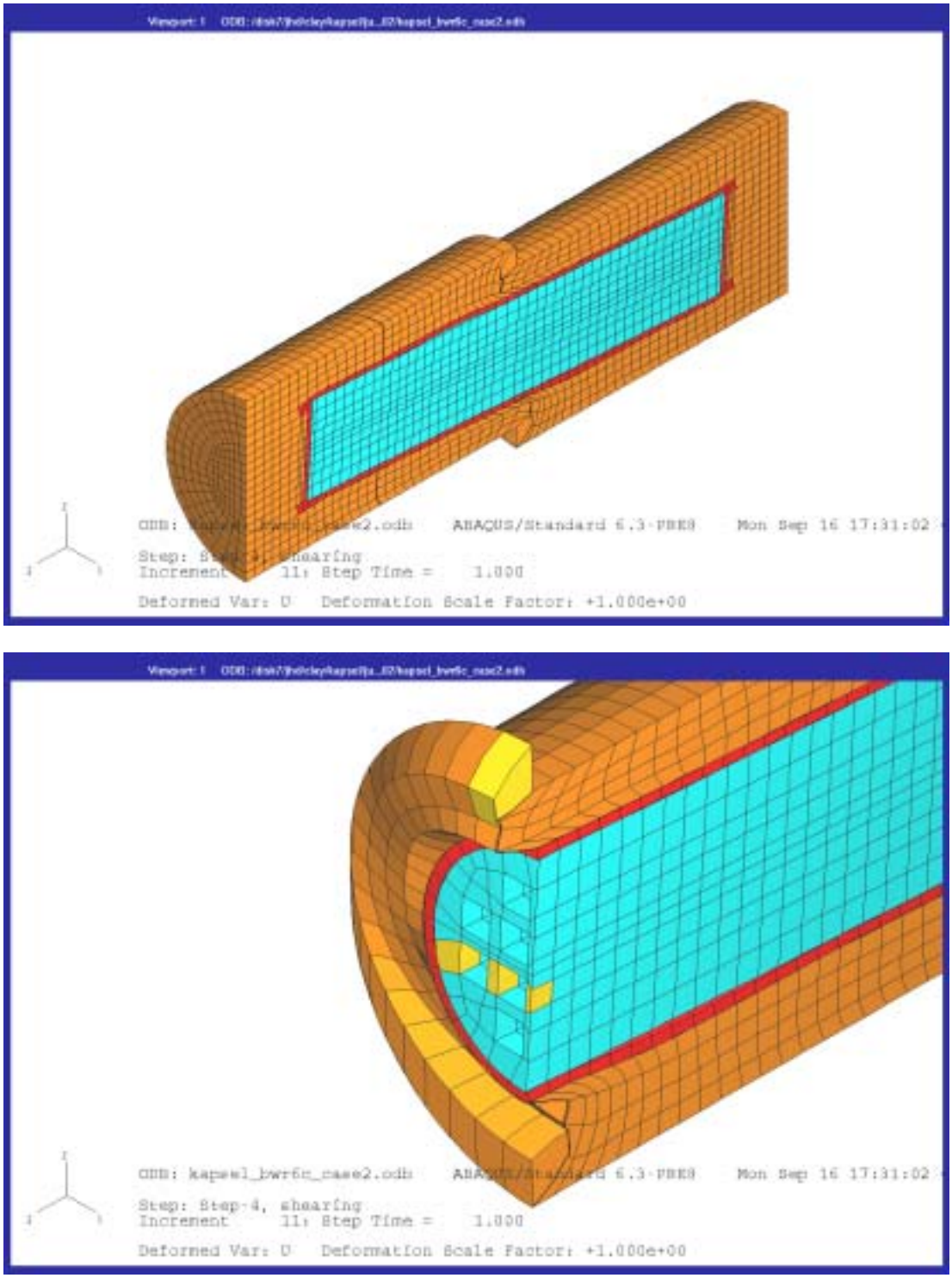

Figure A5-1. *Deformed structure after 20 cm rock displacement (upper) and a detail cut at the shear plane (lower). The three elements in the cast iron insert that are studied in more detail are marked yellow. The numbers are 945 (front element), 948 (central) and 949 (furthest element).*

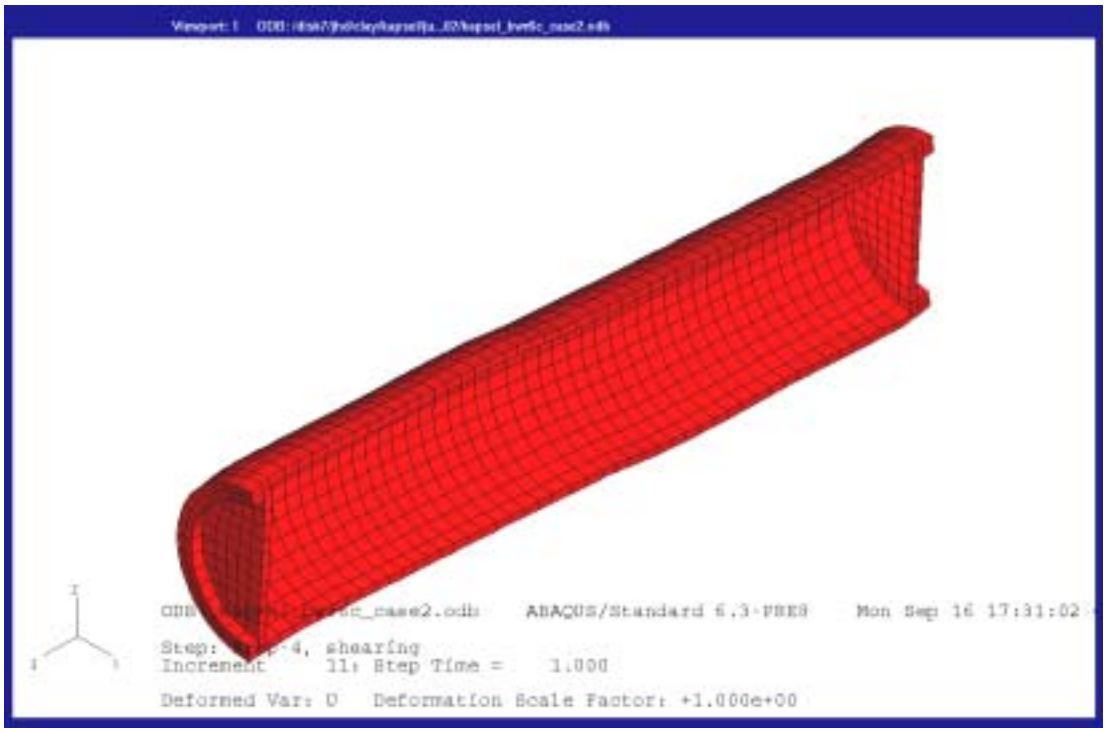

Figure A5-2. *Deformed copper canister after 20 cm rock displacement.*

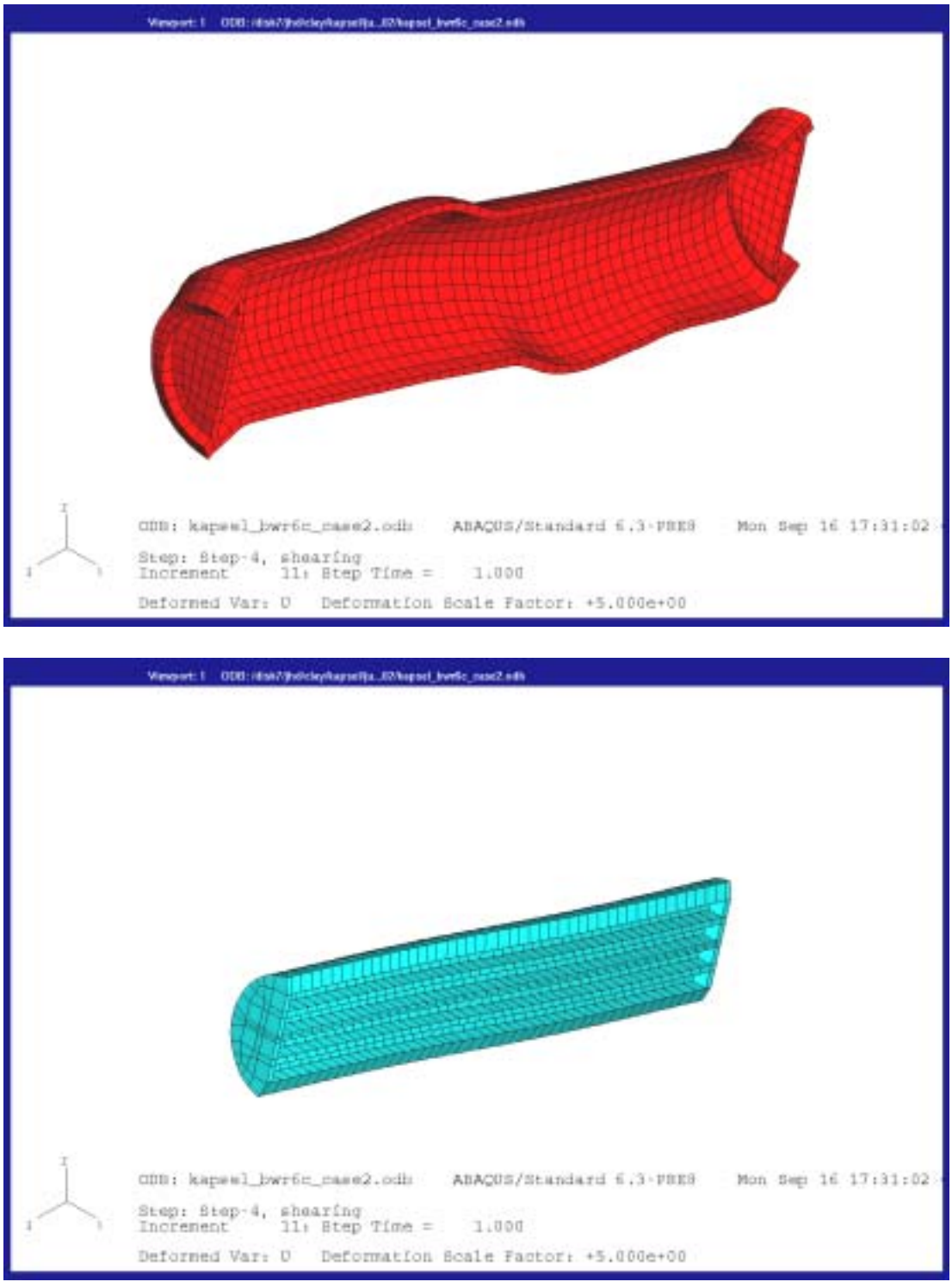

Figure A5-3. *Deformed copper canister (upper) and cast iron insert (lower) after 20 cm rock displacement with a deformation magnification factor of 5.*

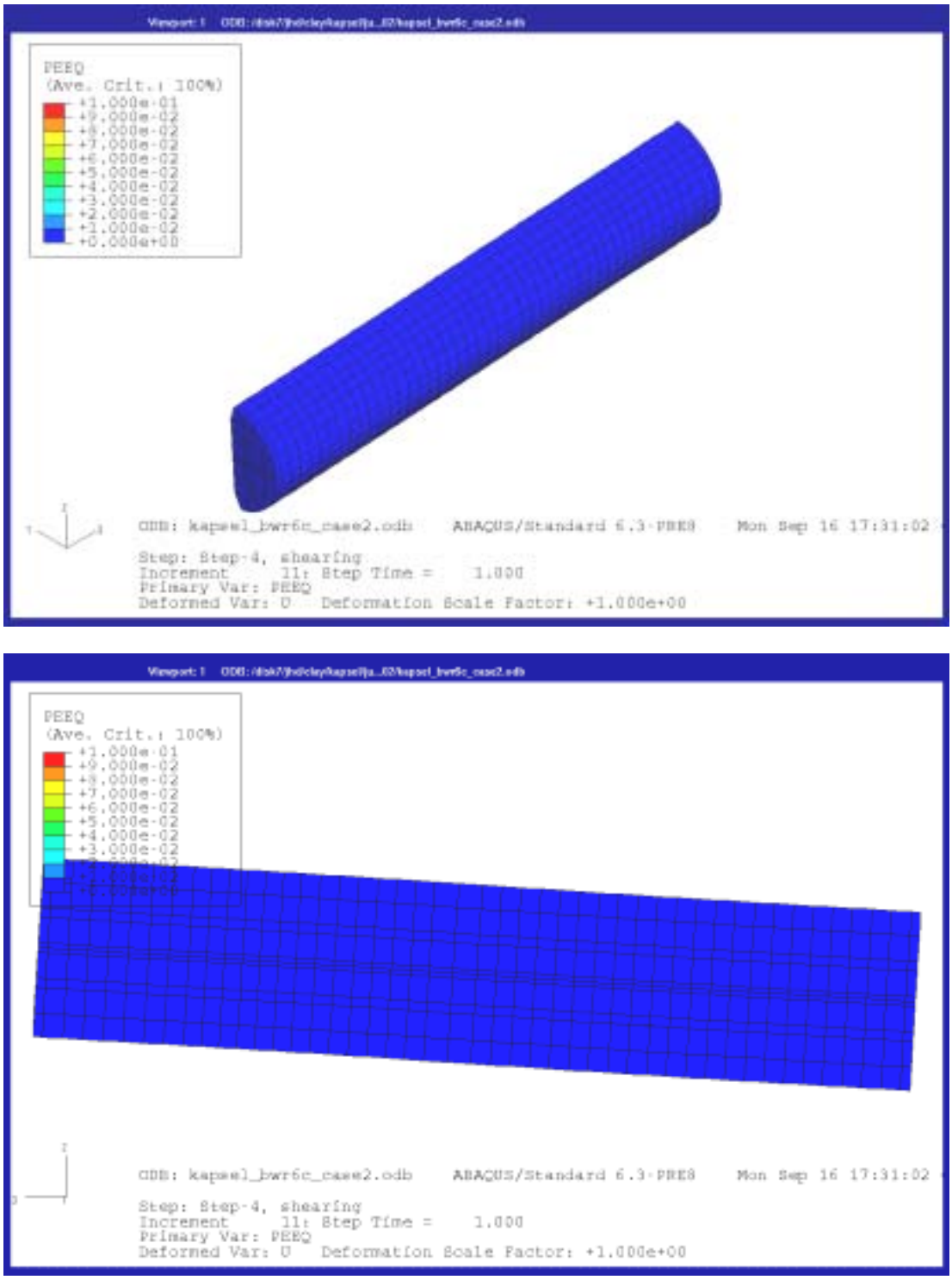

Figure A5-4. *Contour plots of the plastic strain in the cast iron insert seen from "behind" (upper) and straight "from the front" (lower) after 20 cm rock displacement. The shear plane is located in the centre.*

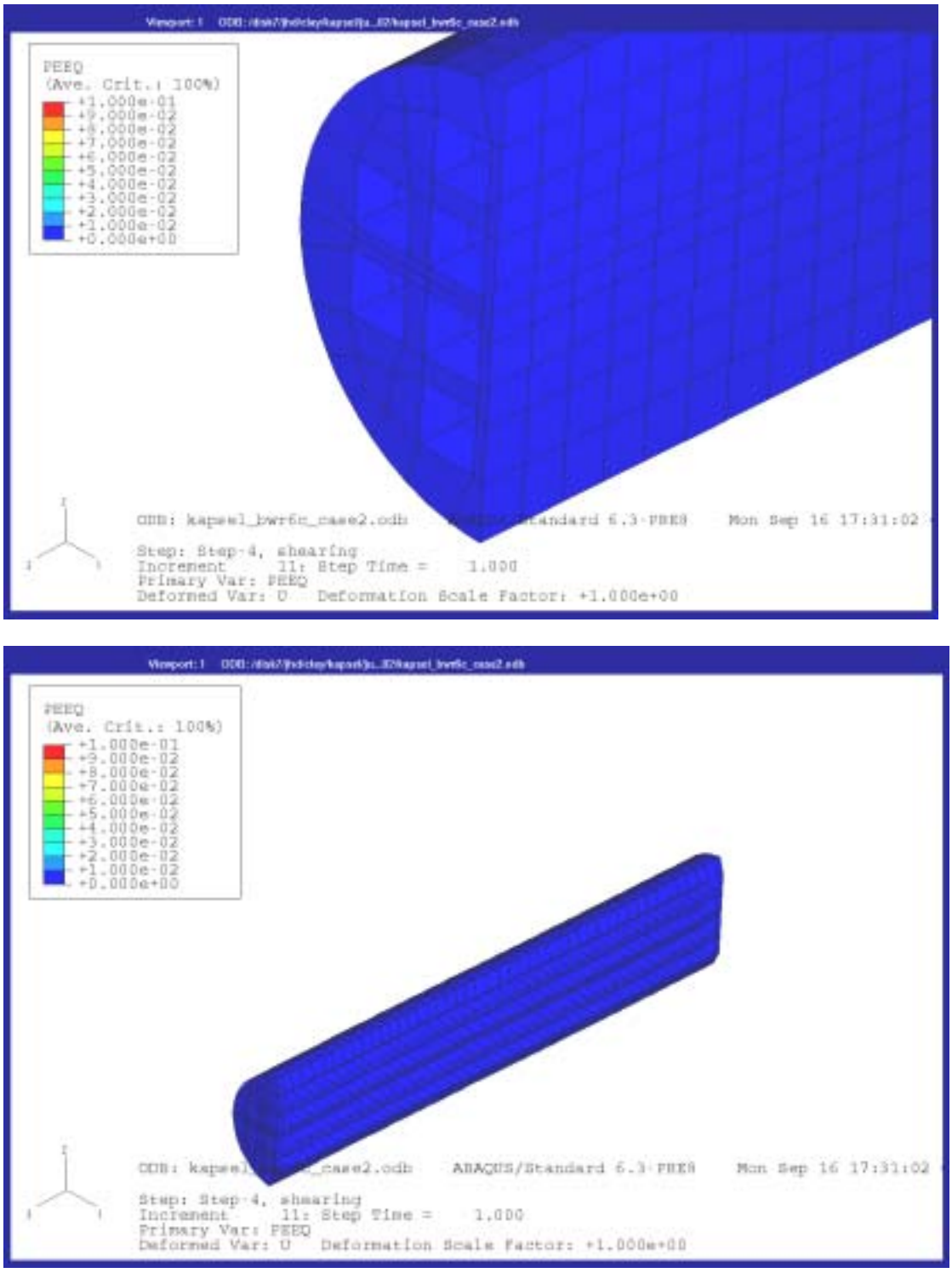

Figure A5-5. *Plastic strain in the cast iron insert after 20 cm rock displacement at a section cut perpendicular to the axis in the most stressed part (upper) and parallel to the axis (lower).*

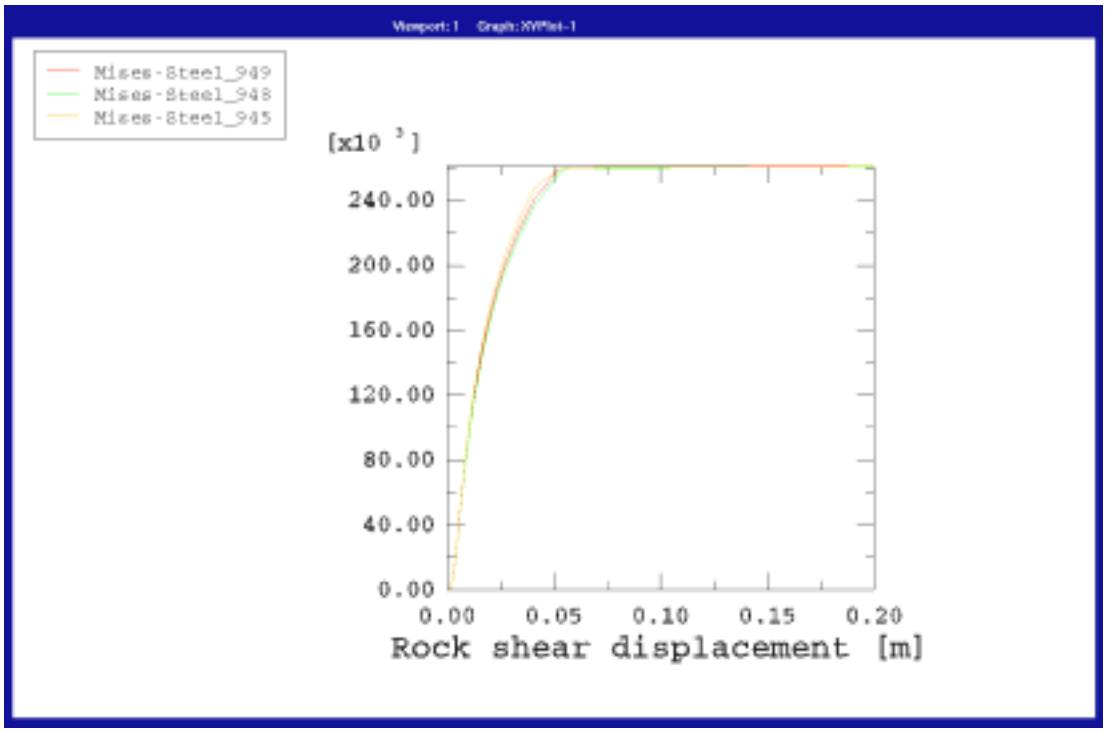

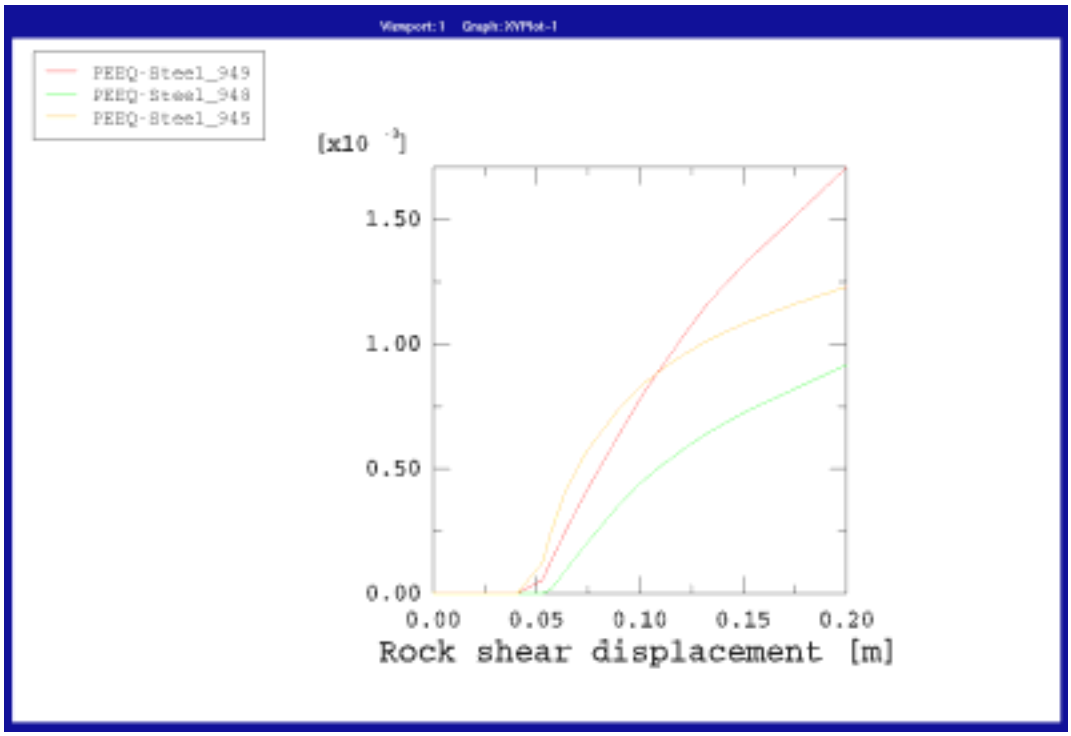

Figure A5-6. *Mises stress (kPa) (upper) and plastic strain (lower) as function of the rock shear displacement (m) for three elements located in the most stressed section. Element 945 is located in the axial symmetry plane while elements 948 and 949 are located in more peripheral parts (see Figure A4-1).*

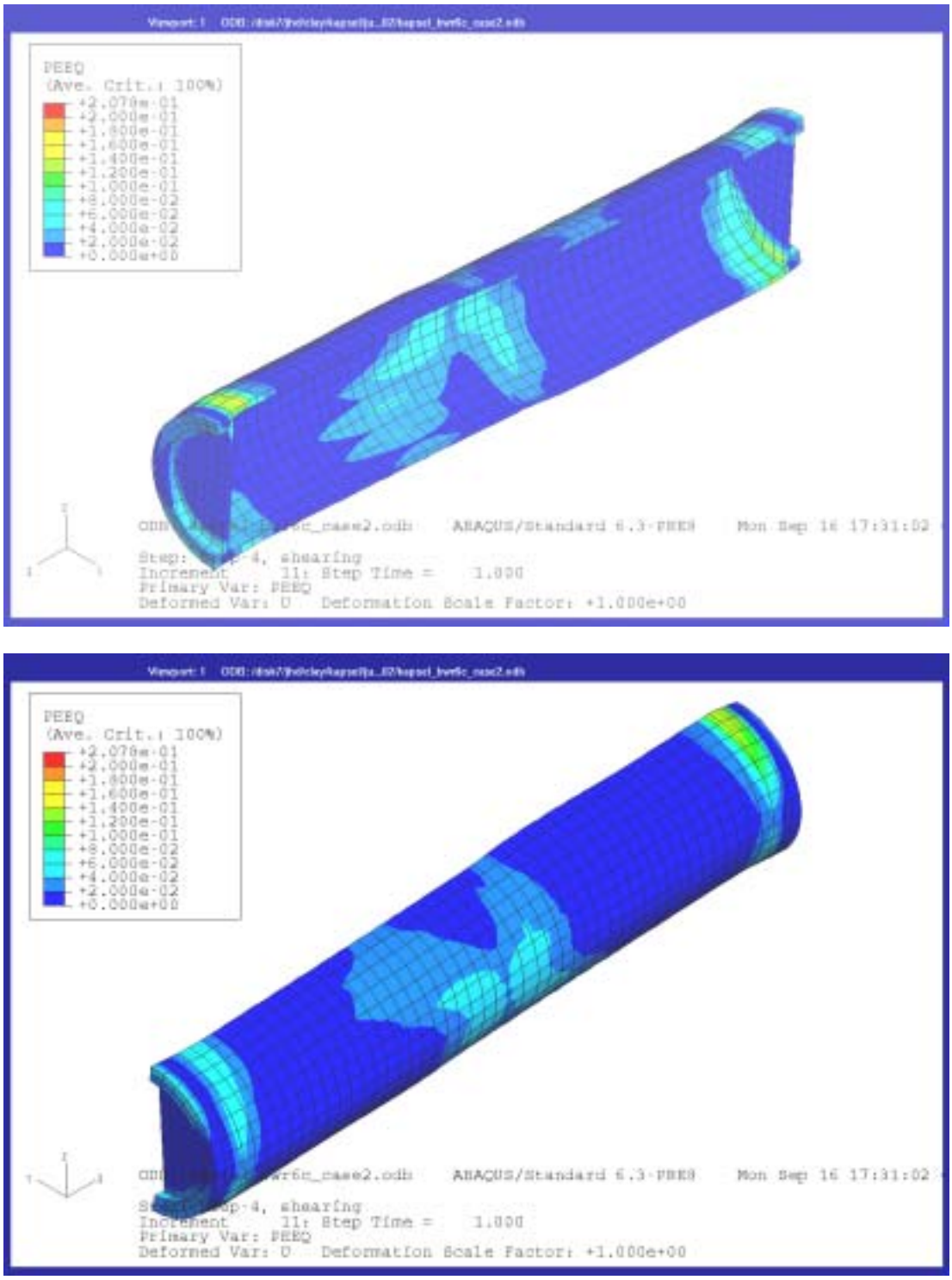

Figure A5-7. *Plastic strain in the copper canister after 20 cm rock displacement.*

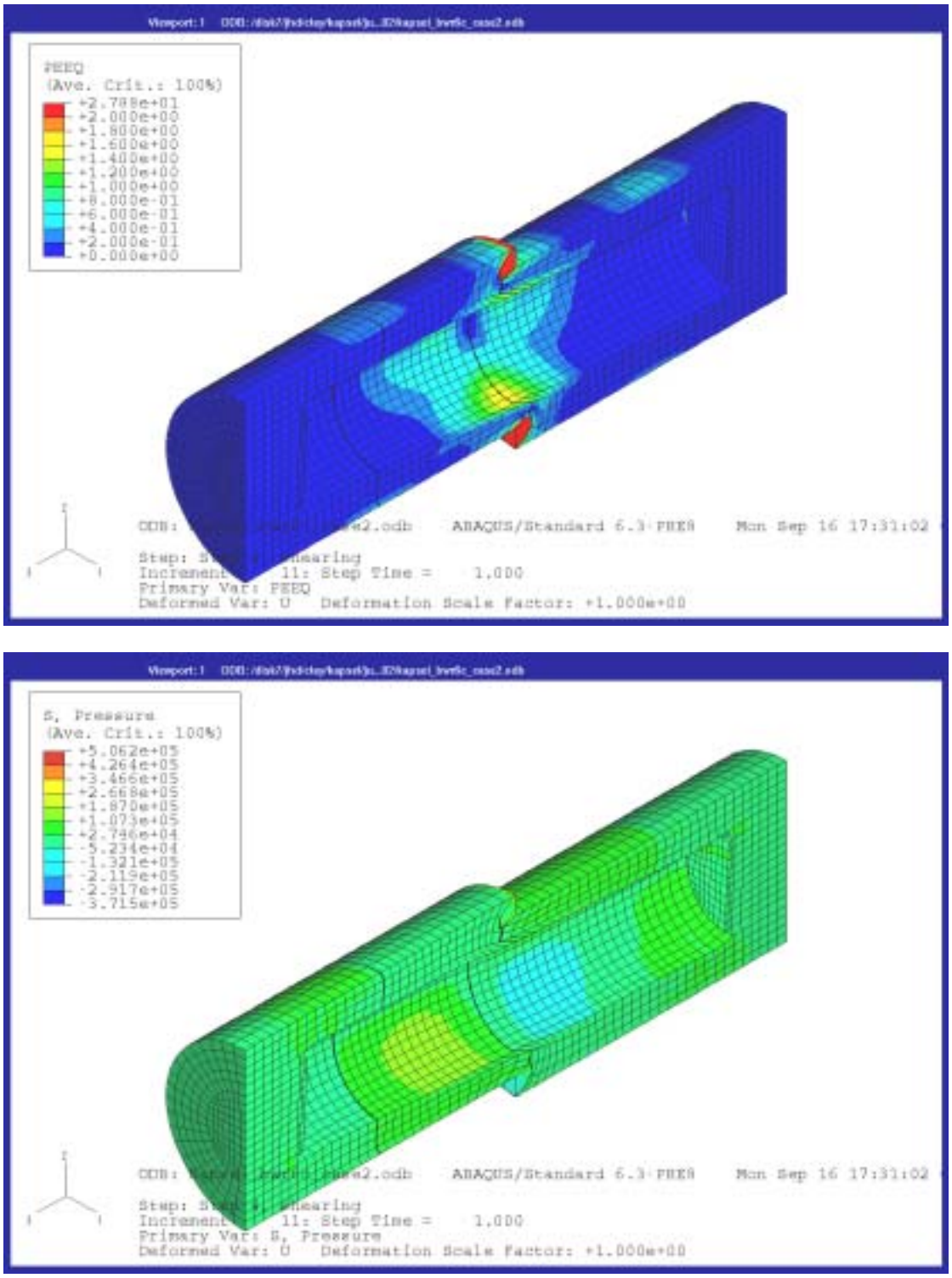

Figure A5-8. *Plastic strain (upper) and average stress (kPa pressure) (lower) in the bentonite buffer after 20 cm rock displacement.*

Appendix 6

Calculation *6c_case3*
Symmetric shear at the buffer density 2050 kg/m^3

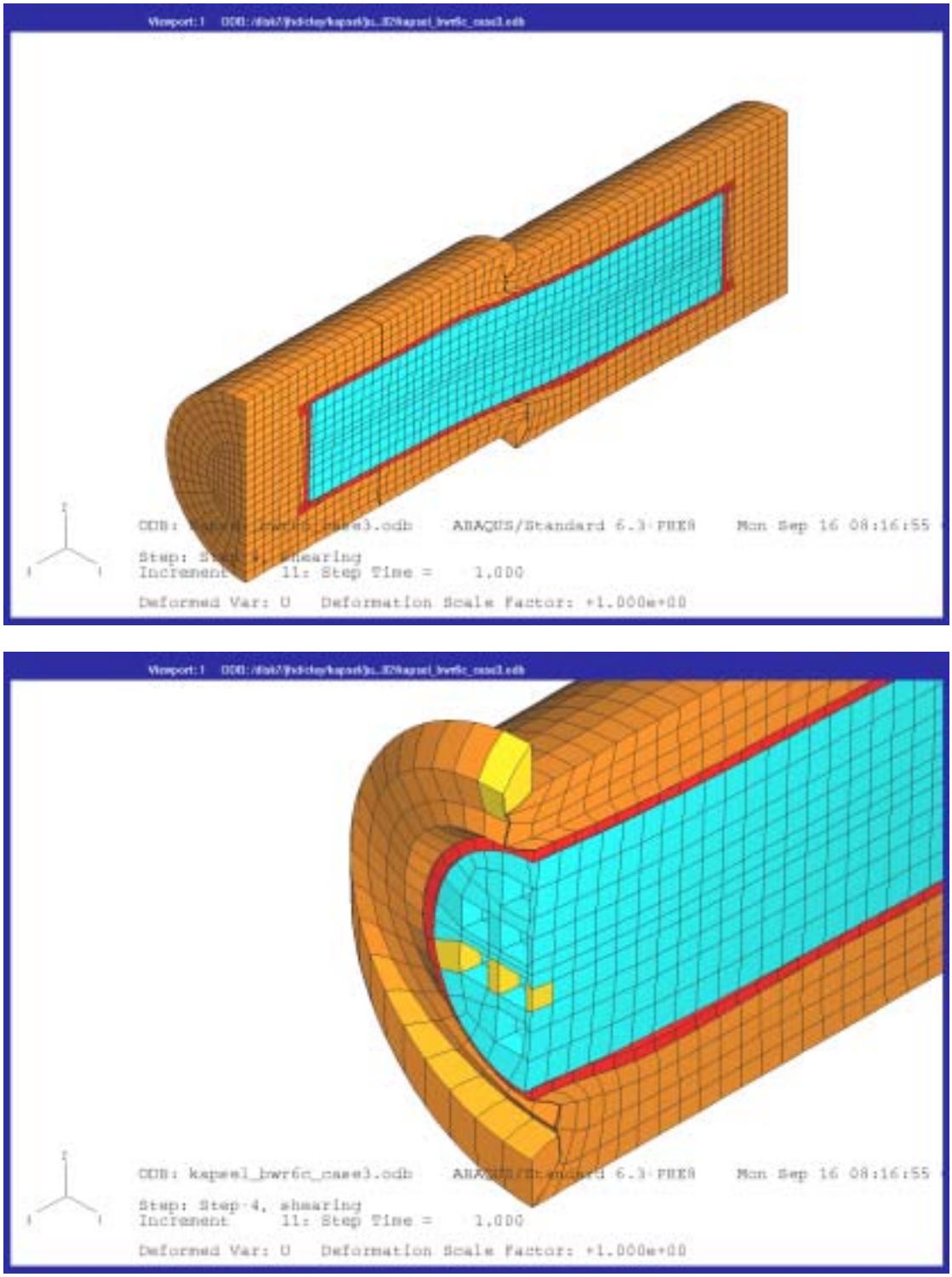

Figure A6-1. *Deformed structure after 20 cm rock displacement (upper) and a detail cut at the shear plane (lower). The three elements in the cast iron insert that are studied in more detail are marked yellow. The numbers are 945 (front element), 948 (central) and 949 (furthest element).*

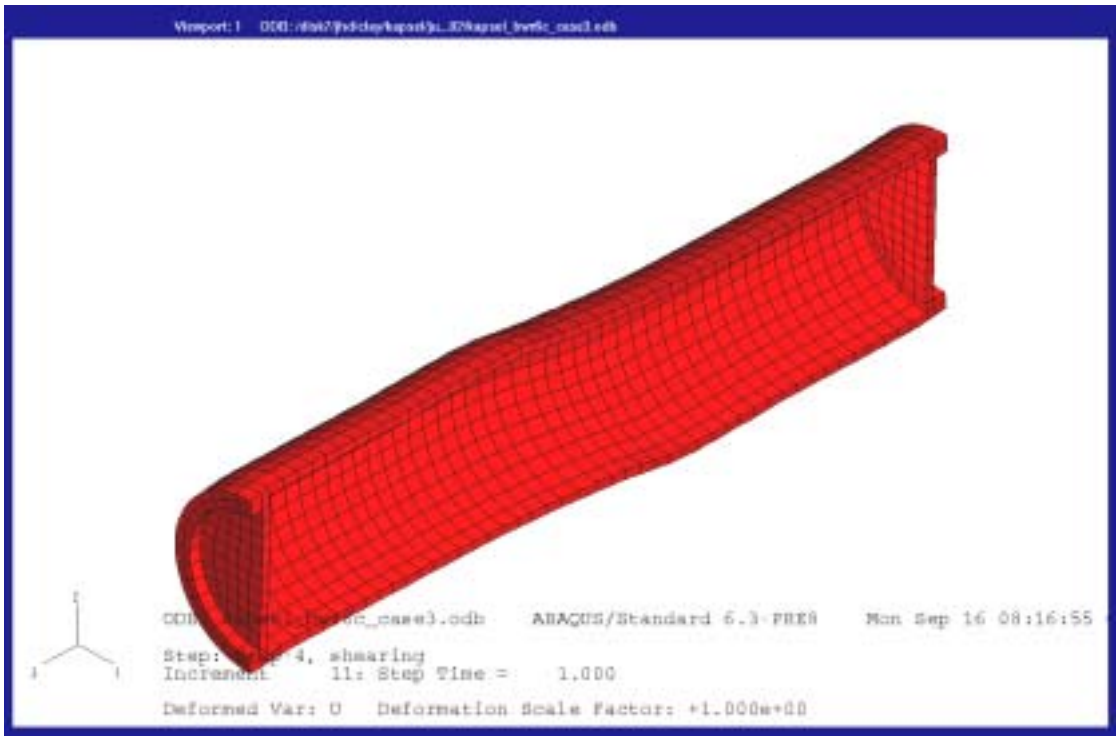

Figure A6-2. *Deformed copper canister after 20 cm rock displacement.*

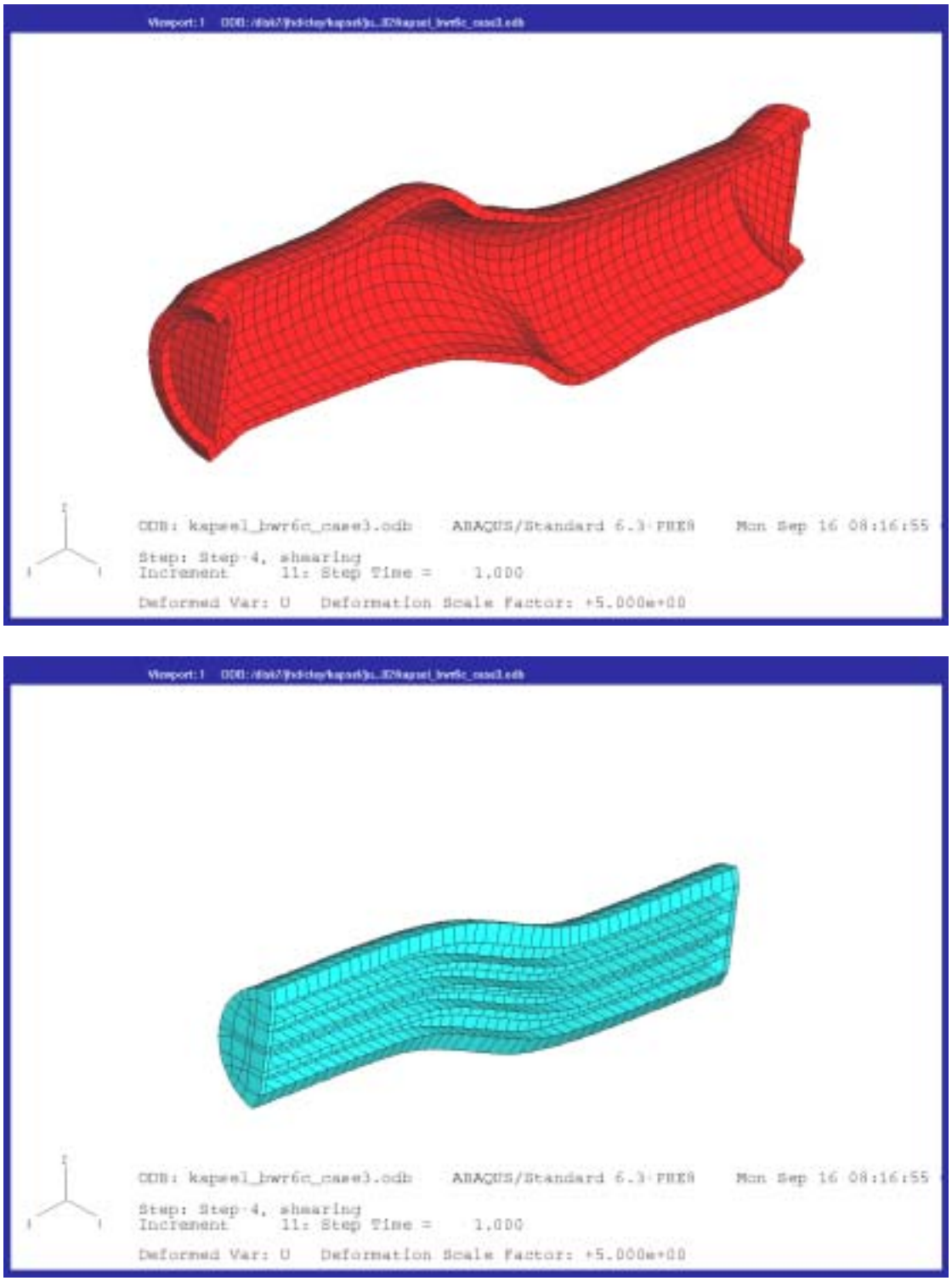

Figure A6-3. *Deformed copper canister (upper) and cast iron insert (lower) after 20 cm rock displacement with a deformation magnification factor of 5.*

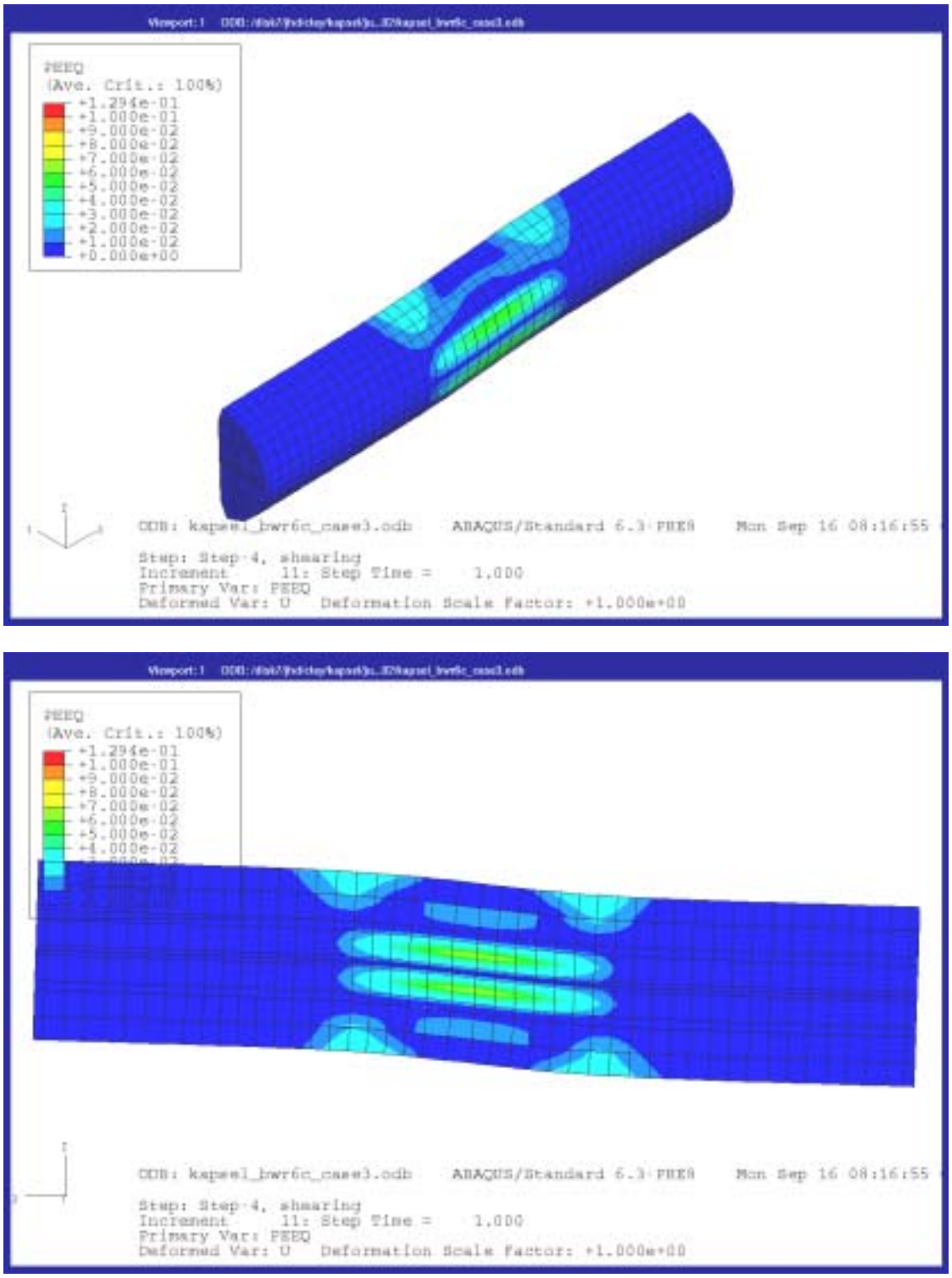

Figure A6-4. *Contour plots of the plastic strain in the cast iron insert seen from "behind" (upper) and straight "from the front" (lower) after 20 cm rock displacement. The shear plane is located 8 elements from the left side in the lower figure.*

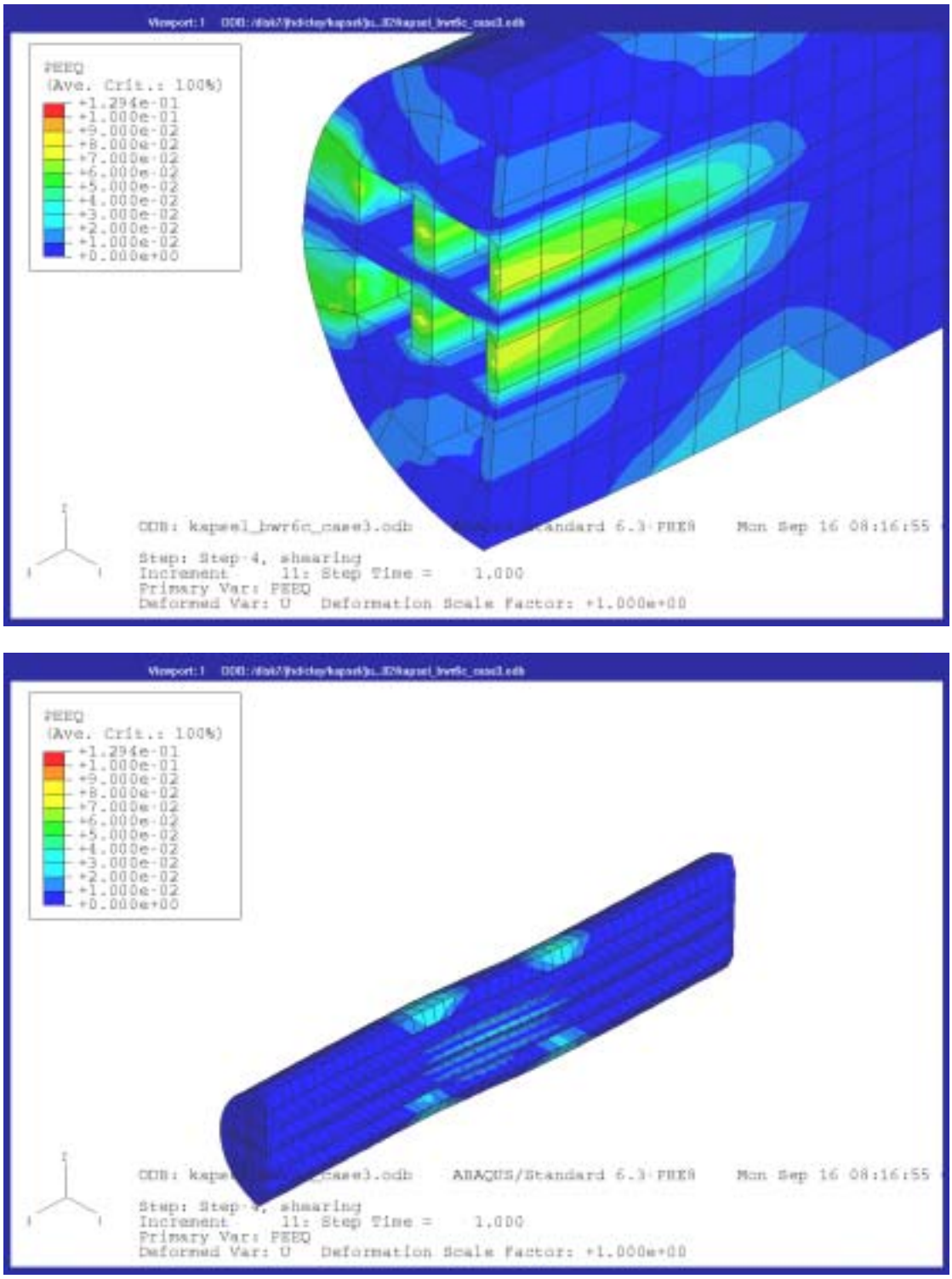

Figure A6-5. *Plastic strain in the cast iron insert after 20 cm rock displacement at a section cut perpendicular to the axis in the most stressed part (upper) and parallel to the axis (lower).*

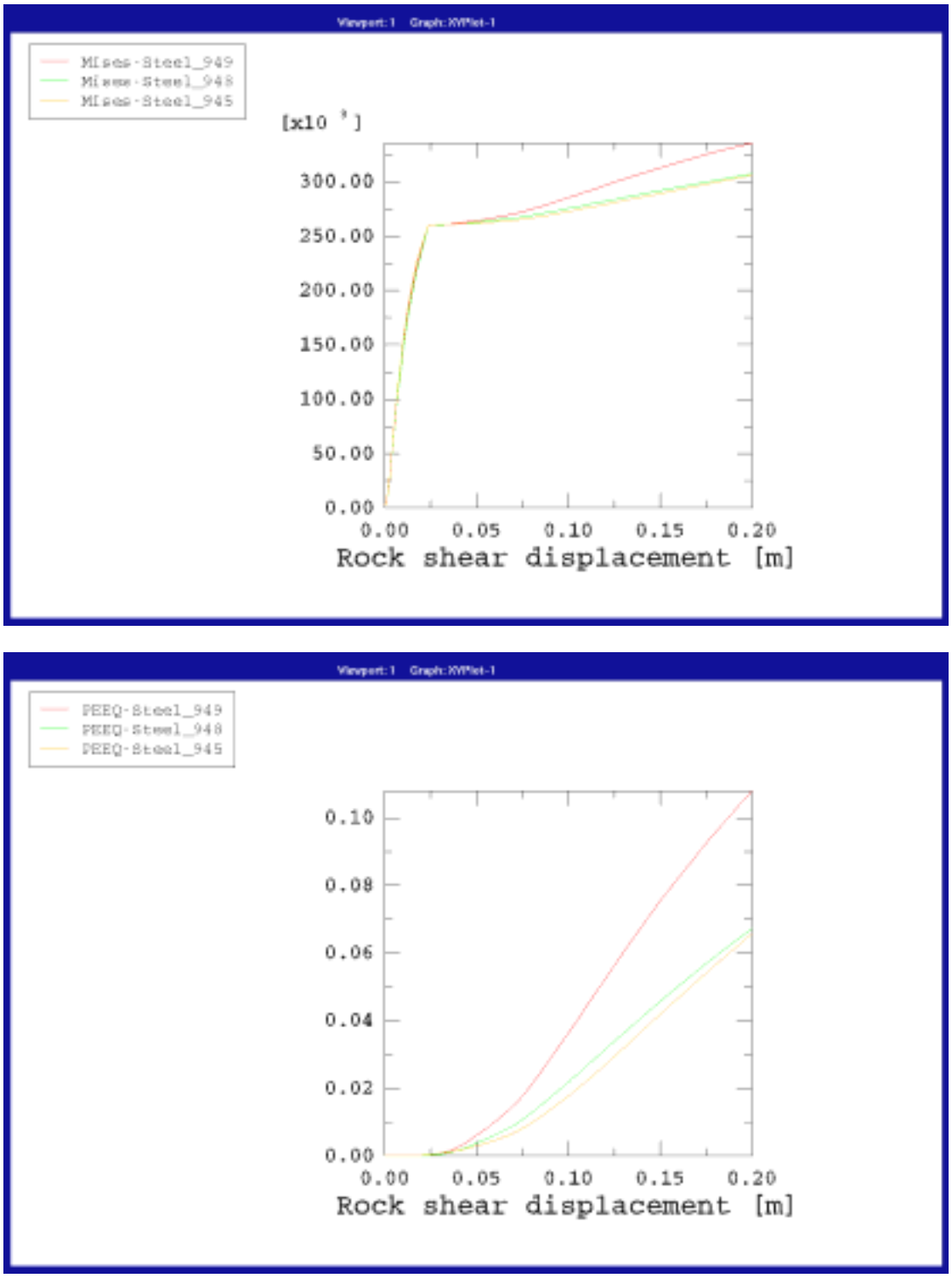

Figure A6-6. *Mises stress (kPa) (upper) and plastic strain (lower) as function of the rock shear displacement (m) for three elements located in the most stressed section. Element 945 is located in the axial symmetry plane while elements 948 and 949 are located in more peripheral parts (see Figure A3-1).*

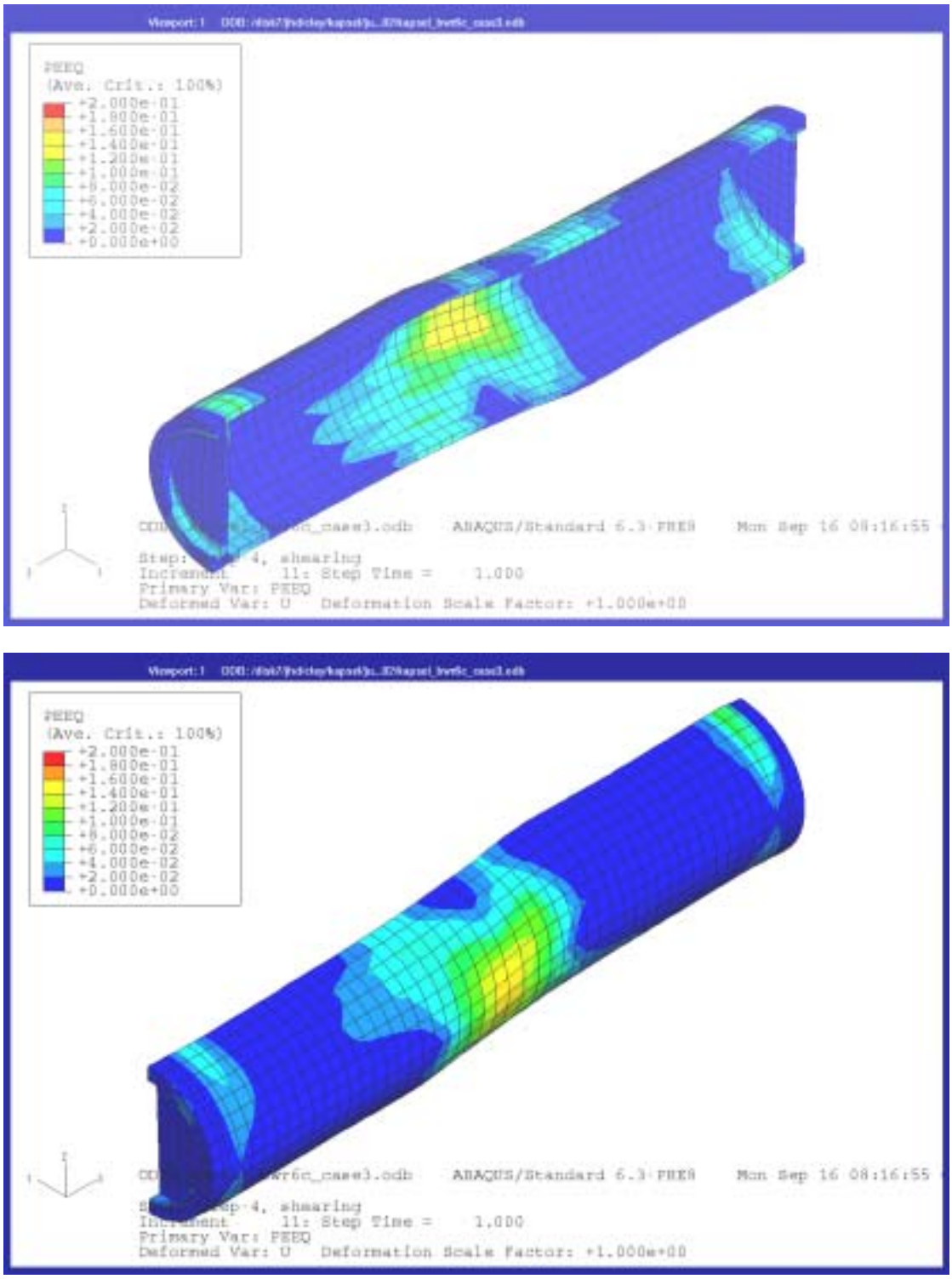

Figure A6-7. *Plastic strain in the copper canister after 20 cm rock displacement.*

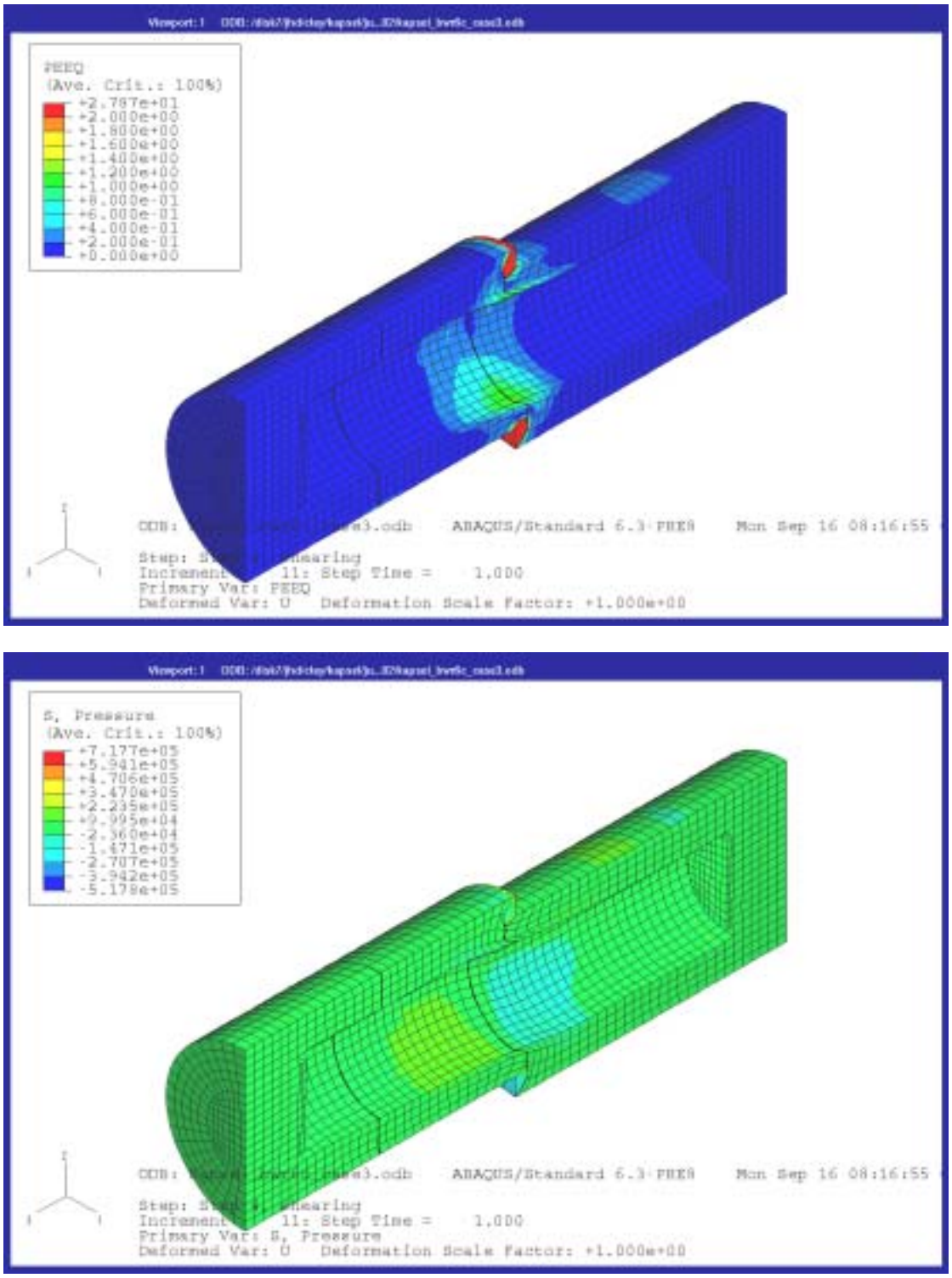

Figure A6-8. *Plastic strain (upper) and average stress (kPa pressure) (lower) in the bentonite buffer after 20 cm rock displacement.*

Appendix 7

Calculation *6c_case4*
Symmetric shear at the buffer density 2010 kg/m^3

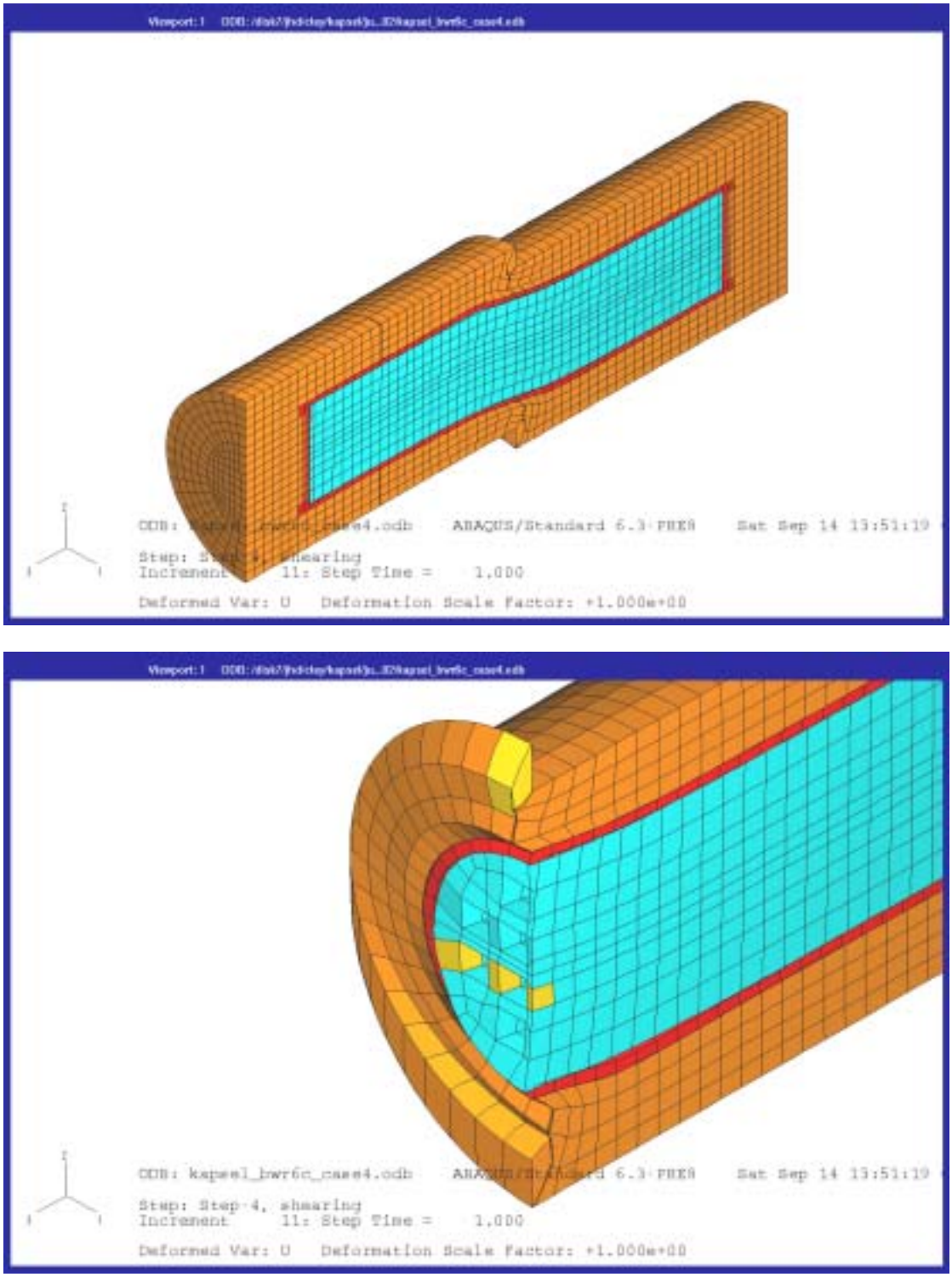

Figure A7-1. *Deformed structure after 20 cm rock displacement (upper) and a detail cut at the shear plane (lower). The three elements in the cast iron insert that are studied in more detail are marked yellow. The numbers are 945 (front element), 948 (central) and 949 (furthest element).*

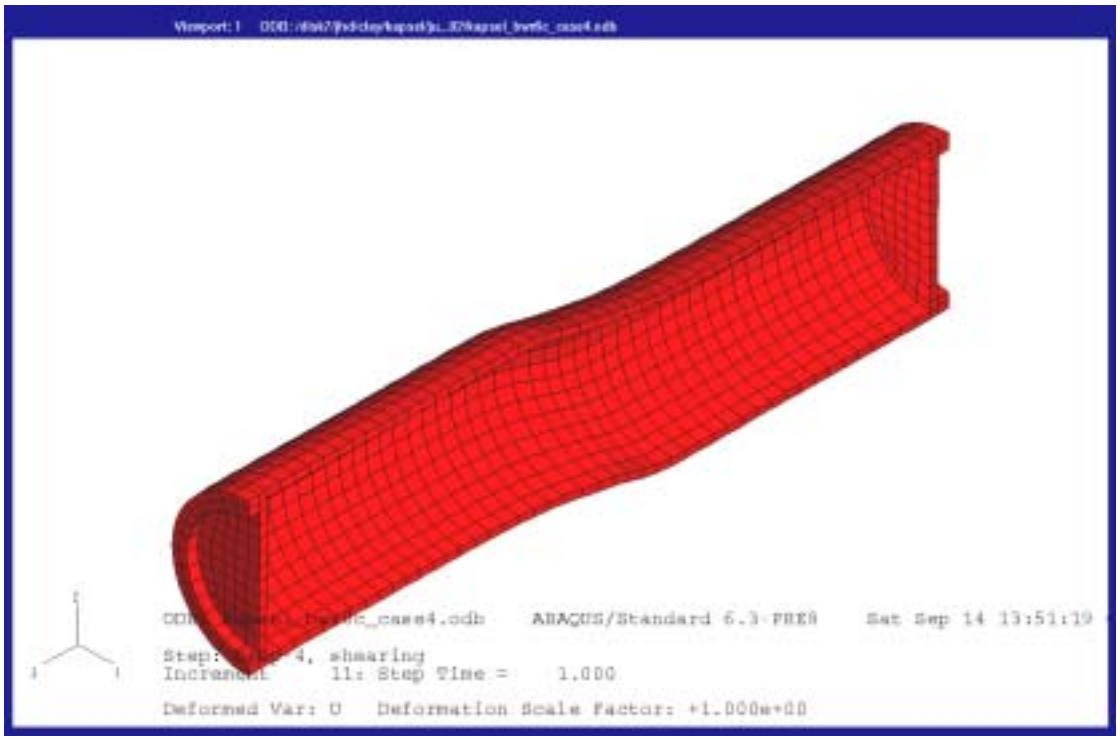

Figure A7-2. *Deformed copper canister after 20 cm rock displacement.*

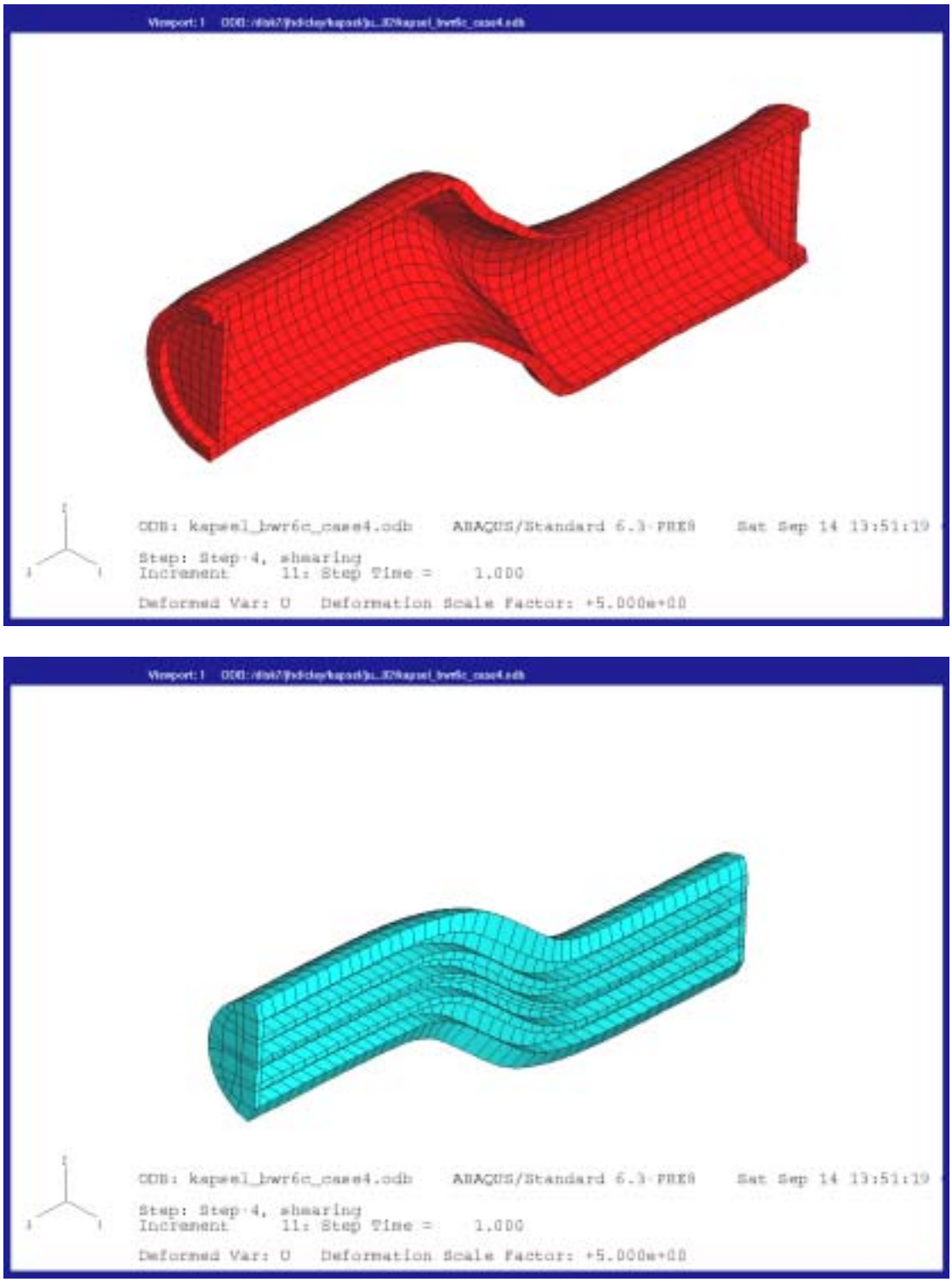

Figure A7-3. *Deformed copper canister (upper) and cast iron insert (lower) after 20 cm rock displacement with a deformation magnification factor of 5.*

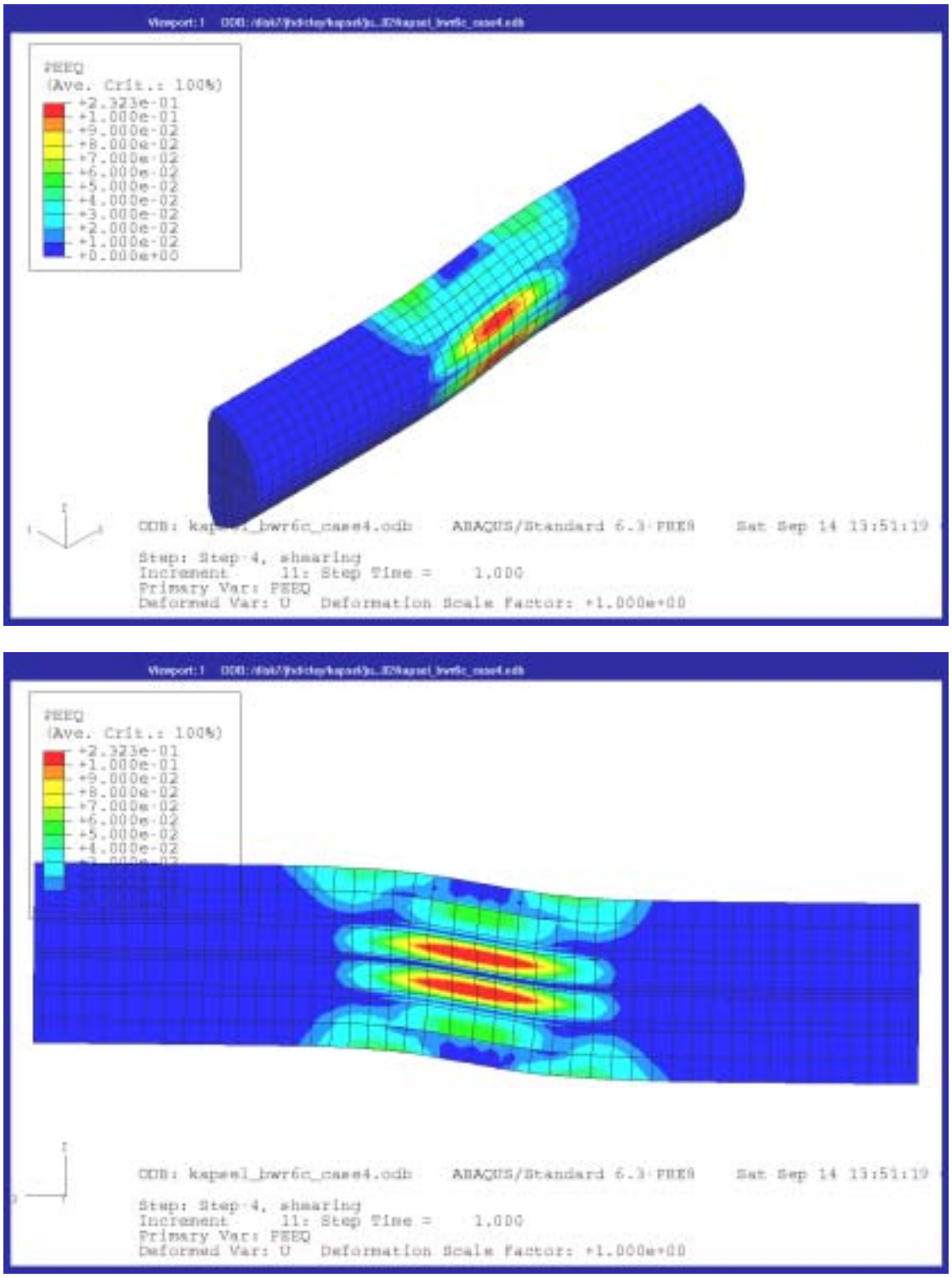

Figure A7-4. *Contour plots of the plastic strain in the cast iron insert seen from "behind" (upper) and straight "from the front" (lower) after 20 cm rock displacement. The shear plane is located 8 elements from the left side in the lower figure.*

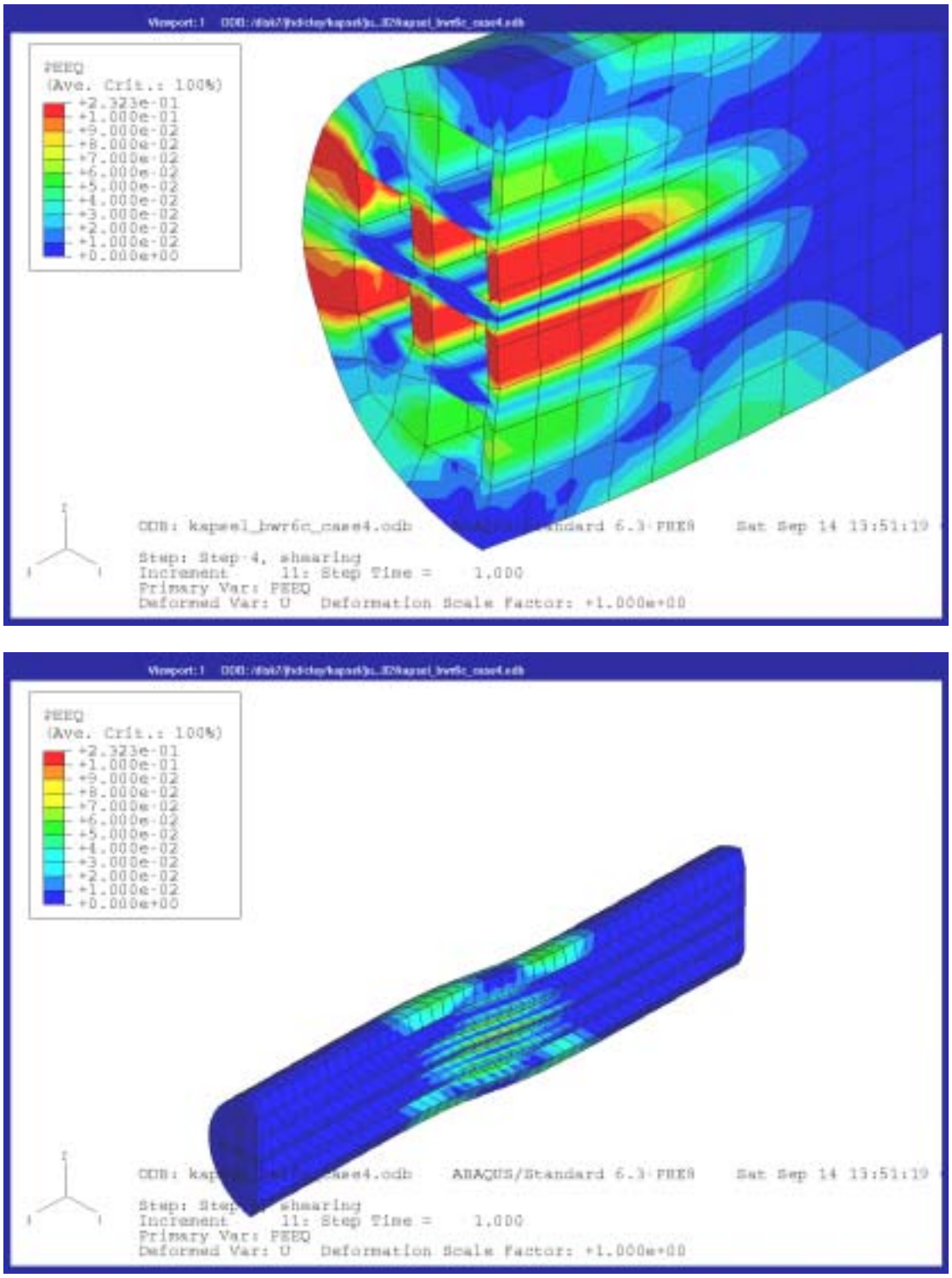

Figure A7-5. *Plastic strain in the cast iron insert after 20 cm rock displacement at a section cut perpendicular to the axis in the most stressed part (upper) and parallel to the axis (lower).*

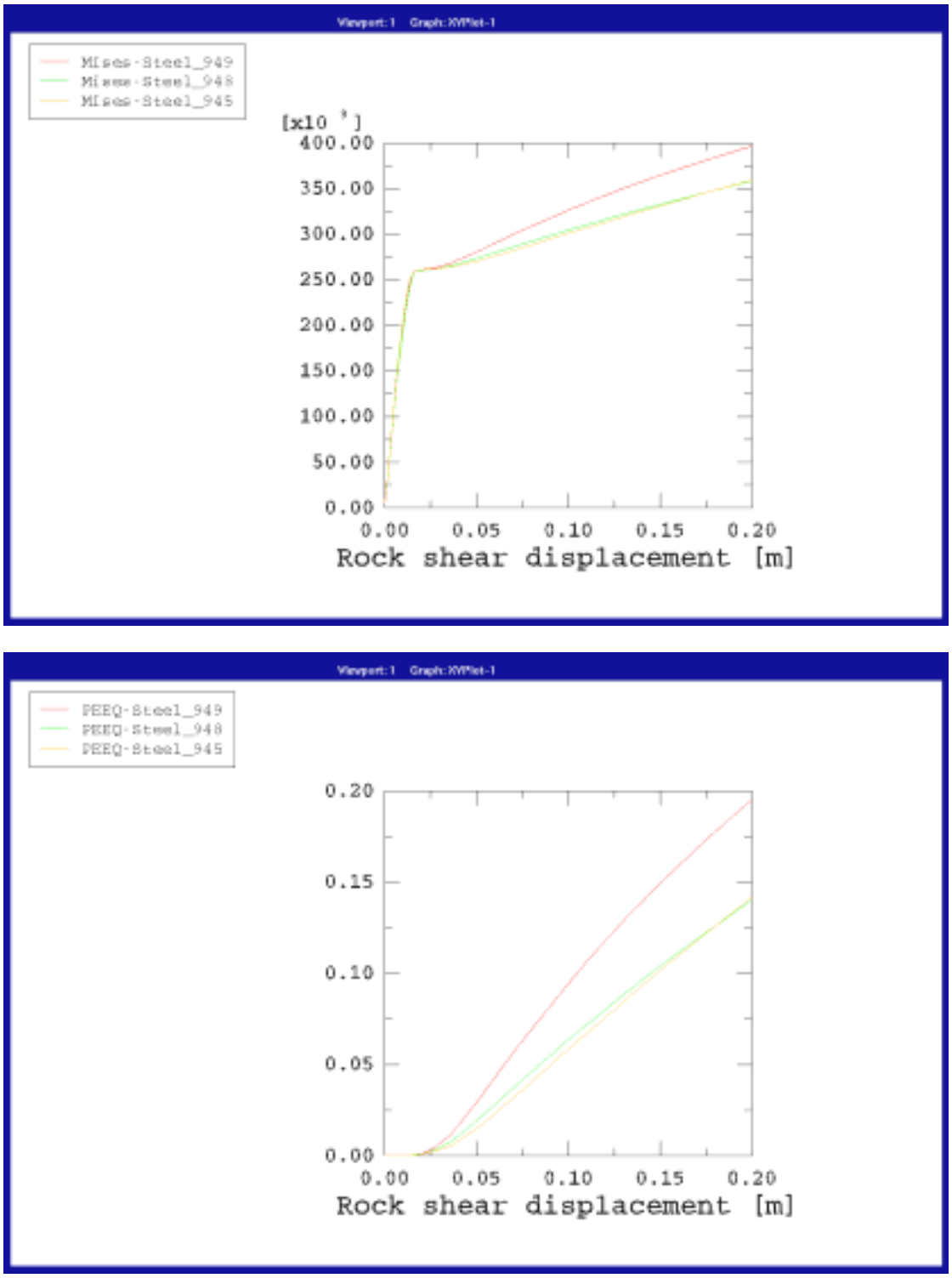

Figure A7-6. *Mises stress (kPa) (upper) and plastic strain (lower) as function of the rock shear displacement (m) for three elements located in the most stressed section. Element 945 is located in the axial symmetry plane while elements 948 and 949 are located in more peripheral parts (see Figure A7-1).*

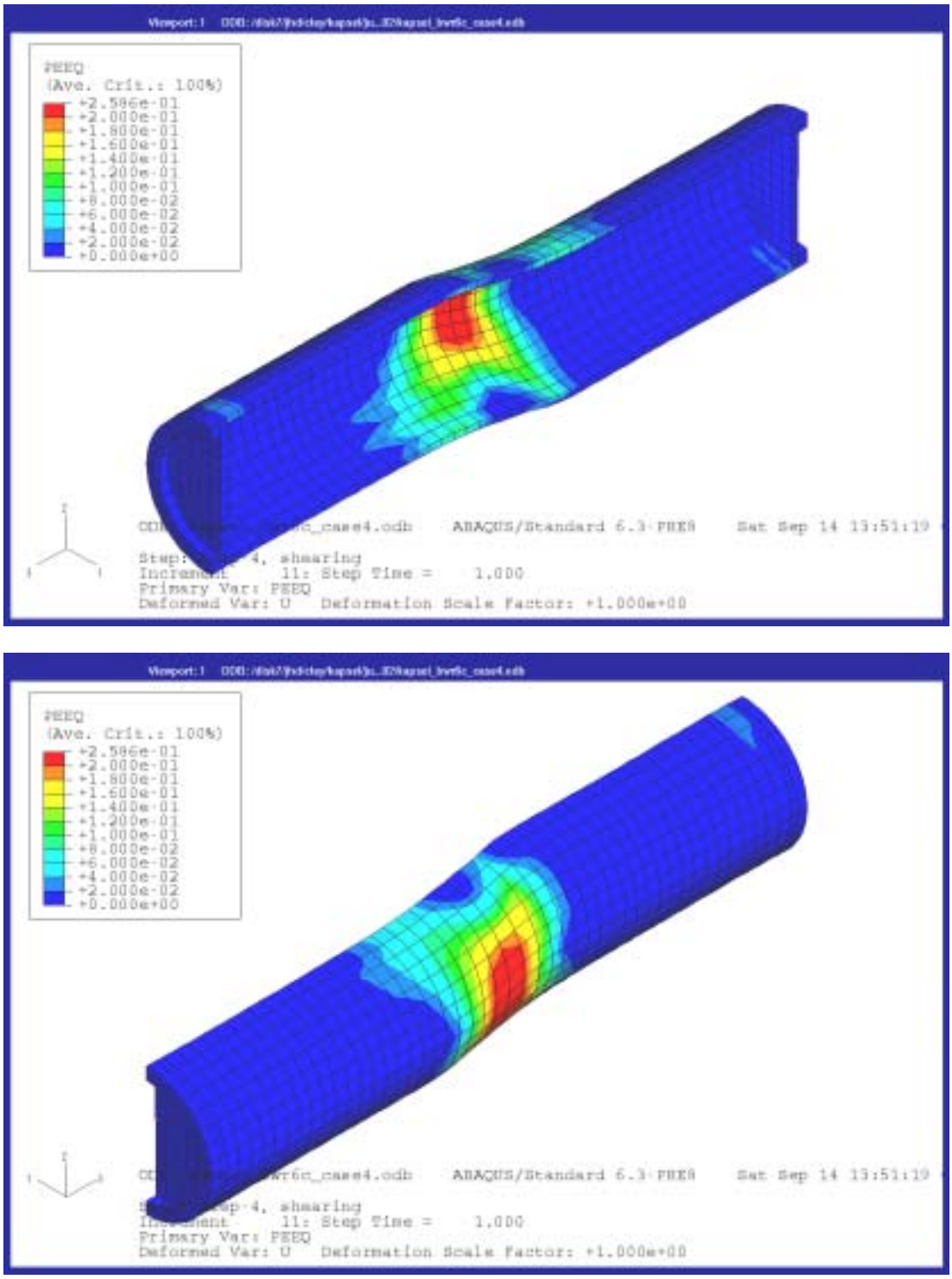

Figure A7-7. *Plastic strain in the copper canister after 20 cm rock displacement.*

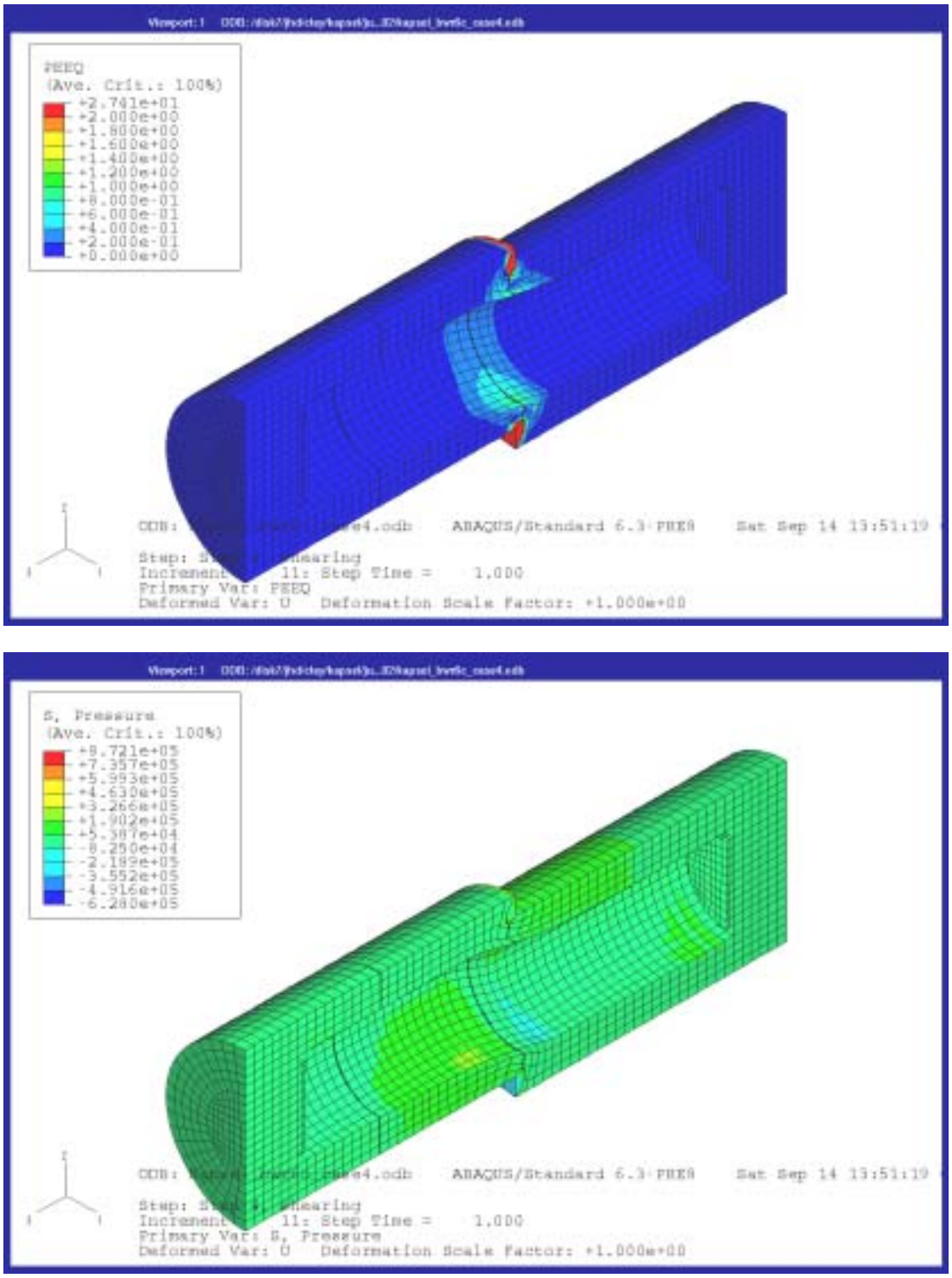

Figure A7-8. *Plastic strain (upper) and average stress (kPa pressure) (lower) in the bentonite buffer after 20 cm rock displacement.*

Appendix 8

Calculation *5b3_case2*
Asymmetric shear at the buffer density 2000 kg/m^3

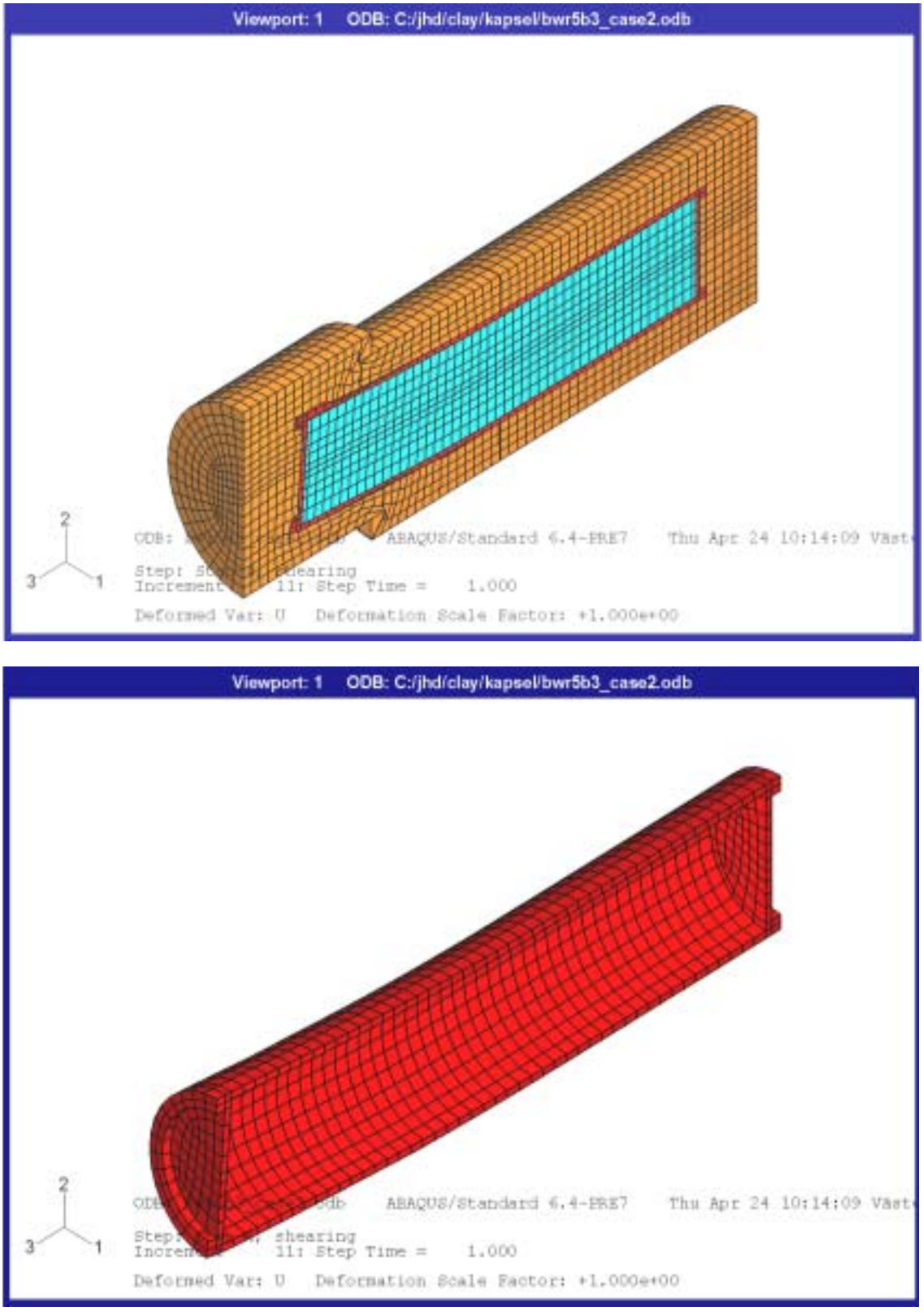

Figure A8-1. *Deformed structure after 20 cm rock displacement (upper) and the deformed copper canister (lower).*

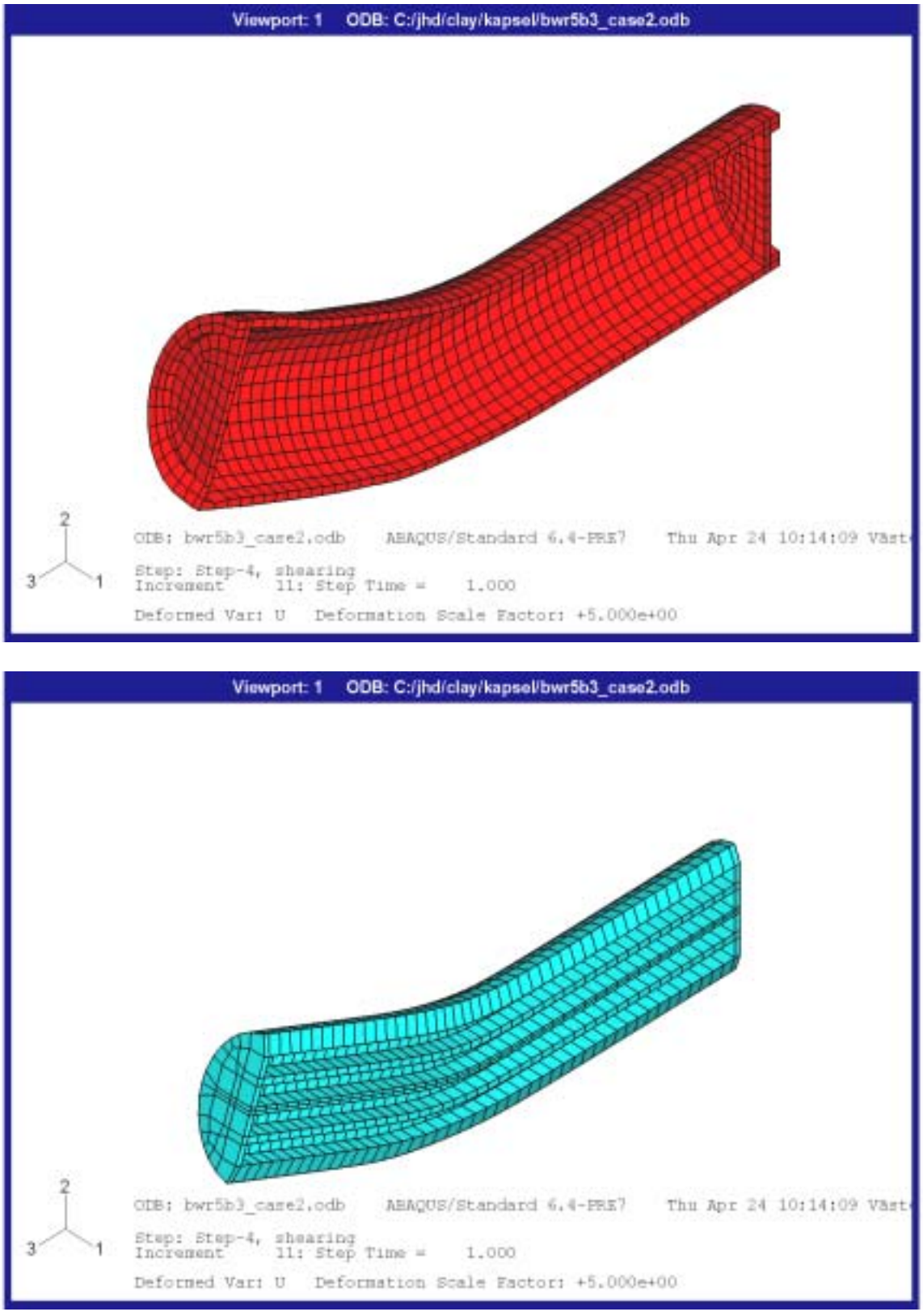

Figure A8-2. *Deformed copper canister (upper) and cast iron insert (lower) after 20 cm rock displacement with a deformation magnification factor of 5.*

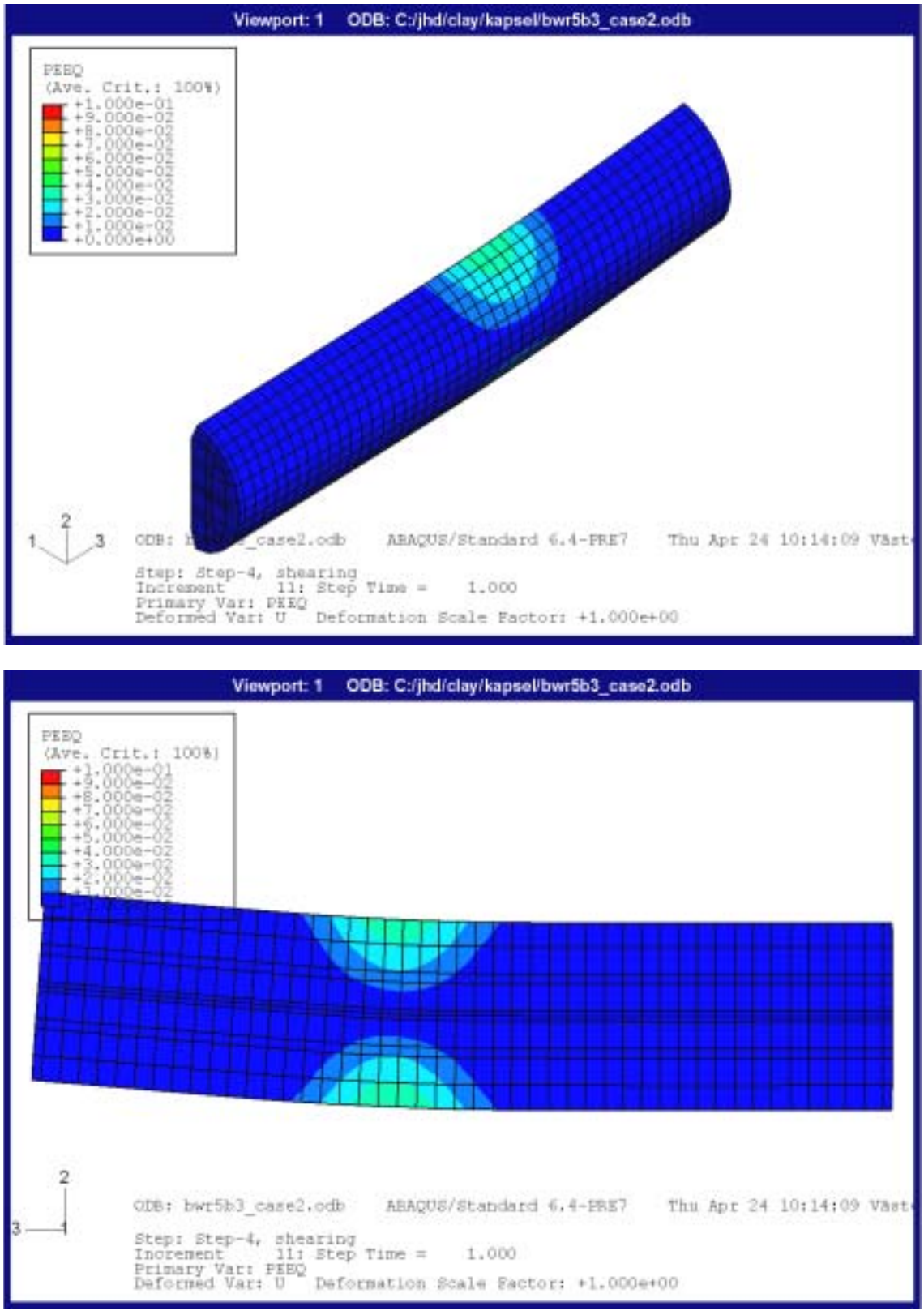

Figure A8-3. *Contour plots of the plastic strain in the cast iron insert seen from "behind" (upper) and straight "from the front" (lower) after 20 cm rock displacement. The shear plane is located 8 elements from the left side in the lower figure.*

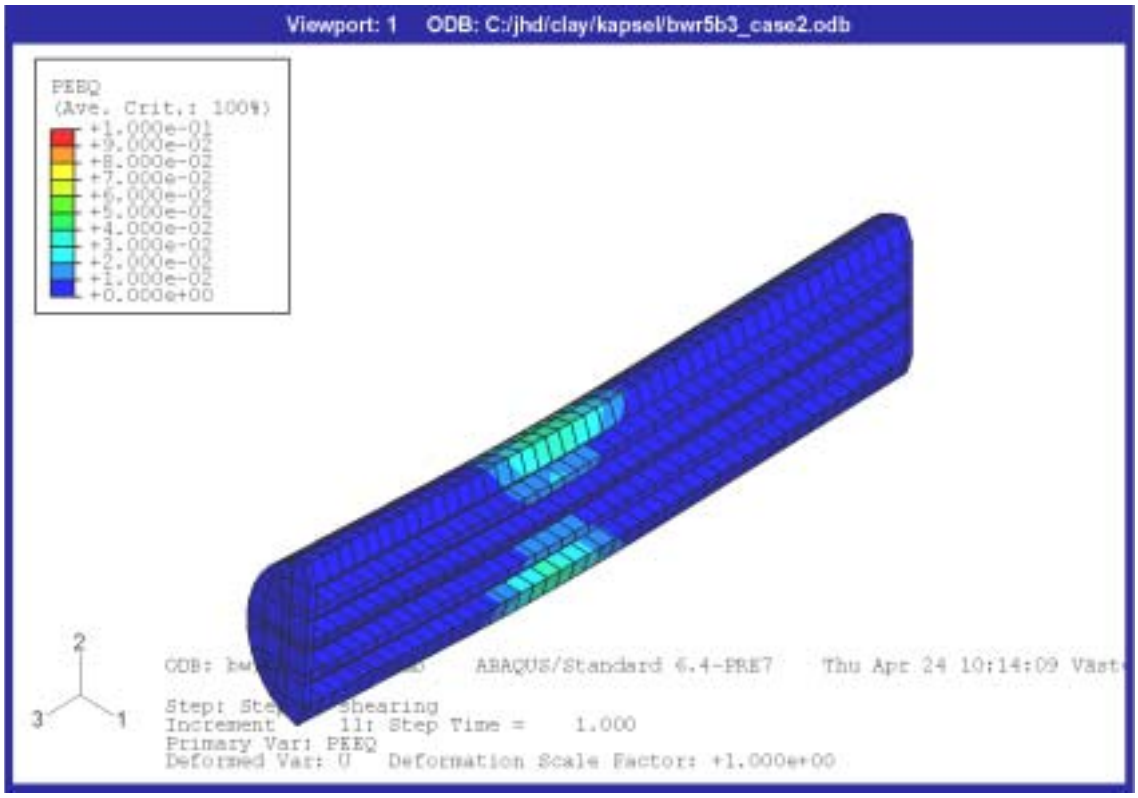

Figure A8-4. *Plastic strain in the cast iron insert after 20 cm rock displacement at a section cut parallel to the axis.*

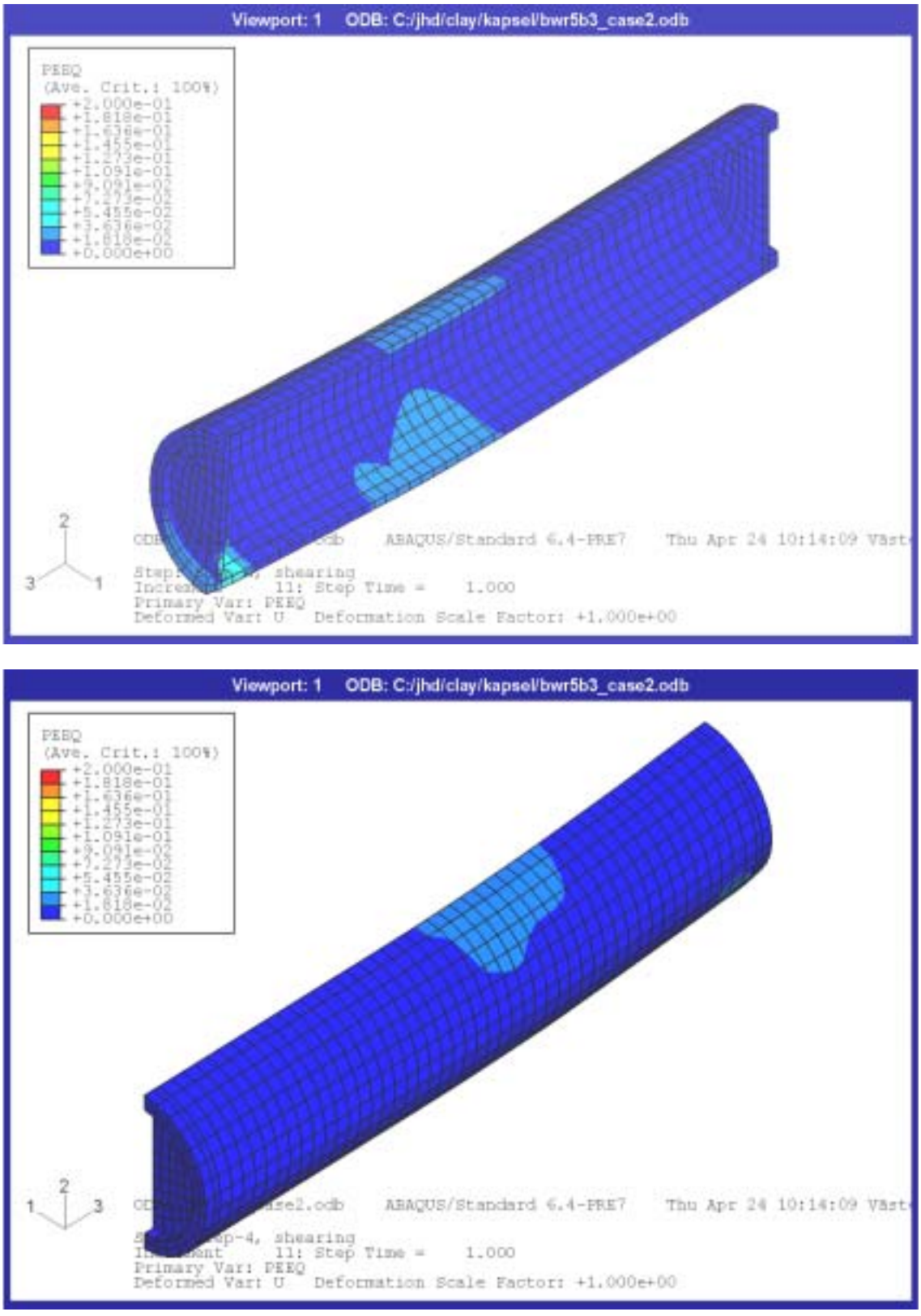

Figure A8-5. *Plastic strain in the copper canister after 20 cm rock displacement.*

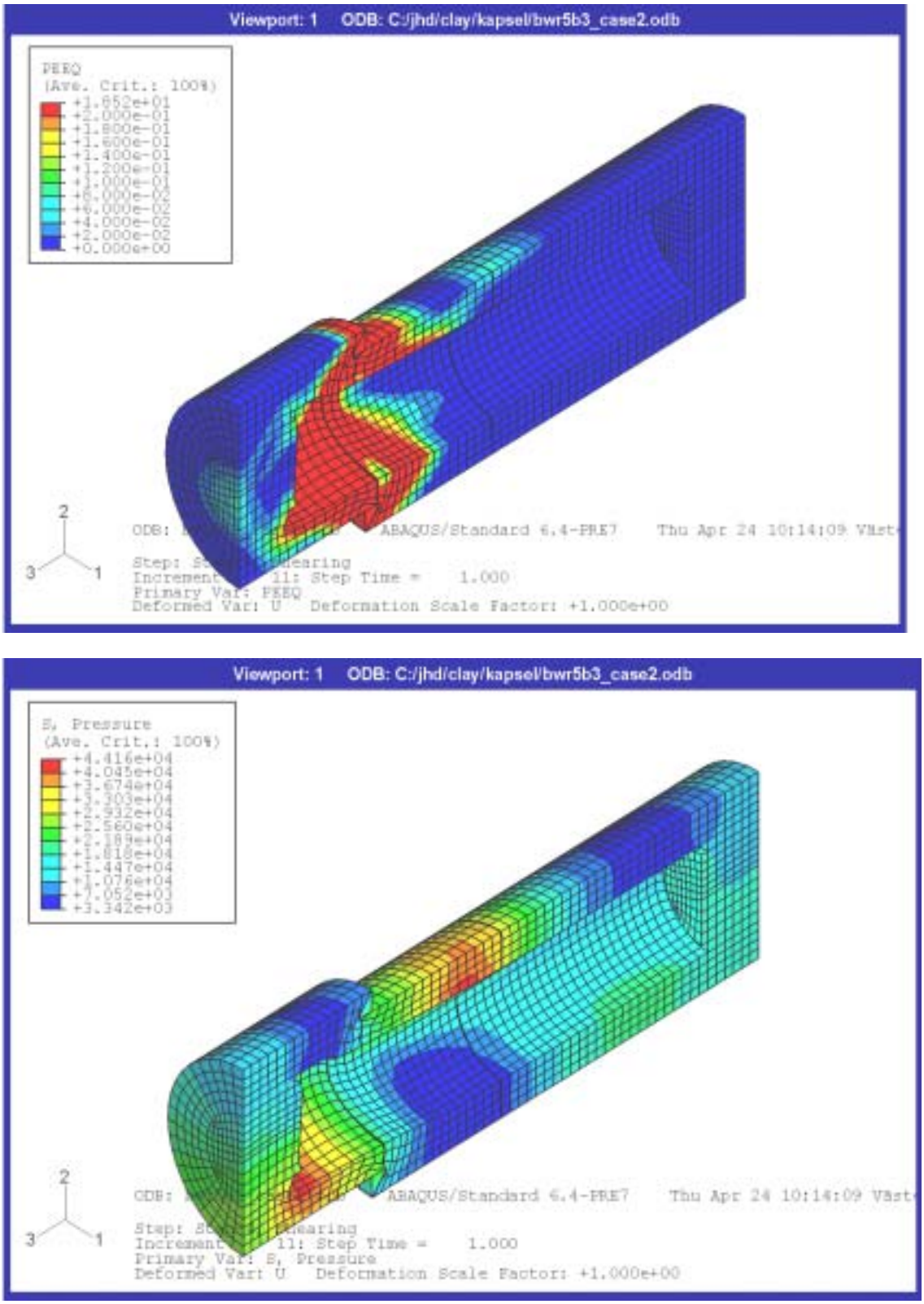

Figure A8-6. *Plastic strain (upper) and average stress (kPa pressure) (lower) in the bentonite buffer after 20 cm rock displacement.*

ISSN 1404-0344

CM Digitaltryck AB, Bromma, 2004